





3 1293 01686 3346

This is to certify that the

dissertation entitled

LIGAND BINDING PROPERTIES OF METALLOPORPHYRINS:  
FACTORS THAT INFLUENCE THEIR CHEMICAL PROPERTIES AND  
RELATIONSHIPS TO PROTEINS

presented by

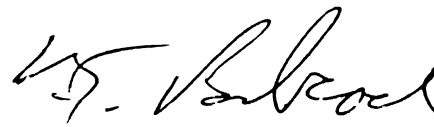
Einhard Schmidt

has been accepted towards fulfillment  
of the requirements for

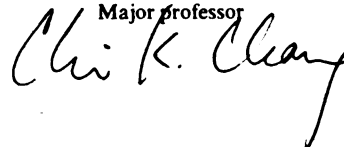
Ph.D. degree in Chemistry

Date

11/13/95



Major professor



**LIBRARY**  
**Michigan State**  
**University**

**PLACE IN RETURN BOX**  
to remove this checkout from your record.  
**TO AVOID FINES** return on or before date due.

DATE DUE	DATE DUE	DATE DUE
<hr/>	<hr/>	<hr/>
<hr/>	<hr/>	<hr/>
<hr/>	<hr/>	<hr/>
<hr/>	<hr/>	<hr/>
<hr/>	<hr/>	<hr/>

**LIGAND BINDING PROPERTIES OF METALLOPORPHYRINS:  
FACTORS THAT INFLUENCE THEIR CHEMICAL PROPERTIES AND  
RELATIONSHIPS TO PROTEINS**

**By**

**Einhard Schmidt**

**A DISSERTATION**

**Submitted to  
Michigan State University  
in partial fulfillment of the requirements  
for the degree of**

**DOCTOR OF PHILOSOPHY**

**Department of Chemistry**

**1995**

## ABSTRACT

### LIGAND BINDING PROPERTIES OF METALLOPORPHYRINS: FACTORS THAT INFLUENCE THEIR CHEMICAL PROPERTIES AND RELATIONSHIPS TO PROTEINS

By

Einhard Schmidt

This dissertation concerns the use of porphyrins as model compounds to mimic the active site of proteins. The use of models in place of actual proteins has several advantages. The obvious advantages being cost and convenience; however, the major reason and most important is the isolation of the active site of the protein itself. With the active site porphyrin isolated from the protein it is possible to establish the influence of the protein on the active site. The model compounds are typically actual active site porphyrins or representative synthetic substitutes. In many cases the synthetic porphyrins are altered to represent proposed protein influences. The models that I used are represented by previously established porphyrin models as well as newly synthesized intramolecular hydrogen bonding compounds.

Resonance Raman spectroscopy was used to study the effects of hydrogen bonding on the vibrational frequency of  $\nu(\text{V}=\text{O})$ ,  $\nu(\text{Ru}-\text{CO})$  and  $\nu(\text{Fe}-\text{CO})$ . The studies done on NKAP(V=O) and NKAmP(V=O) established the hydrogen bonding nature of this model by removal of the acidic proton of the acid with the non-coordinating base DBN.

The room temperature oxidation of Co(II)OEP with AgClO<sub>4</sub> produced the cation radical cobalt porphyrin (Co(II)OEP<sup>+·</sup>)[ClO<sub>4</sub><sup>-</sup>]. When the resulting cation radical is subsequently exposed to carbon monoxide an intramolecular electron transfer takes place. The resulting carbon monoxide ligated cobalt porphyrin was studied with RR, IR and UV-vis spectroscopic techniques. In this study we established the  $\nu(\text{C}\equiv\text{O})$  and  $\nu(\text{Co-CO})$  vibrational modes for both the 5 and 6-coordinated complexes. Information from the titration curve was used in calculating the pressure dependent equilibrium constants.

## ACKNOWLEDGMENTS

This section is where I have the opportunity to point out the special people that gave valuable assistance to the finality of this dissertation. Some of this help was in the scientific area that included specific discussions that were directly related to my work. This would, of course, include my advisors Chris Chang and Gerry Babcock and members of each of their respective groups who sat through many group meetings offering many insights and ideas. My committee was completed by Kris Berglund and John McCracken whom I thank for reviewing this dissertation and keeping me honest. I thank Dan Noccera for taking me to several meetings, I really appreciated the opportunities to experience the scientific community that you are associated with. This list would not be complete without mentioning Mel Sahyun of 3M corporation. You gave me a chance to experience basic research and convinced me to go to graduate school, both of which I found most interesting.

The help to escape from the scientific realm often falls on the family members. I have no doubt that it was not always pleasant when I was in one of my "I have to get away" moods. Fortunately for me one of them was always within reach. In addition to my family the MSU Judo club was extremely helpful to my personal sanity. Without ever knowing why they were often the channel where I could and would vent built up aggression.

There is the bridge that crosses the above mentioned two worlds. In this area falls fellow students who understand the drill. This list is much too long to specifically mention everyone that helped but it never went unnoticed. There are, however, some people that must be mentioned. First is the Vlassiks, Deena and Paul, you fed me, gave me a place to stay and always had beer on hand, I can't thank you enough. To Eric Hendrickson, the nights at the Peanut Barrel will be remembered. The one person that I can never thank enough is Ying Liang (Lora). You were instrumental in my research, but what is more important is that you are a very good friend.

## TABLE OF CONTENTS

	<b>Page</b>
List of Tables.....	vii
List of Figures.....	viii
 <b>CHAPTER 1 - GENERAL INTRODUCTION</b>	
1.1 Background.....	1
1.2 Theoretical Background.....	6
1.2.1 Historical Development.....	8
1.2.1.1 Four Orbital Model.....	9
1.2.2 Spectroscopic Significance.....	13
1.2.3 Raman Theory.....	15
1.2.3.1 Resonance Raman.....	18
1.2.3.2 Established Porphyrin Vibrations.....	23
1.3 Core Metals and Oxidation States.....	27
1.3.1 $\pi$ -Cation Radicals.....	31
1.4 Environmental factors.....	33
1.4.1 Solvent.....	33
1.4.2 Atmosphere.....	34
1.4.3 Temperature.....	35
1.4.4 Hydrogen bonding.....	36
1.5 Aims Of This Research.....	40
References.....	41

<b>CHAPTER 2 - Preparation and Characterization of 5 and 6 Coordinated (CO)Co<sup>III</sup>OEP(ClO<sub>4</sub><sup>-</sup>) Complexes, Electron and Vibrational Spectroscopies and Normal Coordinate Analysis.....</b>	<b>47</b>
2.1 Overview.....	47
2.2 Introduction.....	48
2.3 Experimental.....	51
2.4 Results	
2.4.1 Optical Spectroscopy.....	53
2.4.2 Resonance Raman spectroscopy.....	53
2.4.3 FTIR spectroscopy.....	67
2.4.4 Carbon monoxide titration.....	67
2.5 Discussion	
2.5.1 Analysis of Cobalt-CO vibrations.....	70
2.5.1.1 Group theoretical analysis.....	70
2.5.1.2 Vibrational spectroscopy.....	71
2.5.2 Calculation of equilibrium constants and P <sub>1/2</sub> values for reactions (1) - (3).....	73
2.5.3 Comparison of [(CO)Co(III)OEP]ClO <sub>4</sub> to BrCo(III)OEP and other complexes.....	74
References.....	77

**CHAPTER 3 - Optical and Vibrational Spectroscopic Properties of  
Oxovanadyl Porphyrin Compounds, Evidence of Hydrogen  
Bonding to the Oxo Ligand**

3.1 Introduction.....	81
3.2 Experimental.....	83
3.2.1 Oxo[5-(8-Kempacid-1-Naphthyl)-2,8,13,17-Tetraethyl- 3,7,12,18-Tetramethyl Porphine]vanadium (1).....	83
3.2.2 Instrumentation.....	84
3.3 Results.....	84
3.3.1 Optical Properties.....	87
3.3.2 Resonance Raman.....	92

3.4 Conclusions.....	105
References.....	107

#### CHAPTER 4 - Cyanide Titrations of (Cl<sup>-</sup>)Fe(III)porphyrins Followed by Optical Spectroscopy

4.1 Introduction.....	110
4.1.1 Sol-gel systems.....	110
4.1.2 Cyanide detection systems.....	111
4.1.3 Properties of substituted phenyl tetraphenyl porphyrins.....	112
4.2 Experimental.....	112
4.3 Results.....	113
4.4 Discussion.....	122
References.....	125

#### CHAPTER 5 Resonance Raman Evidence of the Hydrogen Bonding Effect on n(M-CO) where M = Fe(II) or Ru(II).

5.1 Background.....	126
5.1.1 Proposed ligand discriminations.....	128
5.2 Mutagenesis of HisE7 and the effect on CO affinity.....	129
5.2.1 CO ligated myoglobin and vibrational spectroscopy.....	130
5.3 Oxygen binding and hydrogen bonding.....	131
5.4 Experimental.....	132
5.5 Results	
5.5.1 Carbon monoxide bound RuNKAP.....	133
5.5.2 Carbon monoxide bound FeNKAP.....	138
5.6 Discussion.....	144
References.....	145



## LIST OF TABLES

	<b>Page</b>
Table 2-I. Structural sensitive vibrational frequencies ( $\text{cm}^{-1}$ ) observed in resonance Raman spectra obtained at the given excitation wavelengths (nm).....	58
Table 2-II. Observed and calculated frequencies ( $\text{cm}^{-1}$ ) and normal mode assignments of cobalt-carbonmonoxy vibrations for 5 and 6-coordinate $[(\text{CO})_n\text{Co(III)OEP}]\text{ClO}_4$ complexes.....	70
Table 4-I. Equilibrium constants for the binding of cyanide anion the Fe(III) porphyrins.....	114
Table 4-II. Half-wave potentials of different (P)Fe(R) and (P)Fe(Cl) complexes in PhCN (0.1) M (TBA)PF <sub>6</sub> . Reproduced from reference 11.....	122
Table 5-I. Rate and equilibrium constants for O <sub>2</sub> and CO binding for Mb wild type and mutants. (Reproduced from Springer, B. A.; Sligar, S. G.; Olson, J. S. and Phillips, G. N., Jr. <i>Chem. Rev.</i> , <b>1994</b> , 94, 699-714).....	130
Table 5-II. The observed $\nu(\text{M-CO})$ {M = Fe(II) or Ru(II)} frequencies for OEP, NKAP, NKEP or NKAmP in methylene chloride. Raman excitations were obtained from $\lambda_{\text{ex}} = 406.7 \text{ nm}$ .....	146

## LIST OF FIGURES

	<b>Page</b>
Figure 1-1	(a) Structure of ferriprotoporphyrin IX, typical structure found in heme proteins. (b) Structure of chlorophyll a, structure found in green plants, essential in the light harvesting photoreaction center. (c) Corrin structure found at the center of B <sub>12</sub> . ( Reference 6) .....3
Figure 1-2	Aromatic $\pi$ -electron system of the porphyrin macrocycle. The 18 $\pi$ -electron ring is shown by the heavy dark lines. (Reference 3).....5
Figure 1-3	Porphyrin carbon-nitrogen skeleton that shows the D <sub>4h</sub> symmetry of the porphyrins, In this representation the x,y axes become degenerate, this is the typical case in unligated metalloporphyrins(Reference 3).....7
Figure 1-4	Pictorial representation of the HOMOs (b1 and b2) and LUMOs (c1 and c2) of the porphyrin four essential orbitals. The size of the circles are proportional to the orbital coefficients. Solid circles represent positive values and dashed circles represent negative values. The heavy lines indicate nodal planes..... 10
Figure 1-5	Relative orbital energy representations for porphyrin and chlorin. An equivalent energy d has been added to b1 and subtracted from b2 to make these orbitals degenerate in the porphyrins..... 11

Figure 1-6	Some possible consequences of a photon of light interacting with a molecule. The lengths of the arrows are proportional to the frequency of light that is either incoming (upward), scattered (downward) or emitted (downward).(Reference 7c).....	17
Figure 1-7	Porphyrin vibrational modes that are sensitive to the oxidation or spin state of the central metal or the core size of the the porphyrin itself. vibrational values given are for NiOEP in methylene chloride. (Reference 13).....	26
Figure 1-8	Simplified mechanism for the reduction of O <sub>2</sub> and proton translocation in cytochrome oxidase. The binuclear center is represented as [a <sub>3</sub> CuB]. The reaction is initiated by O <sub>2</sub> binding to the reduced form of this center, to produce oxy, and then peroxy intermediates. Reduction and protonation of the peroxy species is coupled to the translocation of two protons, which is indicated by the heavy, shaded arrow. Oxygen-oxygen bond cleavage is also driven, in this step, to produce the ferryl intermediate. Reduction and protonation of this species is also coupled to the translocation of two protons, which is indicated by the second heavy, shaded arrow. The hydroxy product of this reaction is subsequently reduced by two electrons, to complete the cycle.(Figure courtesy of G. T. Babcock).....	29
Figure 1-9	Proposed mechanism for the formation of compound I of Cytochrom c peroxidase. a) Representation of the native enzyme. b) The activated complex with the distal histidine acting as an acid-base catalyst and the active site argenine stabilizing a partial negative charge forming on RO-Ofc. c) The oxoferryl p-cation radical intermediate. d) Compound I after the intramolecular electron transfer to to produce the oxoferryl and free radical X.(Reference 19).....	30
Figure 1-10	(a) Structures of OEP and TPP, synthetic porphyrins that have been well established as models for a variety of biologically related structures. (b) The structure of the recently synthesized naphthyl Kemp's acid etio type porphyrin (NKAP) model compound that is capable of intramolecular hydrogen bonding.....	38
Figure 2.1	a) (—) Neutral Co <sup>II</sup> OEP in CH <sub>2</sub> Cl <sub>2</sub> b) (---) One electron oxidized Co <sup>II</sup> OEP <sup>+</sup> ·(ClO <sub>4</sub> <sup>-</sup> ) in CH <sub>2</sub> Cl <sub>2</sub> under an N <sub>2</sub> atmosphere. c) (···) One electron oxidized Co <sup>II</sup> OEP <sup>+</sup> ·(ClO <sub>4</sub> <sup>-</sup> ) in CH <sub>2</sub> Cl <sub>2</sub> under a CO atmosphere.....	54

Figure 2.2	Resonance Raman spectra of one electron oxidized $\text{Co}^{\text{II}}\text{OEP}^+\cdot(\text{ClO}_4^-)$ under a) an $\text{N}_2$ atmosphere, b) a $^{12}\text{CO}$ atmosphere, c) a $^{13}\text{CO}$ atmosphere. The excitation wavelength in all spectra was 363.8nm at 5mW of power. The samples were prepared in dry $\text{CH}_2\text{Cl}_2$ , UV-vis spectra were taken prior to and following the Raman spectroscopy to verify the integrity of the samples.....	57
Figure 2.3	High range resonance Raman spectra of one electron oxidized $\text{Co}^{\text{II}}\text{OEP}^+\cdot$ under a CO atmosphere, The excitation wavelength in the spectra was prepared 413.1 nm at 5 mW of power. The sample in dry $\text{CH}_2\text{Cl}_2$ , UV-vis spectra were taken prior to and following the Raman spectroscopy to verify the integrity of the sample.....	60
Figure 2.4	High range resonance Raman spectra of one electron oxidized $\text{Co}^{\text{II}}\text{OEP}^+\cdot$ under a) a $^{12}\text{CO}$ atmosphere, b) a $^{13}\text{CO}$ atmosphere. The excitation wavelength in all spectra was 363.8nm at 5mW of power. The samples were prepared in dry $\text{CH}_2\text{Cl}_2$ , UV-vis spectra were taken prior to and following the Raman spectroscopy to verify the integrity of the samples.....	63
Figure 2.5	Resonance Raman spectra of one electron oxidized $\text{Co}^{\text{II}}\text{OEP}^+\cdot(\text{ClO}_4^-)$ a) under an $^{12}\text{CO}$ atmosphere, b) under an $^{13}\text{CO}$ atmosphere. The excitation wavelength in all spectra was 413.1nm at 5mW of power. The samples were prepared in dry $\text{CH}_2\text{Cl}_2$ , UV-vis spectra were taken prior to and following the Raman spectra to verify the integrity of the samples.....	65
Figure 2.6	Titration spectra of the $\text{Co}^{\text{II}}\text{OEP}^+\cdot(\text{ClO}_4^-)$ with carbon monoxide gas. The sample was prepared in the usual way in dry $\text{CH}_2\text{Cl}_2$ , the path length of the optical cell was 5mm. The titration vessel was 135ml capacity and the partial pressure of CO was calculated by starting under vacuum, then systematically injecting into the vessel a known volume of CO gas. Ideal gas law properties were assumed and the partial pressure was calculated from $(V_{\text{inj}}/V_{\text{vessel}})*760\text{Torr}$ . The pressure within the gas tight syringe was allowed to equilibrate to atmospheric pressure, estimated at 760 Torr.....	68

Figure 3-1	(a) The Structure of free base naphthyl Kemp's acid porphyrin showing the acid proton coordinated over the center of the porphyrin ring. (b) The structure of oxovanadyl naphthyl Kemp's acid porphyrin showing the potential for hydrogen bonding between the acid proton and the oxo ligand.....	86
Figure 3.2	The optical absorption spectra of oxovanadyl naphthyl Kemp's acid porpyrin, (a) (—) in pure methylene chloride and (b) (----) in methylene chlorided with 1-2% 1,5-diazabicyclo[4,3,0]one-5-ene.....	89
Figure 3..3	The optical absorption spectra of oxovanadyl octaethyl porphyrin (—) in pure methylene chlorided and (----) in a mixture of 50% methylene chlorided and 50% acetic acid.....	91
Figure 3.4	Resonance Raman spectra obtained from 413.1 nm excition of OEP(VO) in (a) 95% methylene chloride and 5% acedic acid (b) 25% methylene chloride and 75% acedic acid(c) in 50% methylene chloride and 50% deuterated acetic acid (d) in methylene chloride and an excess of tetrabutyl ammonium acetate. Optical absorption spectra were taken before and after the Raman spectra to ensure the integrity of the sample.....	94
Figure 3.5	Resonance Raman spectra obtained from the 413.1 nm excitation of oxovanadyl naphthyl Kemp's acid porpyrin, (a) in pure methylene chloride and (b) in methylene chlorided with 1-2% 1,5-diazabicyclo[4,3,0]one-5-ene. Optical absorption spectra were taken before and after the Raman spectra to ensure the integrity of the sample.....	97
Figure 3.6	Resonance Raman spectra obtained from 413.1 nm excition of OEP(VO) in (a) in pure methylene chloride and (b) in methylene chlorided with an excess of 1,5-diazabicyclo [4,3,0]one-5-ene. Optical absorption spectra were taken before and after the Raman spectra to ensure the integrity of the sample.....	99
Figure 3.7	Resonance Raman spectra obtained from the 413.1 nm excitation of oxovanadyl naphthyl Kemp's amide porpyrin, (a) in pure methylene chloride and (b) in methylene chlorided with 1,5-diazabicyclo[4,3,0]one-5-ene. Optical absorption spectra were taken before and after the Raman spectra to ensure the integrity of the sample.....	102

Figure 3.8	(a) Resonance Raman spectra obtained from the 406.7 nm excitation of oxovanadyl naphthyl Kemp's amide porphyrin, in N-Methyl Imidazole. (b) Resonance Raman spectra obtained from the 406.7 nm excitation of oxovanadyl octaethy porphyrin, in N-Methyl Imidazole. (c) Resonance Raman spectra obtained from the 441.8 nm excitation of oxovanadyl naphthyl Kemp's amide porphyrin, in N-Methyl Imidazole. (d) Resonance Raman spectra obtained from the 441.8 nm excitation of oxovanadyl octaethy porphyrin, in N-Methyl Imidazole.....	105
Figure 4.1	Titration curve of (para-fluoro) tetraphenyl porphyrin (Fe <sup>III</sup> )chloride (Fe <sup>III</sup> (P-F)TPPCL) in acetonitrile (CH <sub>3</sub> CN) titrated with tetrabutyl ammonium cyanide in CH <sub>3</sub> CN.....	116
Figure 4.2	Titration curve of tetraphenyl porphyrin (Fe <sup>III</sup> )chloride (Fe <sup>III</sup> TPTMPCl) in acetonitrile (CH <sub>3</sub> CN) titrated with tetrabutyl ammonium cyanide in CH <sub>3</sub> CN.....	117
Figure 4.3	Titration curve of (pentafluoro) tetraphenyl porphyrin (Fe <sup>III</sup> )chloride (Fe <sup>III</sup> (PentaF)TPPCL) in acetonitrile (CH <sub>3</sub> CN) titrated with tetrabutyl ammonium cyanide in CH <sub>3</sub> CN.....	118
Figure 4.4	Titration curve of Octaethyl porphyrin (Fe <sup>III</sup> )chloride (Fe <sup>III</sup> OEPCl) in acetonitrile (CH <sub>3</sub> CN) titrated with tetrabutyl ammonium cyanide in CH <sub>3</sub> CN.....	119
Figure 4.5	Titration curve of tetraphenyl porphyrin (Fe <sup>III</sup> )chloride (Fe <sup>III</sup> TPPCL) in acetonitrile (CH <sub>3</sub> CN) titrated with tetrabutyl ammonium cyanide in CH <sub>3</sub> CN.....	120
Figure 4.6	Titration curve of porphycene (Fe <sup>III</sup> )chloride (Fe <sup>III</sup> Por) in acetonitrile (CH <sub>3</sub> CN)titrated with tetrabutyl ammonium cyanide in CH <sub>3</sub> CN.....	121
Figure 5-1	The high frequency resonance Raman spectra obtained with $\lambda_{ex} = 406.7$ nm of (a) carbon monoxide bound ruthenium naphthly Kemp's esterporphyrin (b) carbon monoxide bound ruthenium naphthly Kemp's acidporphyrin (c) carbon monoxide bound ruthenium naphthly Kemp's amideporphyrin.....	137

Figure 5-2	The low frequency resonance Raman spectra obtained with $\lambda_{\text{ex}} = 406.7$ nm of (a) carbon monoxide bound ruthenium naphthly Kemp's esterporphyrin (b) carbon monoxide bound ruthenium naphthly Kemp's acidporphyrin (c) carbon monoxide bound ruthenium naphthly Kemp's amideporphyrin.....	139
Figure 5-3	The high frequency resonance Raman spectra obtained with $\lambda_{\text{ex}} = 406.7$ nm of (a) carbon monoxide bound iron(II) octaethylporphyrin in $\text{CH}_2\text{Cl}_2$ (b) carbon monoxide bound iron(II) naphthly Kemp's esterporphyrin (c) carbon monoxide bound iron(II) naphthly Kemp's amideporphyrin (d) carbon monoxide bound iron(II) naphthly Kemp's acidporphyrin.....	141
Figure 5-4	The low frequency resonance Raman spectra obtained with $\lambda_{\text{ex}} = 406.7$ nm of (a) carbon monoxide bound iron(II) octaethylporphyrin in $\text{CH}_2\text{Cl}_2$ (b) carbon monoxide bound iron(II) naphthly Kemp's esterporphyrin (c) carbon monoxide bound iron(II) naphthly Kemp's amideporphyrin (d) carbon monoxide bound iron(II) naphthly Kemp's acidporphyrin.....	143
Figure 5-5	The low frequency resonance Raman spectra obtained with $\lambda_{\text{ex}} = 406.7$ nm of (a) carbon monoxide bound iron(II)NKAP in $\text{CH}_2\text{Cl}_2$ . Iron was inserted into free base NKAP in the form of iron(II)carbonyl carbonate. The carbonate anion left the $\text{COFe(II)NKAP}$ complex in the deprotonated five-coordinate form. (b) carbon monoxide bound iron(II)NKAP in $\text{CH}_2\text{Cl}_2$ and 2mL of HOAc that would leave the $\text{COFe(II)NKAP}$ complex in the protonated five-coordinate form.....	145

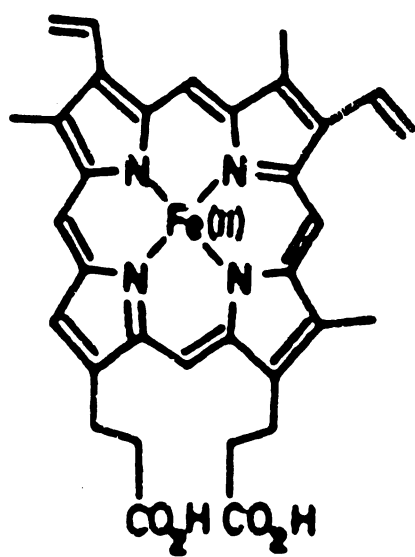
## CHAPTER 1

### GENERAL INTRODUCTION

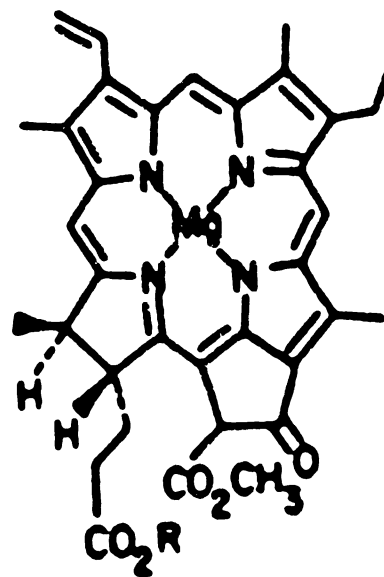
Every form of life depends on some form of four pyrrole macrocycles that take on a variety of characteristics (Figure 1)[1]. The cores of these macrocycles are commonly linked by an aromatic 18  $\pi$ -electron system (Figure 2). The resonance structure of the system is such that two of the nitrogens in the core of the macrocycle are each a single anion. The core of the macrocycle is subject to bonding by either two protons to give the free base form, or with a metal in the 2<sup>+</sup> or higher oxidation state to give a metalloporphyrin (MP). In the fully oxidized form, the macrocycles have the aromatic 18  $\pi$ -electron system and 2 additional  $\pi$ -bonds these are classically known as porphines, A macrocycle with a singly reduced  $\pi$ -bond is a chlorin; when there are two reduced  $\pi$ -bonds they are classified as either bacteriochlorins or isobacteriochlorins. Classically, these structures all fall under the general heading of porphyrin [2]. However, the term porphyrin has now come to signify the fully oxidized structure that was originally designated as porphine.

In this thesis, I will concentrate on the fully oxidized porphyrin as the starting material. The terminology described in the paragraph above will be

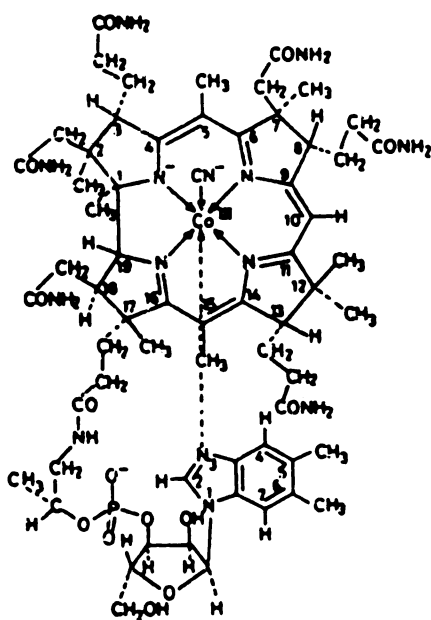
**Figure 1-1** (a) Structure of ferriprotoporphyrin IX, typical structure found in heme proteins. (b) Structure of chlorophyll a, typical structure found in green plants, essential in the light harvesting photoreaction center. (c) Corrin structure found at the center of B<sub>12</sub> systems.



a)



b)



c)

adhered to and the term porphyrin will be used throughout. If any of the other structures are referred to, the specifically defined names above will be used.

In nature, the central core of the porphyrin is found to contain a variety of transition metals [3]. In hemoproteins, the core is occupied by an iron atom that can bind oxygen and, at the same time, retain the oxidation state of the iron. Hemoglobin and myoglobin are the best known and most characterized, reversible oxygen binding hemeproteins. An isolated heme in solution has an affinity for carbon monoxide that is 25,000 times greater than that for oxygen. However, in the proteins hemoglobin and myoglobin, the heme has a binding affinity for carbon monoxide only 200 times that of oxygen [4]. The protein's ability to reduce the carbon monoxide binding affinity is a defense mechanism designed to prevent asphyxiation by endogenously produced carbon monoxide. The mechanism that these proteins use for achieving this reduced carbon monoxide binding affinity, is for the most part fully characterized and understood, however, at this time, certain details remain unresolved [5]. Cytochrome c oxidase, which is also an oxygen binding heme protein, initially binds oxygen in the  $\text{Fe}^{\text{II}}$  state and sequentially goes through  $\text{Fe}^{\text{III}}$  and  $\text{Fe}^{\text{IV}}$  states while reducing  $\text{O}_2$  to  $\text{H}_2\text{O}$ . Similar mechanism are found in catalases and other oxidases.

Cobalt occupies the center of a corrin ring in cyanocobalamin (Vitamin  $\text{B}_{12}$ )[6a]. The corrin ring has an altered carbon-nitrogen skeleton where one of the bridging carbons, known as the meso carbon, is entirely removed from the ring. However, the use of cobalt porphyrins as models to gain an understanding of vitamin  $\text{B}_{12}$  chemistry is well documented [6b]. The cobalt center of both the models and the vitamin can be oxidized to  $\text{Co}(\text{III})$  [6c] or reduced to  $\text{Co}(\text{I})$ . The  $\text{Co}(\text{I})$  of models, like that of vitamin  $\text{B}_{12}$ , can and does undergo oxidative addition with alkyl halides to give the corresponding alkyl cobalt porphyrins [6d].

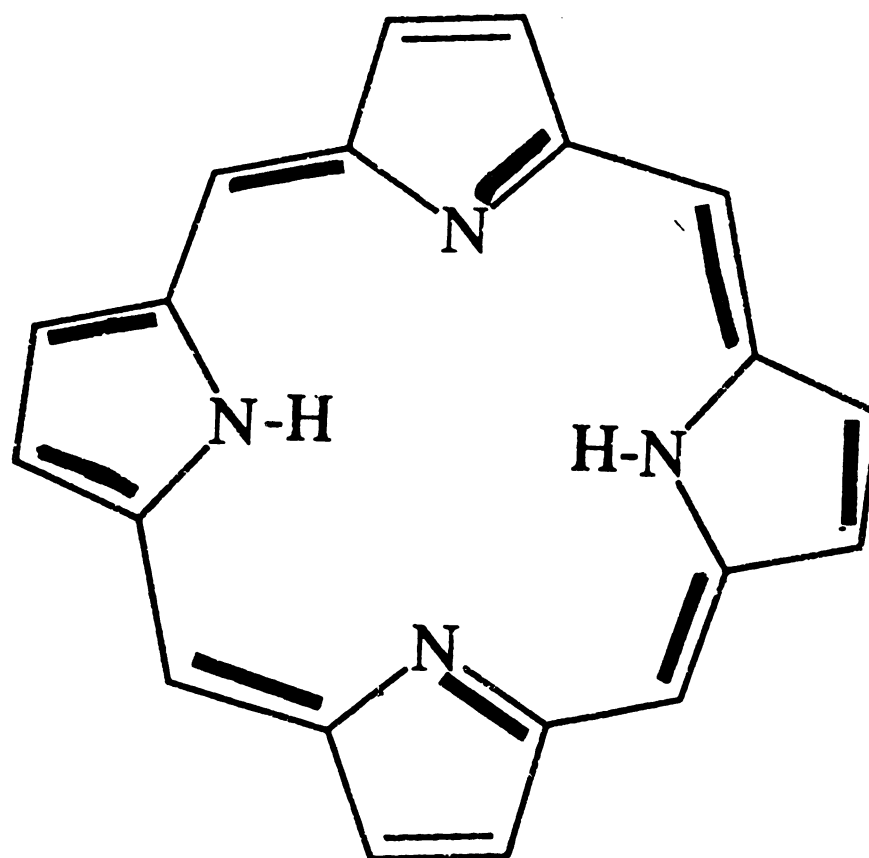
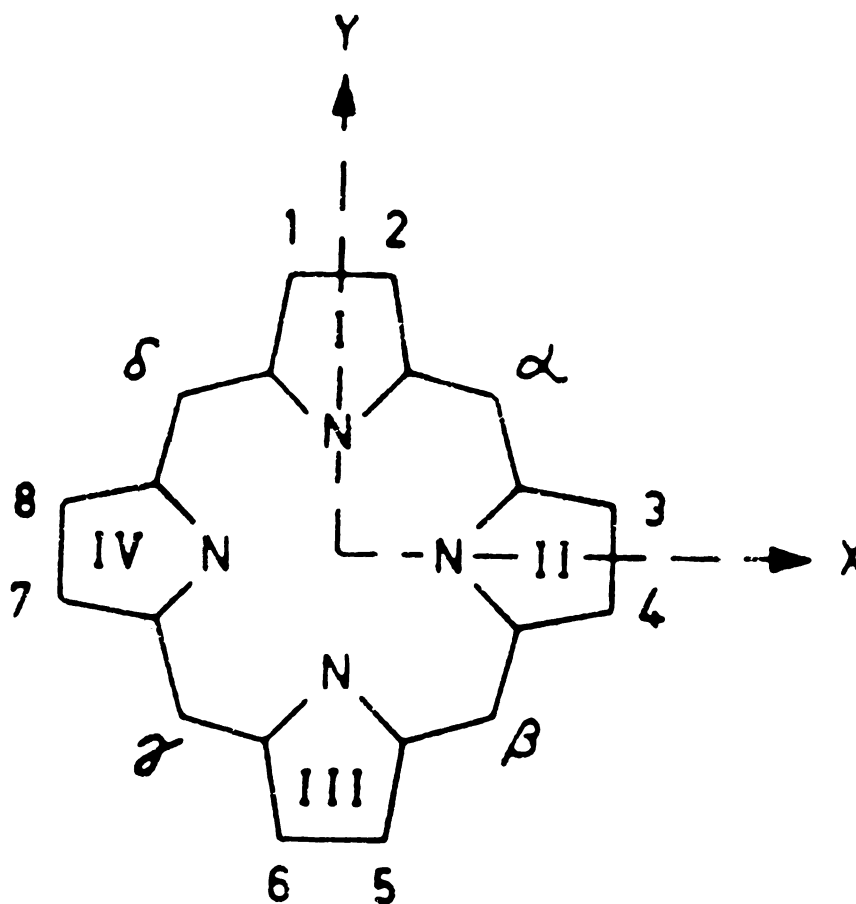


Figure 1-2 Aromatic  $\pi$ -electron system of the porphyrin macrocycle. The 18 p-electron ring is shown by the heavy dark lines. (Reference 3).

## 1.2 Theoretical Background

Many of the colors found in biology are produced by porphyrins, porphyrinoid structures, or their oxidation products. The colorful nature of porphyrins also makes them ideally suited to study by optical spectroscopic techniques. Many theories have been presented to explain the optical properties of the porphyrins and porphyrinoid systems. The currently accepted model, known as the four orbital model, was first presented by Martin Gouterman in 1959 [2a]. The four orbital model is based on the carbon-nitrogen skeleton of the macrocycle only (Figure 3). Therefore, it applies to the fully oxidized porphyrin as well as the partially reduced chlorins, bacteriochlorins and isobacteriochlorins. Before giving the details of the four orbital model, some nomenclature related to optical spectra must be introduced. Detailed explanations of the optical spectra will follow the four orbital model explanation.

The optical spectra of porphyrins are separated into two basic regions. In the near UV, the intense B band maximum (also known as the Soret band) typically occurs between 350 and 450 nm. The Q bands lie in the visible light region encompassing 450-700 nm, and are approximately one tenth as intense as the Soret band. Figure 3 is a representation of the carbon-nitrogen skeleton that shows the basic  $D_{4h}$  symmetry of the porphyrin. Peripheral substituents, or ligands bound to the core metal of metalloporphyrins, as well as the free base form, may cause deviations from pure  $D_{4h}$  symmetry. Common examples of four pyrrole macrocycles with lowered symmetry are chlorins, free base porphyrins and the naturally occurring ferriprotoporphyrin IX (Figure 1a). These examples all have  $C_{2v}$  symmetry. The effect of lowering the  $D_{4h}$  symmetry to that of  $C_{2v}$  is that the x axis and the y axis are no longer degenerate. When the  $D_{4h}$  symmetry of the porphyrins is effectively lowered the Q bands, as well as the B band, are



**Figure 1-3** Porphyrin carbon-nitrogen skeleton that shows the  $D_{4h}$  symmetry of the porphyrins. In this representation the x,y axes become degenerate, this is the typical case in unligated metalloporphyrins (Reference 3).

subsequently split into  $Q_x$ ,  $Q_y$  and  $B_x$ ,  $B_y$  transitions. The  $Q_x$  and  $Q_y$  bands are clearly identified in optical spectra when a lowered symmetry occurs, however, the  $B_x$  and  $B_y$  transitions are too closely oriented in their absorption maximum to be resolvable except for a few known cases [44]. The theory presented here, which is rigorous only for the pure  $D_{4h}$  is, nonetheless, still applicable for explaining optical spectral bands in porphyrin systems that deviate from the  $D_{4h}$  case. The effects of lowering the symmetry will be explained in section 1.2.2.

### 1.2.1 Historical Development

In 1949 Simpson was able to predict qualitatively the occurrence of the higher energy B and lower energy Q bands by treating the  $18-\pi$  electron system of the porphyrins as free electron wire rings [2b]. In a model of this type the orbitals take the form of  $\exp(i \ell \phi)$  with an energy of  $\hbar^2 \ell^2 / 4\pi m R^2$ , where  $\hbar$  is Planck's constant,  $m$  is the electron mass and  $R$  is the radius of the ring. Orbitals of the form  $\ell = 0, \pm 1, \pm 2, \pm 3, \pm 4$  are occupied in the ground state and  $\ell = \pm 4$  is the highest occupied molecular orbital (HOMO). The lowest unoccupied molecular orbital (LUMO) is the  $\ell = \pm 5$  orbital. The lowest-energy excited states are constructed as transitions from  $\ell = \pm 4 \rightarrow \ell = \pm 5$ . There are four transitions with total angular momentum  $L_z = \pm 1$  and  $\pm 9$ ; each transition gives rise to one state with  $S = 0$  and three states with  $S = 1$ . The corresponding 16 excited states will have energy transitions of  $(\hbar^2 / 4\pi m R^2)(5^2 - 4^2)$ . A ring of radius 4 Å gives a transition energy congruent with 580 nm light. Thus, from Simpson's theoretical model a ring the size of a porphyrin is predicted to have transitions in the region that they are actually seen in experimentally. From Hund's rule we can qualitatively predict that the lowest excited energy state should be a triplet, and that the singlet states with  $L_z = \pm 1$  should have higher energy than those with  $L_z = \pm 9$ . Since the ground state is a closed shell with  $L_z$

$= \pm 0$ , the normal selection  $\Delta L_z = \pm 1$  predicts that the higher energy singlet is allowed and the lower energy singlet is forbidden. With these arguments the  $L_z = \pm 1$  singlet excited state was assigned to the Soret band and the  $L_z = \pm 9$  singlet excited state was assigned to the visible bands.

In 1954, Moffitt extended Simpson's studies to a cyclic polyene and obtained the same results as Simpson with the added benefits of correctly explaining the  $Q_x$  and  $Q_y$  energy levels [2c]. In 1950, Longuet-Higgins, Rector and Platt used MO calculations and reported the  $a_{1u}$  and  $a_{2u}$  orbitals, in  $D_{4h}$  notation, as the HOMOs and the  $e_g$  orbitals as the LUMOs [2d]. These orbitals are analogous to the free electron orbitals  $\ell = \pm 4$  and  $\ell = \pm 5$  [2e, 10a]. An electron, excited to a higher energy level, can be either an  $a_{2u} \rightarrow e_g$  and  $a_{1u} \rightarrow e_g$  transition. The excited state configurations are denoted  $(a_{2u}e_g)$  and  $(a_{1u}e_g)$ . These assignments were consistent with the corresponding wavelengths seen in the optical spectra of porphyrins. However, as a shortcoming the theoretical models still, incorrectly, predicted equal intensities for both the Q and B bands. In 1959, Gouterman added configuration interaction (CI) to the pioneering work of Simpson's free electron model, Moffitt's cyclic polyene and Longuet-Higgins and coworkers' molecular orbital (MO) calculations. This has come to be known as Gouterman's four orbital model.

#### 1.2.1.1 Four Orbital Model

The four orbital model is based on the simple Hückel model developed by Simpson and Moffitt, combined with the MO calculations of Longuet-Higgins. This model considers the two nearly degenerate HOMO orbitals labeled by Gouterman as  $b_1$  and  $b_2$  and are of  $a_{2u}$  and  $a_{1u}$  symmetries, respectively. The use of the  $b_1$  and  $b_2$  labels are due to the fact that the assigned  $a_{2u}$  and  $a_{1u}$  symmetries are only appropriate for the full  $D_{4h}$  symmetric porphyrin. However,

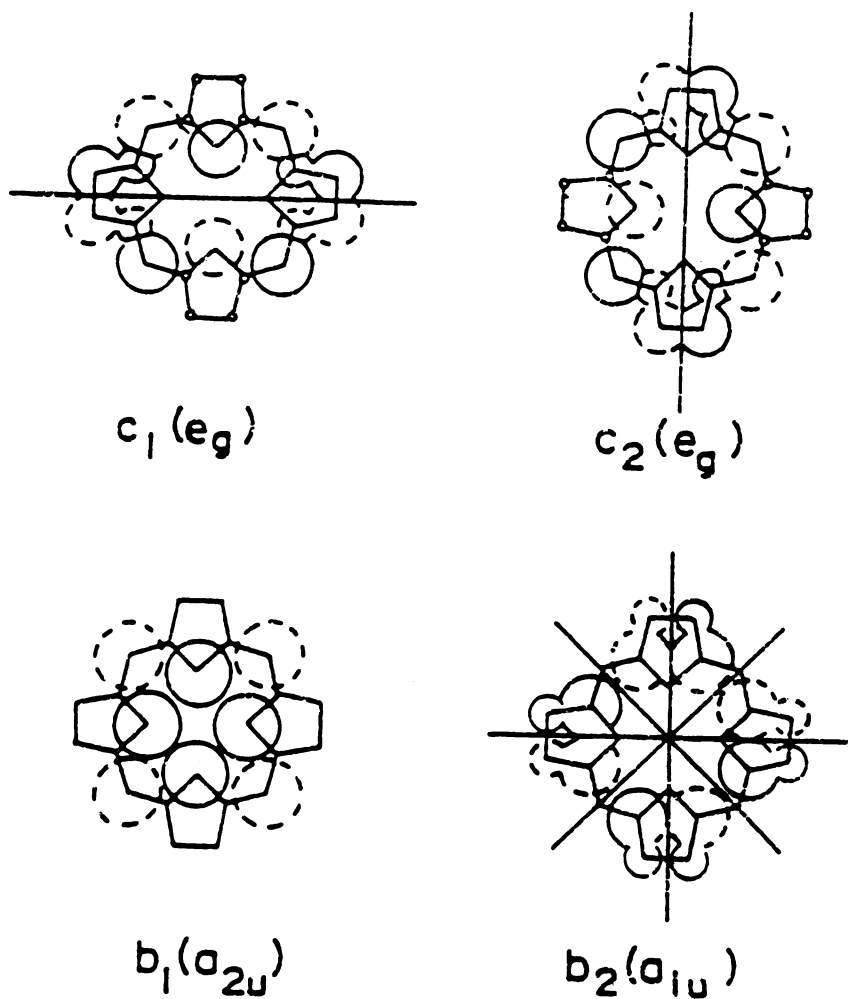
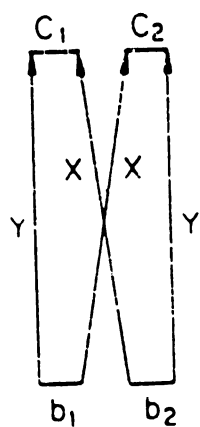
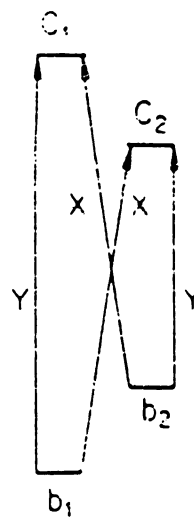


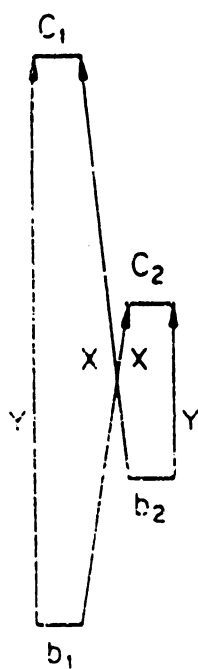
**Figure 1-4** Pictorial representation of the HOMOs ( $b_1$  and  $b_2$ ) and LUMOs ( $c_1$  and  $c_2$ ) of the porphyrin four essential orbitals. The size of the circles are proportional to the orbital coefficients. Solid circles represent positive values and dashed circles represent negative values. The heavy lines indicate nodal planes.



PORPHINE



CHLORIN



OPP-(THP)



ADJ-(THP)

Figure 1-5 Relative orbital energy representations for porphyrin and chlorin. An equivalent energy  $d$  has been added to  $b_1$  and subtracted from  $b_2$  to make these orbitals degenerate in the porphyrins.

as mentioned above, the four orbital model has been taken as applicable to all four pyrrole macrocycles. The degenerate LUMO orbitals labeled by Gouterman as  $c_1$  and  $c_2$  are each of  $e_g$  symmetry in the full  $D_{4h}$  symmetric porphyrin. The  $c_1$  and  $c_2$  labels are applicable to pyrroles that are not of  $D_{4h}$  symmetry. The orbitals are represented schematically in Figure 4. The atomic orbital (AO) coefficients are proportional to the size of the circles. The dashed circles show a change in sign and the heavy lines represent nodal planes. The approach Gouterman took to combine the partial explanations of the previous workers was to assume CI as of prime importance to explain the optical properties of the porphyrins. The other assumptions in Gouterman's considerations were that full  $D_{4h}$  symmetry is in effect and that the HOMO orbitals are accidentally degenerate. It was shown that these assumptions were valid for explaining the porphyrin and porphyrinoid structures.

If the  $b_1$  and  $b_2$  orbitals are degenerate then electron interaction would cause the singlet transitions to mix as follows:

$$\frac{B_x^o}{Q_x^o} \Big\} = [(b_1 \rightarrow c_2) \pm (b_2 \rightarrow c_1)](2)^{-\frac{1}{2}} \quad \text{eq. 1}$$

$$\frac{B_y^o}{Q_y^o} \Big\} = [(b_1 \rightarrow c_1) \pm (b_2 \rightarrow c_2)](2)^{-\frac{1}{2}}$$

Figure 5a is a representative diagram of the nearly degenerate case. Figure 5b is a diagram of the transitions if the x and y degeneracy is lifted. In the case of chlorins, which has no x,y degeneracy, we might expect that the x-polarized states would still be defined by eq. 1 because the two transitions remain nearly degenerate. However, the y-polarized states would become:

$$\begin{aligned}
 B_y &= \cos \eta (b_1 \rightarrow c_1) + \sin \eta (b_2 \rightarrow c_2) \\
 Q_y &= \sin \eta (b_1 \rightarrow c_1) - \cos \eta (b_2 \rightarrow c_2)
 \end{aligned}
 \tag{eq. 2}$$

where  $\eta$  is chosen so that the lower energy transition ( $b_2 \rightarrow c_2$ ) is more heavily weighted in the lower energy state  $Q_y$ . If ( $b_1 \rightarrow c_1$ ) and ( $b_2 \rightarrow c_2$ ) have roughly equal transition dipoles, then the ratio of absorption strengths will be:

$$\frac{\ell^2(Q_y)}{\ell^2(B_y)} = \frac{1 - \sin 2\eta}{1 + \sin 2\eta}
 \tag{eq. 3}$$

In eq. 3 we see that as the energy of the two transitions ( $b_1 \rightarrow c_1$ ) and ( $b_2 \rightarrow c_2$ ) become increasingly unequal,  $\eta$  drops below  $\pi/4$ , and the  $Q_y$  band gains intensity at the expense of the  $B_y$  band. The orbital energies of Fig. 5 are essentially those of a simple Hückel calculation with a  $\delta$  energy added to  $b_2$  and subtracted from  $b_1$  to make  $b_2$  and  $b_1$  fully degenerate. Since the two x-polarized transitions remain nearly degenerate the wavelengths and absorption strengths of  $Q_x$  and  $B_x$  remain similar even when the x and y degeneracy is no longer present. However, as the x and y degeneracy is lost the  $Q_y$  band will red shift and become intensified. This is very evident in the optical spectra of chlorins. Thus, it is seen that the four orbital model can be used to explain the observed optical spectra of porphyrins and porphyrinoid compounds.

### 1.2.2 Spectroscopic Significance

Electronic absorption spectroscopy of porphyrins can be explained by the four orbital model. Electronic transitions, are produced by the absorbance of light and give either B or Q bands. The B band, also known as the Soret band, comes from the allowed transition of the  $\pi$  to  $\pi^*$  state. The Q bands in the visible region

come from configuration interaction of the four orbitals with some vibronic coupling of the Q bands with the Soret band [12]. In Q bands there are transitions of the Q(0,0) referred to as the  $\alpha$  band. The symbolism Q(0,0), used here, represents the electronic transition of the ground state at the lowest vibrational level to the excited state lowest vibrational state. To the blue side of the  $\alpha$  bands are transitions of Q(0,1) known as the  $\beta$  bands. The Q(0,1) symbol would represent the electronic transition of the ground state  $v = 0$  to the excited state  $v = 1$  and so on. In a few highly coupled porphyrins the Q(0,2) transitions are also discernible. In the Soret band the transitions are less obvious owing to the intensity of the B(0,0) band. The B(0,1) is seen as a shoulder on the blue side of the Soret band. The visible bands, on the other hand, are readily resolvable into the various transitions. These transitions, although weakly allowed, have approximately one tenth the intensity of the Soret band. In addition to the visible bands of the porphyrin, metalloporphyrins have charge transfer bands that are, as a rule, not observable. Notable cases of observable charge transfer bands are found in  $\text{Mn}^{3+}$  etioporphyrin I [8a, 8b], high spin  $\text{Fe}^{3+}$  metalloporphyrins [8c] and most importantly in cytochrome c oxidase spectra [9].

Because all of the optical absorption bands fall in the visible light region we can complement optical spectroscopy with the use of Raman spectroscopy. Raman spectroscopy has become particularly useful in elucidating protein structure and functionality[7b, 13]. When Raman spectra are taken so that the excitaiton wavelength is within one of the optical absorption bands, we can obtain Raman spectra that have enhanced vibrational modes related to the specific optical band. In other words, we can isolate chromophoric properties related to specific optical transitions.

### 1.2.3 Raman Theory

An explanation of Raman spectroscopy has its origin in classical theory [13]. If we start with a light wave of frequency  $\nu$  and an associated electric field of strength  $E$  that is dependent on frequency  $\nu$ , then:

$$E = A \cos 2\pi \nu t \quad \text{eq. 4}$$

where  $A$  represents the amplitude and  $t$  represents the time. If we use the light associated with eq. 4 to irradiate a diatomic molecule, we can calculate the induced dipole moment from:

$$P = \alpha E = \alpha A \cos 2\pi \nu t \quad \text{eq. 5}$$

where  $\alpha$  represents the polarizability. A molecule vibrating at frequency  $\nu_1$  has a nuclear displacement  $q$  that can be calculated from:

$$q = q_0 \cos 2\pi \nu_1 t \quad \text{eq. 6}$$

where  $q_0$  represents the vibrational amplitude.

If vibrational amplitudes are small, then  $\alpha$  is a linear function of  $q$ . Thus:

$$\alpha = \alpha_0 + q(\partial\alpha/\partial q)_0 \quad \text{eq. 7}$$

where  $\alpha_0$  represents the polarizability at the equilibrium position and  $(\partial\alpha/\partial q)_0$  is the rate of change in polarizability with respect to the change in vibrational

amplitude, evaluated at the equilibrium position. We can now combine equations 1-3 and obtain the following:

$$\begin{aligned}
 P &= \alpha A_0 \cos 2\pi \nu t \\
 &= \alpha_0 A_0 \cos 2\pi \nu t + (\partial \alpha / \partial q)_0 q_0 A_0 \cos 2\pi \nu t \cos 2\pi \nu_1 t \\
 &= \alpha_0 A_0 \cos 2\pi \nu t \\
 &\quad + 1/2 (\partial \alpha / \partial q)_0 q_0 A_0 \{ \cos [2\pi (\nu + \nu_1) t] + \cos [2\pi (\nu - \nu_1) t] \} \quad \text{eq. 8}
 \end{aligned}$$

From classical theory we can assign the terms of eq. 8 as follows. The first term represents an oscillating dipole that radiates light at frequency  $\nu$ ; this is known as Rayleigh scattering. The second term describes the Raman scattering of light frequencies  $\nu - \nu_1$  and  $\nu + \nu_1$ . These terms are known as Stokes and anti-Stokes scattering, respectively. From eq. 8, we see that if  $(\partial \alpha / \partial q)_0$  goes to zero then the second term goes to zero and there is no Raman scattering. In other words, if the polarizability of a molecule does not change during the vibration, then the molecule is not Raman active. Figure 6 is a diagram representing some of the possible effects of a photon-molecule interaction. The Stokes lines arise when an excitation light source of  $\nu$  is impinged on a molecule in the  $\nu = 0$ , or ground vibrational state. The frequency of the scattered light ( $\nu_s$ ) that is collected by the detector is equal to the frequency of the exciting laser line ( $\nu$ ) minus the frequency ( $\nu_1$ ) corresponding to the molecular transition of the ground vibrational state to first vibrational state of  $\nu = 1$ . The anti-Stokes line is the frequency of the exciting laser line plus the frequency corresponding to the energy difference between the first vibrational state and the ground vibrational state. It is in fact, true that the anti-Stokes lines have the same vibrational information as the Stokes lines, however at a much lower intensity. The lowered intensity of the anti-Stokes lines can be explained by the Maxwell-Boltzman

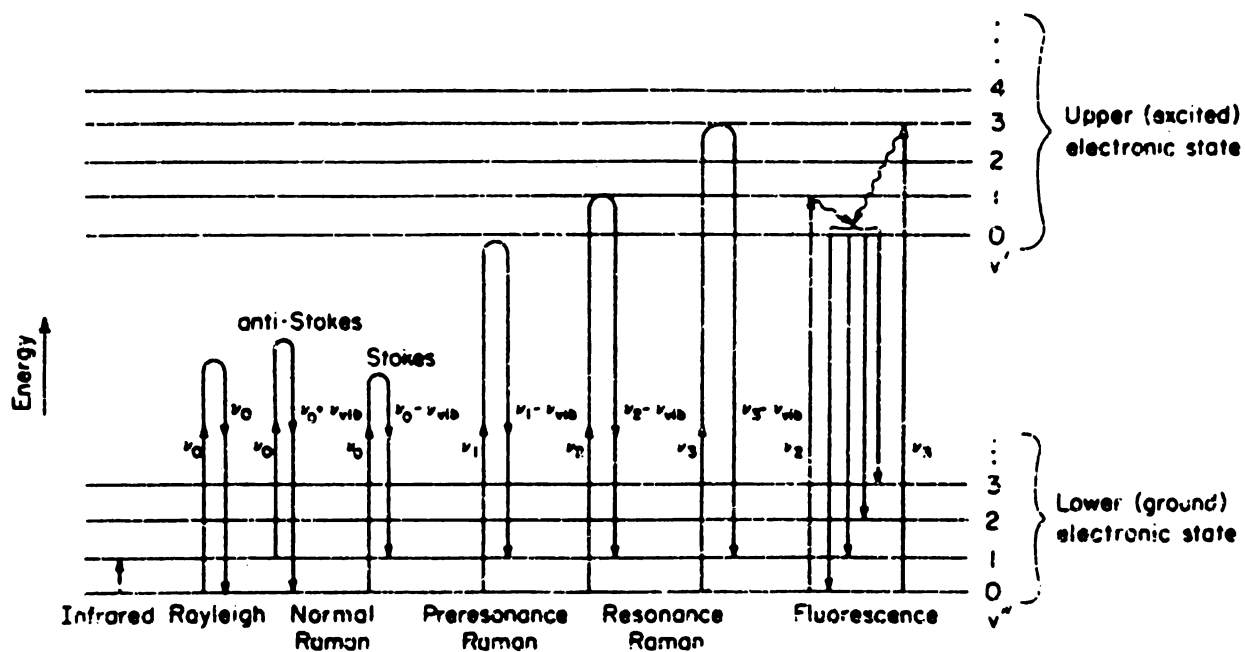


Figure 1-6 Some possible consequences of a photon of light interacting with a molecule. The lengths of the arrows are proportional to the frequency of light that is either incoming (upward), scattered (downward) or emitted (downward). (Reference 7c).

distribution law. That is, the number of molecules in the  $v = 0$  vibrational state by far exceeds the number in the  $v = 1$ , or first vibrational state. Due to this fact all the Raman spectra shown in this thesis are Stokes scattering Raman spectra.

### 1.2.3.1 Resonance Raman

The theory given above for Raman theory also applies to resonance Raman spectroscopy (RR). The major difference between the two types of spectroscopy is that in standard Raman the energy of the excitation line falls below the energy level necessary to excite the molecule into the excited state. However, in RR the frequency of the excitation laser line is of a wavelength that is of sufficient energy to place the molecule into the excited state. Although conceptually this could be mistaken for resonance fluorescence (RF), there are some major experimental differences. One in particular applies to RR of porphyrins and that is that RF lines are all polarized, and in RR spectroscopy some lines are polarized and some lines are depolarized.

The classical theory of Raman spectroscopy is sufficient to explain the energy of the scattered light, however, it does not explain the Raman vibrational band intensity [7c]. To explain the intensity  $I$ , we must incorporate quantum theory. For the Stokes process we will start with the classical expression for the Raman intensity of the scattered light:

$$I = K(\nu_0 - \nu_{\text{vib}})^4 I_0 (d\alpha_{\text{ss}} / dr)^2 \quad \text{eq. 9}$$

where  $K$  is a constant,  $I_0$  is the incident light intensity, and  $r$  is the distance separating nuclei  $m_1$  and  $m_2$ . From eq. 9 we see that the intensity of the Raman light is proportional to the fourth power of the scattered light. It is also apparent from eq. 6 that the intensity is dependent on the change in polarizability of the

molecule. The change in polarizability is the basis of the bond polarizability theory [7d], which tries to explain Raman intensity from the classical approach. However, the theory is concerned only with the properties of the ground electronic state. This theory works well for Raman intensities that are far from resonance, but inappropriate for explaining resonance Raman intensity.

In the quantum mechanical treatment we have the following:

$$I = K(\nu_0 \pm \nu_{\text{vib}})^4 I_0 \sum_{\sigma\rho} |(\alpha_{\sigma\rho})_{mn}|^2 \quad \text{eq. 10}$$

where  $\nu_{mn}$  represents the frequency resulting from a molecular transition from state m to n and  $|(\alpha_{\sigma\rho})_{mn}|$  is the transition polarizability tensor .

$$(\alpha_{\sigma\rho})_{mn} = \frac{1}{h} \sum_r \frac{\langle n|\mu_\rho|r\rangle\langle r|\mu_\sigma|m\rangle}{\nu_{rm} - \nu_0 + i\Gamma_r} + \frac{\langle n|\mu_\sigma|r\rangle\langle r|\mu_\rho|m\rangle}{\nu_{rm} + \nu_0 + i\Gamma_r} \quad \text{eq. 11}$$

In equations 10 and 11 the molecule is considered, initially, to be in the molecular state m. An electromagnetic wave of frequency  $\nu_0$  and intensity  $I_0$  causes the transition into the n state, while scattering light of frequency  $\nu_0 \pm \nu_{mn}$ . The sum over r includes all of the quantum mechanical quantum eigenstates of the molecule, h is Plank's constant and  $\Gamma_r$  is a damping constant which takes into account the finite lifetime of each molecular state. The amplitudes of the electric dipole transition moments is represented by the integrals  $\langle n|\mu_\rho|r\rangle$  , etc.; where  $\mu_\rho$  is the electric dipole moment operator along direction  $\rho$ . In eq. 11 we see that as  $\nu_0$  approaches the energy of an allowed molecular transition  $\nu_{rm}$ ,  $(\nu_{rm} - \nu_0 + i\Gamma_r)$  becomes small; consequently, one term in the sum becomes very large. This is, in fact, the resonance condition. If we consider the Born-Oppenheimer

approximation, we can write the molecular states  $m$  and  $n$  as the product of their electronic and vibrational states. Thus, the total wavefunctions can be written as:

$$|m\rangle = |g\rangle|i\rangle, \quad |n\rangle = |g\rangle|j\rangle, \quad |r\rangle = |e\rangle|v\rangle \quad \text{eq. 12}$$

where,  $g$  is the ground state and  $e$  is the electronic excited state. The  $i$  and  $j$  terms represent vibrational states associated with  $g$  and  $v$  is a vibrational state associated with  $e$ . If we now refer to Fig. 6 we can see a correlation with the levels depicted. The lower electronic state corresponds to  $g$  and the upper electronic state corresponds to  $e$ . The  $i$  and  $j$  terms are  $v''$  levels in  $g$  and  $v$  corresponds to a  $v'$  level in  $e$ . If we use eq. 12 we can write the dipole transition moments as:

$$\langle n|\mu_p|r\rangle = \langle j|M_e|v\rangle \quad \text{and} \quad \langle r|\mu_\sigma|m\rangle = \langle v|M_e|i\rangle \quad \text{eq. 13}$$

where  $M_e$ , which is the pure electronic transition moment from the ground to the electronically excited electronic state.

Now, the expressions on the right hand side of the equal signs in equation 10 involve only vibrational wave functions. The electronic wave functions appear in  $M_e$ . and  $M_e$  changes as the nuclear coordinates vary. We can account for these changes by expanding the electronic transition dipole moment in a Taylor series about the equilibrium geometry as a function of the normal coordinate  $Q$ . Hence, we have:

$$M_e = M_e + (\partial M_e / \partial Q)Q + \dots \quad \text{eq. 14}$$

There are equivalent expressions for each of the  $3N-6$  possible normal coordinates. If we now substitute eq. 14 into eq. 13 and subsequently substitute eq. 13 into eq. 11, we get:

$$(\alpha_{op})_{mn} = A + B \quad \text{eq. 15}$$

where

$$A = \frac{M_e^p M_e^q}{h} \sum_v \frac{\langle j|v\rangle \langle v|i\rangle}{\nu_{vi} - \nu_0 + i\Gamma_v} \quad \text{eq. 16}$$

and

$$B = \frac{M_e^p (\delta M_e^q / \delta Q)^o}{h} \sum_v \frac{\langle j|v\rangle \langle v|Q|i\rangle}{\nu_{vi} - \nu_0 + i\Gamma_v} \quad \text{eq. 17}$$

The term  $\nu_{vi}$  represents the energy gap between the  $i$ th vibrational level in the ground state and  $v$ th vibrational level in the excited resonant electronic state. In the right hand side of eq. 16 we have ignored the nonresonant term and the term for which  $p$  and  $q$  are reversed has been omitted.

The dominant contributor to the resonance Raman intensity is the A term. This is the case since, for allowed transitions  $M_e$ , the electronic transition moment, is larger than the change in the dipole moment with respect to the normal coordinate  $Q$  ( $\partial M_e / \partial Q$ ). The vibrational overlap integrals,  $\langle j|v\rangle$  and  $\langle v|i\rangle$  (also known as the Franck-Condon factors) are equal to zero for non-totally-symmetric modes, therefore, only the totally symmetric modes give rise to resonance enhancement.

The A term involves a single electronic state; however, the B term arises from the vibronic mixing of two excited states. The B term active vibration may have any symmetry that is contained in the direct product of the group-theoretical representations of the two electronic states. The vibronic mixing is an

important feature of the B term, however, the major importance of the B term mechanism is the intensity it allows to scattering by non-totally-symmetric modes. What this means is that normally weak vibrations can be observed because they are able to borrow intensity from nearby intense transitions.

We can now make some generalizations about the use of Raman spectroscopy. Equation 9 defines the classical theory of scattered light intensity. We can see from eq. 9 that Raman intensity, far from resonance, is mostly dependent on polarizability of the molecule. That is, the Raman intensity depends on the degree of change of the polarizability caused by a change in the normal coordinate. In resonance Raman there are two terms that add intensity to the Raman scattering. The A term mechanism involves a single excited electronic state, whereas the B term mechanism involves two excited electronic states. The combined results of these terms is that resonance Raman intensity may be enhanced as much as  $10^4$  over the normal Raman intensity. The large intensity enhancements are expected if, for both terms, the excitation frequency is close to the electronic transition, and the absorption intensity of the electronic transition is large. Both terms also experience enhancement if the geometric changes experienced during a particular normal mode are similar to those changes occurring when going from the ground to the excited electronic states. For the A term only some of the products of the Franck-Condon factors  $\langle j|v \rangle$  and  $\langle v|i \rangle$  are large and for the B term, only, the vibration is effective in mixing the two excited electronic states.

The intensity gained by resonance Raman spectroscopy over normal Raman spectroscopy, makes it an ideally suited spectroscopic technique to study porphyrins in both model and biological systems [7b, 13c]. The principle of resonance Raman gives us the opportunity to enhance vibrational properties relevant to a specific electronic absorption band. For example, ligands may be

vibronically coupled to the porphyrin  $\pi$  system. So, excitation into the Soret band allows detectability of the ligand by its vibrational frequency and corresponding isotope shift. If, however, the ligand is not vibrationally coupled to the porphyrin  $\pi$  system, then excitation into the Soret band would not enhance the ligand vibrations. However, excitation into one of the Q bands or a charge transfer band could well enhance vibrations of the ligand. This technique allows us to probe a mixture of compounds and isolate vibrational modes belonging to one specific compound; or in the case of a protein to isolate the active site that contains the porphyrin structure.

### 1.2.3.2 Established Porphyrin Vibrations

Figure 2 shows the label designations for the carbons of the porphyrins. The carbons directly bonded to the nitrogens are known as the alpha carbons ( $C_\alpha$ ). The backbone carbons of the pyrrole rings are designated the beta carbons ( $C_\beta$ ) and the bridging carbons are referred to as the meso carbons ( $C_m$ ). The carbon-nitrogen skeleton that makes up the basic porphyrin has been extensively studied. The various vibrational modes are well known and their sensitivities, although not fully understood, are well characterized. The RR bands in the 1000  $\text{cm}^{-1}$  to 1700  $\text{cm}^{-1}$  region correspond to the in-plane stretching of C-C and C-N bonds. The bands above 1000  $\text{cm}^{-1}$  are not only very sensitive to the peripheral substituents but also indicative of a number of effects on the central metal or macrocycle moiety.

Normal coordinate analyses of nickel [14a], copper [14b], and iron [14c] porphyrins have been used to establish both the RR and IR active vibrational modes of a number of porphyrins. The calculated frequencies, combined with specific isotopic substitution, has allowed for frequency and symmetry assignments of these porphyrins. The normal mode calculations and RR work of

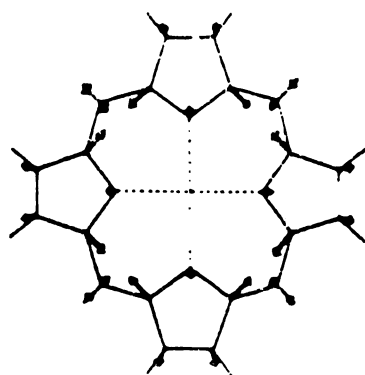
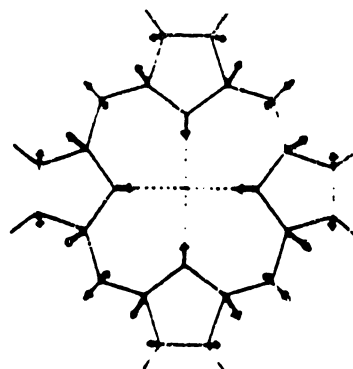
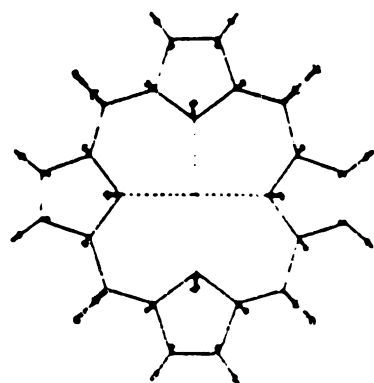
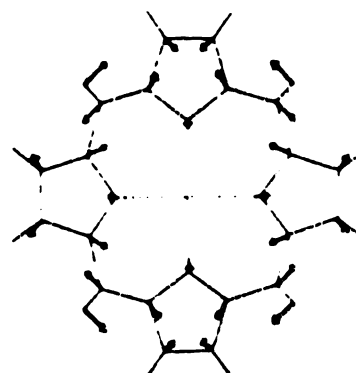
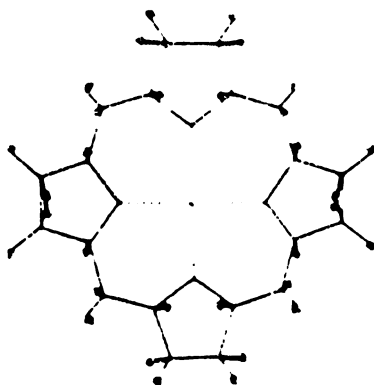
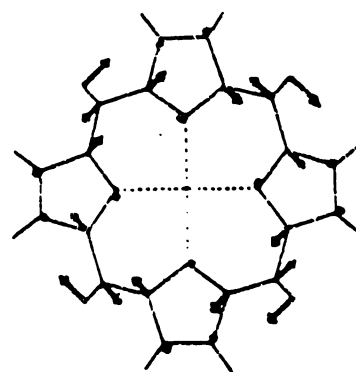
Abe et al.[14a] established the frequency labels that are used in this thesis. The other important information from the work of Abe et al. is that the C $\beta$ -ethyl vibrations only contribute to the porphyrin modes. In other words the internal vibrations of the ethyl groups do not affect the porphyrin vibrations. From an experimental standing this means that substitution of the ethyl groups with other alkyl groups has little or no effect on the porphyrin vibrations.

Typical porphyrin vibrations are generally a mixture of vibrational motions. This is best seen in Figure 7, which shows the basic vibrational motions of the individual atoms for a given frequency assignment. With the mixing of vibrational modes we typically get several vibrational bands that are each sensitive to metalloporphyrin properties. These coupled vibrational bands follow certain systematic trends that give us an opportunity to characterize a variety of metalloporphyrin traits.

Some of the more informative characterizations that we can get from RR spectra are the distinction between five and six coordinated porphyrin complexes, the oxidation and spin states of the central metal and many environmental factors that affect the coordinated ligands and/or the metal or the porphyrin itself.

Specific Raman active vibrations of interest are the vibrational modes known as  $\nu_2$ ,  $\nu_3$ ,  $\nu_4$ ,  $\nu_{10}$ ,  $\nu_{11}$  and  $\nu_{19}$ . The designated vibrational modes come from the assignments of Abe et alii. These modes are known as the oxidation state marker ( $\nu_4$ ), core size markers ( $\nu_3$ ,  $\nu_{10}$  and  $\nu_{19}$ ) and spin state markers ( $\nu_2$  and  $\nu_{11}$ ). The major contributing factors associated with these vibrations are  $\nu(\text{C}\alpha\text{N})$ ,  $\nu(\text{C}\alpha\text{C}_m)$  and  $\nu(\text{C}\beta\text{C}\beta)$ , respectively.

**Figure 1-7** Porphyrin vibrational modes that are sensitive to the oxidation or spin state of the central metal or the core size of the the porphyrin itself. vibrational values given are for NiOEP in methylene chloride. (Reference 13).


 $\nu_3 (A_{1g}) \quad 1519$ 

 $\nu_4 (A_{1g}) \quad 1383$ 

 $\nu_7 (A_{1g}) \quad 674^*$ 

 $\nu_{10} (B_{1g}) \quad 1655$ 

 $\nu_{11} (B_{1g}) \quad 1576$ 

 $\nu_{19} (A_{2g}) \quad 1603$

The oxidation state marker band  $\nu_4$  is the most intense porphyrin vibration observed when the porphyrin is excited near or in the Soret band. It is named, accordingly, due to its sensitivity to the oxidation state of the central metal. The  $\nu_4$  vibration is particularly sensitive to the oxidation state of iron porphyrins. In ferric heme proteins  $\nu_4$  is detected at approximately  $1375\text{ cm}^{-1}$ , while in ferrous heme proteins  $\nu_4$  is located at approximately  $1355\text{ cm}^{-1}$ . All the vibrational modes above  $1450\text{ cm}^{-1}$  have an inverse linear relationship with core size. The modes that are particularly sensitive to the core size are the ones that have their major potential energy distribution in the  $C_{\alpha}$ - $C_m$  vibrations.

The core size markers and particularly  $\nu_{10}$  are good indicator bands for distinguishing between five- or six-coordinated metalloporphyrins. This is, in effect, due to the out-of-plane nature of the five coordinate complexes. In five coordinated complexes the ligand pulls the metal out of the porphyrin skeletal plane. The metal nitrogen bonds are subsequently drawn toward the metal, which causes the pyrrole ring to tilt. This does, in one sense, increase the core size of the porphyrin which does of course affect the core size marker bands. However, tilting of the pyrrole rings also causes a torsional strain on the meso carbon and  $\alpha$  carbon bonds that is detectable in the vibrational modes that have their major potential energy distribution contributed by these bonds.

### 1.3 Core Metals and Oxidation States

As mentioned earlier, the functionality of iron ranges from  $O_2$  transportation in hemoglobin and  $O_2$  storage in myoglobin to electron transportation in the oxidase cycle of cytochrome c oxidase (CcO). During the reduction of  $O_2$  to  $H_2O$  in CcO heme  $a_3$ , coupled in proximity with  $Cu_B$ , receives an electron from cyt. c, through heme a and  $Cu_A$  to become an  $Fe^{II}$  (Figure 8).

**Figure 1-8** Simplified mechanism for the reduction of O<sub>2</sub> and proton translocation in cytochrome oxidase. The binuclear center is represented as [a<sup>3</sup> CuB]. The reaction is initiated by O<sub>2</sub> binding to the reduced form of this center, to produce oxy, and then peroxy intermediates. Reduction and protonation of the peroxy species is coupled to the translocation of two protons, which is indicated by the heavy, shaded arrow. Oxygen-oxygen bond cleavage is also driven, in this step, to produce the ferryl intermediate. Reduction and protonation of this species is also coupled to the translocation of two protons, which is indicated by the second heavy, shaded arrow. The hydroxy product of this reaction is subsequently reduced by two electrons, to complete the cycle.(Figure courtesy of G. T. Babcock).

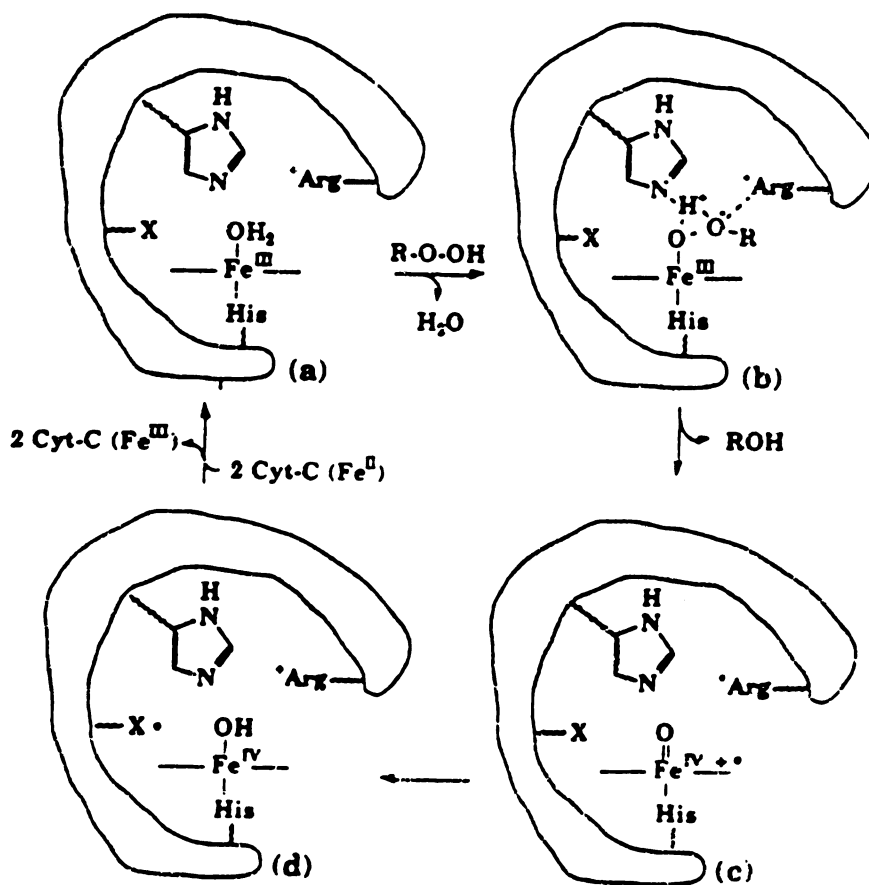


**Figure 1-9** Proposed mechanism for the formation of compound I of Cytochrom c peroxidase. a) Representation of the native enzyme. b) The activated complex with the distal histidine acting as an acid-base catalyst and the active site arginine stabilizing a partial negative charge forming on  $\text{RO-OFe}$ . c) The oxoferryl  $\pi$ -cation radical intermediate. d) Compound I after the intramolecular electron transfer to to produce the oxoferryl and free radical X.(Reference 19).

Subsequent steps of electron and proton transfer take heme a<sub>3</sub> to an O=Fe<sup>IV</sup> complex [18]. Peroxidase binds peroxide (H<sub>2</sub>O<sub>2</sub>) in the ferric form. Subsequent oxidation produces an oxoferryl cation radical that is the active oxidizing form of the enzyme that carries out nonspecific oxidation of a number of substrates (Figure 9)[19]. Catalases react the same as peroxidases in their initial steps. They are never found in the ferrous state naturally and virtually impossible to reduce to the ferrous form. The major difference between the catalases and peroxidases is that the catalases are very substrate specific. Cytochrome P-450 is a drug metabolizing defense mechanism in animal life. Although not all of the intermediates are fully characterized it is reasonably accepted that the highly oxidizing intermediate is also an O=Fe<sup>IV</sup>P<sup>+</sup> complex [19].

Virtually every metal has, at some time, been inserted into synthetic porphyrins. The usefulness of metalloporphyrins not naturally found in biology are many fold. For example, oxoferryl model compounds are unstable above -30°C, [45] so oxovanadyl porphyrins have been used to study environmental effects on the oxo ligand [46]. Zinc and magnesium octaethyl and tetraphenyl porphyrins, for example, were instrumental in setting the ground work in the study of  $\pi$ -cation radicals.

### 1.3.1 $\pi$ -Cation Radicals

One electron oxidation of metalloporphyrins may take place at either the core metal or the  $\pi$ -system of the macrocycle. The major factors that influence the site from which the electron is removed are the substitution pattern on the macrocycle skeleton, the central metal, and environmental conditions. Much attention has been given to the understanding, spectroscopic characterization, and predictability of which orbital the electron is removed from when a  $\pi$ -cation radical is formed. In the formation of a  $\pi$ -cation radical, it is possible to remove an

electron from either one of the HOMO's ( $a_{1u}$  and  $a_{2u}$ ), depending on which is lower in energy for a given MP. Examples of  $\pi$ -cation radicals of the  $^2A_{1u}$  and  $^2A_{2u}$  forms are both known from the work of Dolphin and coworkers [15a]. From ESR studies it was possible, to first, establish the oxidized products of zinc and magnesium octaethyl and tetraphenyl porphyrins as  $\pi$ -cation radicals. From the electron density distribution of the ESR work it was also possible to determine which of the  $\pi$ -cation radical types were formed. It was established that both ZnOEP and MgOEP had  $^2A_{1u}$  ground electron states, while ZnTPP and MgTPP both had  $^2A_{2u}$  ground electron states. The established ground electron states have unique optical spectroscopic properties. The optical properties and subsequent optical spectra are referred to as  $A_{1u}$  for the  $^2A_{1u}$  ground electron state and  $A_{2u}$  for the  $^2A_{2u}$  ground electron state. The work of Dolphin and coworkers was instrumental in establishing the formation of  $\pi$ -cation radicals in model compounds and then relating the model compounds to optical spectroscopic patterns in biological intermediates [15b].

Many types of spectroscopic techniques that have been used to characterize  $\pi$ -cation radicals. In addition to the optical and ESR techniques mentioned above, there are MCD [29], NMR [30], IR [31], X-ray crystallography [32] and RR, which will be focused on here. Detailed RR studies of  $\pi$ -cation radicals have identified the structurally sensitive vibrational modes [16, 11a]. The vibrational modes sensitive to oxidation of the macrocycle, as one might expect, are the same modes that are structurally informative in the parent porphyrin. These modes are  $\nu_2$ ,  $\nu_3$ ,  $\nu_4$ ,  $\nu_{10}$ ,  $\nu_{11}$ , and  $\nu_{19}$ ; their vibrational character was described earlier.

The work of Oertling et al. [11a] on  $MOEP^{+\cdot}$  ( $M = Cu, Zn, Co$ ) [11] and the work of Czernuszewicz et. al. on  $MTPP^{+\cdot}$  [16b] and  $MOEP^{+\cdot}$  ( $M = Cu, Ni$  and  $Fe$ ) has shown that the the structurally sensitive Raman bands of these porphyrin

cation radicals have systematic trends. For the octaethyporphyrins the modes involving primarily  $C_{\alpha}C_m$  stretching character ( $\nu_3$  and  $\nu_{10}$ ) decreased in frequency relative to the parent compound. Those bands whose primary stretching character was in the  $C_{\beta}C_{\beta}$  portion of the ring ( $\nu_{11}$  and  $\nu_2$ ) increased in frequency relative to the parent compound. The frequency of  $\nu_4$ , which is primarily a  $C_{\alpha}N$  stretch, decreased relative to the parent.

The vibrational modes for the cation radicals of MTPP shift somewhat differently than the corresponding modes of the cation radicals of MOEP. Particularly, the mode  $\nu_2$ , that increased in the  $MOEP^{+\cdot}$ , decreased in the  $MTPP^{+\cdot}$  case. The down shift of  $\nu_4$  is much less in the  $MTPP^{+\cdot}$  compared to the down shift of the  $MOEP^{+\cdot}$ . These differences in mode shifts has been explained in terms of the  $a_{1u}$  and  $a_{2u}$  orbitals being antibonding and bonding, respectively, with respect to the  $C_{\beta}C_{\beta}$  bonds.

## 1.4 Environmental factors

A number of factors influence the binding properties a metalloporphyrins in model studies. The effects on the model compounds can and often do give invaluable insights into the protein's effect on the macrocycle active site. Among some of the factors that effect model compound bindings are temperature, solvent properties and atmosphere.

### 1.4.1 Solvent

When metalloporphyrins are oxidized, solvent effects are a key consideration of where the oxidation takes place [22]. For example, oxidation of metalloporphyrins in coordinating solvents causes oxidation to occur at the metal center. The solvent often becomes either a mono or in most cases, a bis coordinated metalloporphyrin  $(L_nM^{III}P)(n = 1 \text{ or } 2)$  complex. Oxidation of

metalloporphyrins in noncoordinating solvents can, and often does produce metalloporphyrin  $\pi$ -cation radicals ( $MP^{+\cdot}$ ). When metalloporphyrin  $\pi$ -cation radicals are subsequently exposed to coordinating solvents, or other potentially coordinating media, they can undergo an intramolecular electron transfer to give an  $(L_nM^{III}P)(n = 1 \text{ or } 2)$  complex.

Solvent binding to metalloporphyrins can give an understanding of the competitive and hindering effects of water soluble ligands that may be exposed to the active site of a protein. For the most part, aqueous ligands are anions and typically inhibitors of CcO. One of the most commonly studied and best known of these aqueous ions is cyanide. Cyanide ( $CN^-$ ) binds to the  $Fe^{III}$  state much more rapidly and stronger than to the  $Fe^{II}$  state of hemoproteins. This is easily understood due to the fact that a ferric iron state in a porphyrin must be in close proximity, if not actually bound, to an anion. The cyanide anion is a relatively strong anion in terms of nucleophilicity. It, subsequently, is tightly bound to a ferric state iron porphyrin and only weakly attracted and bound to a ferrous iron porphyrin. Once bound to the ferric state of an oxidase protein removal is virtually impossible since the ferrous state of a hemoglobin is the only exchange protein available to oxidase [4]. This results in cyanide being highly toxic to any form of animal life.

### 1.4.2 Atmosphere

A number of metalloporphyrins, when oxidized under an inert atmosphere such as argon or nitrogen, produce a metalloporphyrin  $\pi$ -cation radical ( $MP^{+\cdot}$ ). If, however, they are oxidized under an atmosphere that has coordinating capabilities such as carbon monoxide (CO), nitrous oxide (NO), oxygen ( $O_2$ ), etc., then ligated metal oxidized MP's are formed[23]. Understanding the binding property of gaseous ligands is essential since biological proteins are subjected to

these ligands. Gaseous ligands are in constant competition with O<sub>2</sub> for binding to the metal core of active site hemoproteins. In hemoglobin, for example, carbon monoxide is known to have a much stronger bonding affinity than oxygen and yet the protein moiety functions to discriminate for O<sub>2</sub> binding over CO binding [4, 5]. Debate over the protein's ability to bring about this discrimination has given rise to a variety of model compounds. These models can affect the binding site by either a strap [24], a cap [25], a picket fence [26], even cofacial or face to face diporphyrins [27]. Therefore, the search for a "true" model system and definitive experiment are ever important.

### 1.4.3 Temperature

It might, at first thought, seem that temperature effects on the binding properties of metalloporphyrins has little relationship to biology. For the most part biological systems carry out chemical processes at a controlled and constant temperature. However, since it is virtually impossible to perform isolated ligand binding and spectroscopic studies in vivo the effects of temperature on metalloporphyrin binding rates and strengths can produce invaluable results in understanding the role of the protein that surrounds the active site macrocycle. Temperature is a major factor in the ligating properties of metalloporphyrin model compounds. Exposure of reduced metalloporphyrins to oxygen at high temperatures (typically above 0°C) results in oxidation of the metal. If, however, reduced metalloporphyrins are exposed to oxygen at low temperatures they can form a semi-stable O<sub>2</sub> bound metalloporphyrin complex. The binding abilities of oxidized MP's are sometimes temperature dependent. For example, H<sub>2</sub>O binds reversibly to Co<sup>II</sup>OEP<sup>+</sup>·(ClO<sub>4</sub><sup>-</sup>) only at low temperatures. Methanol, however, readily binds to the Co<sup>II</sup>OEP<sup>+</sup>·(ClO<sub>4</sub>)<sup>-</sup> at room temperature to give a[(MeOH)<sub>2</sub>Co<sup>III</sup>OEP]<sup>+</sup>(ClO<sub>4</sub>)<sup>-</sup> complex[21].

#### 1.4.4 Hydrogen bonding

One of the most important intermolecular forces in chemistry and biology is hydrogen bonding [33]. It is well known that hydrogen bonding is one of the major influences on protein folding [34]. The influence of hydrogen bonding at the active sites of hemoproteins is, however, an issue of much debate [35]. Hemoglobin and myoglobin are subject to binding by ligands that they are in constant contact with. The question that has yet to be answered is what mechanism the protein uses to actively discriminate between oxygen and other available ligands that are better at liganding the bare heme [36]. In cytochrome c oxidase the possibility of a hydrogen bonded oxoferryl intermediate has sparked controversy and is at this time an unresolved issue [37-38].

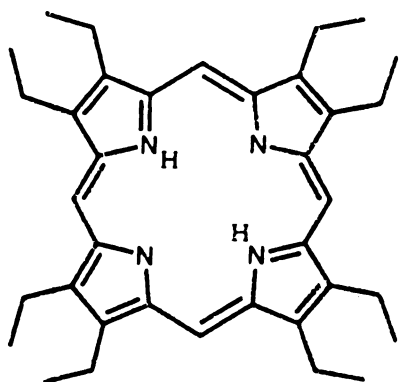
The true nature of the hydrogen bond is in itself an unresolved issue. The classical definition of the hydrogen bond, given by Pauling described it as ionic/electrostatic in nature [33]. At one time it was believed that only complexes consisting of the most electronegative elements nitrogen, oxygen or fluorine could be involved in hydrogen bonding. The ongoing work of Green et al. [45] and Zwier et al. [39] has shown that not only strong electronegative atoms could be involved in hydrogen bonding, but also that  $\pi$ -electron clouds of cyclic polyenes could be hydrogen bond acceptors. These workers not only shed new light into the nature of the hydrogen bond but often relate their findings to biological systems with convincing results [40]. The work of Zwier has shown that chlorohydrocarbons could even be hydrogen bond donors [39a]. With such an active interest in hydrogen bonding in protein structure control and the previously reported cases of potential hydrogen bonding at active site ligation it is only conceivable that this work be carried into the field of biological model compounds.

Intermolecular hydrogen bonding studies have been done for a number of compounds under a variety of conditions. Cobalt substituted myoglobin or hemoglobin bound with oxygen shows a deuterium isotope effect when H<sub>2</sub>O is substituted with D<sub>2</sub>O [41]. Carbon monoxide bound to ferrous cytochrome c is also known to exhibit a deuterium isotope effect on  $\nu(\text{CO})$  when D<sub>2</sub>O is used relative to H<sub>2</sub>O [42-43]. The studies mentioned above were all done with either hemoglobin or myoglobin. However, the possibility and possible role of hydrogen bonding being an active participant in reaction intermediates of oxidases has yet to be answered.

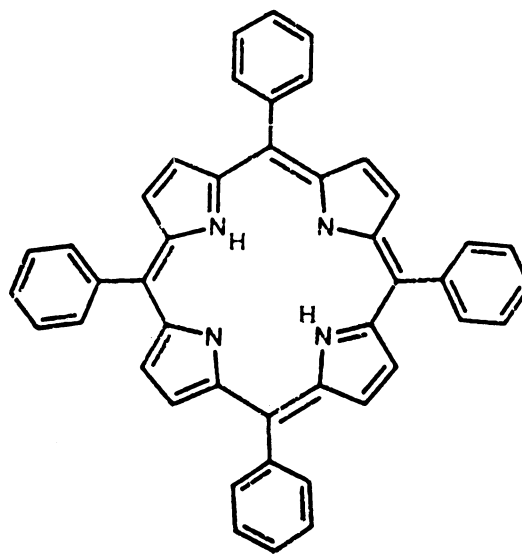
Chang and co-workers have presented a series of compounds where one of the meso carbons is substituted with either a naphthyl or anthryl unit that may contains a functional group capable of effecting intramolecular hydrogen bonding with ligands coordinated to the core metal. Alterations of the functional group from acid to amide to alcohol to ester have given orders of magnitude decreases in O<sub>2</sub> binding ability as measured by titrative methods. This model, however, has a free rotation bond that does not allow for consistent hydrogen bonding effects or lack thereof. To lock the functional group into a position that is consistently in the vicinity of a ligand binding to the metalloporphyrin pocket site they have created the Kemp's acid structure (Figure 10c).

This system, although, not absolutely rigid does allow for only minimal displacement of the acid, amide, alcohol or ester group. The titration results, again show orders of magnitude increases in O<sub>2</sub> binding over any previous O<sub>2</sub> binding models.

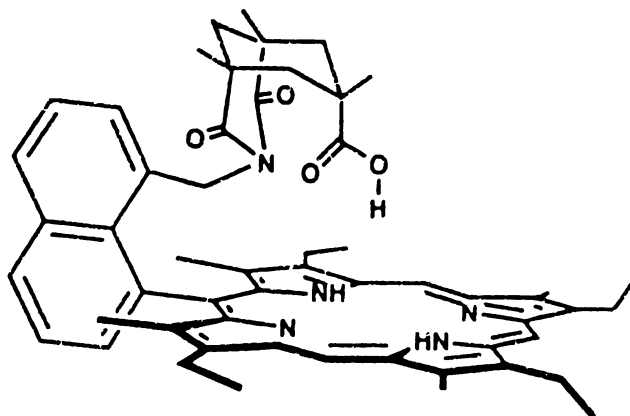
**Figure 1-10** (a) Structures of OEP and TPP, synthetic porphyrins that have been well established as models for a variety of biologically related structures. (b) The structure of the recently synthesized naphthyl Kemp's acid etio type porphyrin (NKAP) model compound that is capable of intramolecular hydrogen bonding.



a)



b)



c)

## 1.5 Aims Of This Research

My research has been oriented toward the use of model compounds to gain an understanding of the role of porphyrin compounds in biological systems. Although some projects used chlorins [47], biological samples [49], or involved the synthesis of non-porphyrin compounds. The theme of this dissertation will focus on the porphyrin chemistry upon which I concentrated. The parent [11a] structures that are the focus of the majority of the work described in this thesis are octaethylporphyrin (OEP), tetraphenylporphyrin (TPP) and naphthyl Kemp's acid porphyrin (NKAP) (Figure 10). Synthesis of NKAP and its derivatives was done by Ying Liang and details of the process will be described in her dissertation and/or corresponding publications. The core metals included cobalt, iron, vanadium, ruthenium and aluminum. The binding ligands were the following: carbon monoxide(CO), oxygen (O<sub>2</sub>), oxo(O=) and cyanide(-CN).

Specific compounds used in my studies are given detailed explanations within the following chapters of this dissertation. Specifically, Chapter 2 will concentrate on  $\pi$ -cation radicals. Chapter 3 will be dedicated to hydrogen bonding. Chapter 4 will be a study in cyanide binding to fluoro-substituted phenyls of tetraphenyl iron porphyrins and Chapter 5 will be a summary of additional projects.

Projects that will not be discussed in this dissertation, although published or submitted, included chlorins,[47] biological samples,[49] and transient lifetimes of manganese OEP cation radical[48].

## REFERENCES

- [1] (a) Dolphin, D. (Ed.); *The Porphyrins*. Academic: New York Vols. VI and VII
- [2] (a) Gouterman, M. *J. Chem. Phys.* 1959, 30, 1139-1161 (b) Simpson, W.T. *J. Chem. Phys.* 1949, 17, 1218-1221 (c) Moffitt, W. *J. Chem. Phys.* 1954, 22, 1820-1829 (d) Longuet-Higgins, Rector, and Platt *J. Chem. Phys.* 1950, 18, 1174-1181 (e) Platt, J.R. *J. Chem. Phys.*, 1954, 22, 1448-1455
- [3] *Metal ions in Biological Systems; Studies of some Biochemical and Environmental Problems*, Plenum Press, New York 1973
- [4] Stryer, L. *Biochemistry*, 3rd Ed., W. H. Freeman and Company, New York 1988
- [5] Springer, B.A., Sligar, S.G., Olson, J.S. and Phillips, G.N.Jr. *Chem. Rev.*, 1994, 94, 699-714
- [6] (a) Pratt, J.M. *Inorganic Chemistry of Vitamin B12*, Academic Press, London, 1972 (b) Herlinger, A.W. and Brown, T.L. *J. Am. Chem. Soc.*, 1971, 93, 1790-1791 (c) Falk, J.E. *Porphyrins and Metalloporphyrins*, Elsevier, Amsterdam, The Netherlands, 1964 (d) Lemberg, R. and Legge, J.W. *Hematin compounds and Bile pigments.*, Interscience, New York, NY, 1949
- [7] (a) Dolphin, D. (Ed.); *The Porphyrins*, Academic: New York Vol. III-V (b) Spiro, T.G. (Ed.); *Biological Applications of Raman spectroscopy*, Vol. 3, 1988 (c) Carey, P.R. *Biochemical Applications of Raman and Resonance Raman Spectroscopies*, Academic: New York, 1982 (d) Hester, R.E. Chapter 4 in *Raman spectroscopy*, Szymanski, H.A. (Ed.), Plenum, New York, NY, 1967
- [8] (a) Asher, S. and Sauer, K. *J. Chem. Phys.*, 1976, 64, 4115-4125 (b) Shelnutt, J.A.; O'Shea, D.C.; Yu, N.-T.; Cheung, L.D. and Felton, R. *J. Chem. Phys.*, 1976, 64, 1156-1165 (c) Smith, D.W. and Williams, R.J.P. *Structure and Bonding*, Springer-Verlag, Berlin, Vol. 7, 1970, 1-45

- [9] (a) Williams, R.J.P. *J. Theoret. Biol.*, 1961, 1, 4 (b) Williams, R.J.P., in *Hemes and Hemoproteins*, eds. Chance, B., Estabrook, R.W. and Yonetani, T., Academic Press, New York, 1966
- [10] (a) Gouterman, M. *J. Mol. Spec.* 1961, 6, 138-163 (b) Gouterman, M.; Wagniere, G.H. and Snyder, L.C. *J. Mol. Spec.* 1963, 11, 108-127 (c) Spellane, P.J.; Gouterman, M.; antipas, A.; Kim, S. and Liu, Y.C. *Inorg. Chem.*, 1980, 19, 386-391
- [11] (a) Oertling, W.A.; Salehi, A.; Chung, Y.C.; Leroi, G.E. Babcock, G.T. and Chang, C.K. *J. Chem. Phys.* 1987, 91, 5887-5898 (b) Sandusky, P.O., Oertling, W.A., Chang, C.K. and Babcock, G.T. *J. Phys. Chem.*, 1991, 95, 4300-4307
- [12] Wang, M.-Y.R. and Hoffman, B.M. *J. Am. Chem. Soc.*, 1984, 106, 4235-4240
- [13] Nakamoto, K. *Infrared and Raman Spectra of Inorganic and Coordination Compounds* 4th Ed., Wiley-Interscience Publication, 1985
- [14] (a) Abe, M.; Kitagawa, T. and Kyogoku, Y. *J. Chem. Phys.* 1979, 69, 4526-4534 (b) Gladkov, L.L. and Solovyov, K.N. *Spectrochimica Acta*. 1986, 42A, 1-10
- [15] Dolphin, D., Muljiani, Z., Rousseau, K., Borg, D.C., Fajer, J. and Felton, R.H. *Annals New York Academy of Sciences*, 1973, 177-209
- [16] (a) Boldt, N.J.; Donohoe, R.J.; Birge, R.R. and Bocian, D.F. *J. Am. Chem. Soc.* 1987, 109, 2284-2298 (b) Czernuszewicz, R.S.; Macor, K.A.; Li, X.-Y.; Kincaid, J.R. and Spiro, T.G. *J. Am. Chem. Soc.*, 1989, 111, 3860-3869
- [17] Lever, A.B.P. and Gray,, H.B., Eds., *Iron Porphyrins*, Parts I-III ,Addison Wesley Reading, Mass. 1983
- [18] (a) Babcock, G.T. and Wikström, M. *Nature*, 1992, 356, 301-309 (b) Wikström, M. and Morgan, J.E. *J. Biol. Chem.*, 1992, 267, 10266-10273
- [19] Watanabe, Y. and Groves, J.T. in *The Enzymes*, Chap. 9, Academic Press, Inc., New York, 1992
- [20] (a) Balch, A.L; Chan, Y.-W. and Olmstead, M.M. *J. Am. Chem. Soc.* 1985, 107, 6510-6514 (b) Balch, A.L; Chan, Y.-W.; Olmstead, M.M. and Renner, M.W. *J. Am. Chem. Soc.* 1985, 107, 2393-2398 (c) Mizutani, Y., Watanabe, Y. and Kitagawa, T. *J. Am. Chem. Soc.* 1994, 16, 3439-3441
- [21] Salehi, A; Oertling, W.A.; Babcock, G.T. and Chang, C.K. *J. Am. Chem. Soc.* 1986, 108, 5630-5631
- [22] (a) Kadish, K.M., Lin, X.Q. and Han, B.C. *Inorg. Chem.*, 1987, 26, 4161-4167 (b) Bottomley, L.A. and Kadish, K.M. *Inorg. Chem.*, 1981, 20, 1348-1357

- [23] (a) Mu, X.H. and Kadish, K.M. *Inorg. Chem.*, 1989, 28, 3743-3747 (b) Kadish, K.M. *Prog. Inorg. Chem.* 1986, 34, 435-605 (c) Chan, R.J.H., Su, Y.O. and Kuwana, T. *Inorg. Chem.*, 1985, 24, 3777-3784
- [24] (a) Yu, N.-T.; Kerr, E.A.; Ward, B and Chang, C.K. *Biochemistry*, 193, 22, 4534-4540 (b) Momenteau, M.; Mispelter, J.; Loock, B. and Lhoste, J.-M. *J. Chem. Soc., Perkin Trans.*, 1985, 221-231 (c) Wijesekera, T.P.; Paine, J.B.III, and Dolphin, D. *J. Org. Chem.*, 1988, 53, 1345-1352
- [25] (a) Hashimoto, T. and Basolo, F. *Comments Inorg. Chem.*, 1981, 1, 199- 206 (b) Hashimoto, T.; Dyer, R.L.; Crossley, J.E.; Baldwin, J.E. and Basolo, F. *J. Am. Chem. Soc.*, 1982, 104, 2101-2109
- [26] Colman, J.P.; Gagne, R.R.; Reed, C.A.; Robinson, W.T. and Rodley, C.A. *Proc. Natl. Acad. Sci.*, 1974, 71, 1326-1329
- [27] (a) Collman, J.P.; Elliot, C.M.; Halbert, T.R. and Tovrog, B.S. *Proc. Natl. Acad. Sci., U.S.A.*, 1977, 74, 18-22 (b) Ward, B.; Wang, C. and Chang, C.K. *J. Am. Chem. Soc.*, 1981, 103, 5236-5238
- [28] Antonini, E. and Brunori, M. *Hemoglobin and Myoglobin in Their Reactions With Ligands*, Elsevier, New York, 1971
- [29] (a) Browett, W.R. and Stillman, M.J. *Inorg. Chim. Acta.*, 1981, 49, 69-77 (b) Browett, W.R. and Stillman, M.J. *J. BioChim. Biophys. Acta.*, 1981, 660, 1-7
- [30] (a) Goff, H.M. and Phillippi, M.A. *J. Am. Chem. Soc.*, 1983, 105, 7567-7571 (b) Godziela, G.M. and Goff, H.M. *J. Am. Chem. Soc.*, 1986, 108, 2237-2243 (c) Morishima, I.; Takamuki, Y. and Shiro, Y. *J. Am. Chem. Soc.*, 1984, 106, 7666-7672
- [31] Shimomura, E.T.; Phillippi, M.A.; Goff, H.M. Scholz, W.F. and Reed, C.A. *J. Am. Chem. Soc.*, 1981, 103, 6778-6780
- [32] (a) Barkigia, K.M.; Spaulding, L.D. and Fajer, J. *Inorg. chem.*, 1983, 22, 349-351 (b) spaulding, L.D.; Eller, P.G.; Bertrand, J.A. and Felton, R.H. *J. Am. Chem. Soc.*, 1974, 96, 982-987
- [33] (a) Pauling, L. *The Nature of the Chemical Bond*, Cornel University Press, Ithaca, 1960 (b) Pimentel, G.C. and McClellen, A.L. *The Hydrogen Bond*, W.H. Freeman and Co., New York, 1960
- [34] (a) Branden, C. and Tooze, J. *Introduction to Protein Structure*, Garland Publishing, New York, 1991 (b) Atwood, J.L., Hamada, F., Robinson, K.D., Orr, G.W. and Vincent, R.I. *Nature*, 1991, 349, 683-684 (c) Jeffrey, G.A. and Saenger, W. *Hydrogen Bonding in Biological Structures*, Springer-Verlag, Berlin Heidelberg New York, 1991

[35] For a current set of review articles on hemoglobin, myoglobin and corresponding model compounds see for example *Chemical Reviews*, May 1994, Volume 94, Number 3

[36] (a) Collman, J.P.; Brauman, J.I.; Iveson, B.L.; Sessler, J.L.; Morris, R.M. and Gibson, Q.H. *J. Am. Chem. Soc.*, **1983**, 105, 3052-3064 (b) Lavalette, D.; Tetreau, C.; Mispelter, J.; Momenteau, M. and Lhoste, J.-M. *Eur. J. Biochem.*, **1984**, 106, 5132-5143 (c) Traylor, T.G.; Koga, N.; Deardurff, L.A.; Mitchell, M. and Styne, J.A. *J. Am. Chem. Soc.*, **1984**, 106, 5132-5143 (d) Traylor, T.G.; Tsuchiya, S.; Campbell, D.; Mitchell, M.; Styne, D. and Koga, N. *J. Am. Chem. Soc.*, **1985**, 107, 604-614 (e) Springer, B.A.; Egeberg, K.D.; Sligar, S.G.; Rohlf, R.J.; Mathews, A.J. and Olson, J.S. *J. Biol. Chem.*, **1989**, 264, 3057-3060

[37] (a) Varotsis, C.; Woodruff, W.H. and Babcock, G.T. *J. Am. Chem. Soc.* **1989**, 111, 6439-6440 (b) Han, S.; Ching, Y.-c. and Rousseau, D.L. *Proc. Natl. Acad. Sci., U.S.A.* **1990**, 87, 2491-2495 (c) Varotsis, C. and Babcock, G.T. *Biochem* **1990**, 29, 7357-7362 (d) Varotsis, C.; Woodruff, W.H. and Babcock, G.T. *J. Biol. Chem* **1990**, 265, 11131-

[38] (a) Varotsis, C.; Zhang, Y.; Appelman, E.H. and Babcock, G.T. *Proc. Natl. Acad. Sci., U.S.A.* **1992**, 90, 237-241 (b) Ogura, T.; Takahashi, S.; Hirota, S.; Shinzawa-Itoh, K.; Yoshikawa, S.; Appelman, E.H. and Kitagawa, J. *J. Am. Chem. Soc.* **1993**, 115, 8527-8536

[39] (a) Garrett, A.W. and Zwier, T.S. *J. Chem. Phys.* **1992**, 96, 9710-9718 (b) Gotch, A.J. and Zwier, T.S. *J. Chem. Phys.* **1990**, 93(10), 6977-6986

[40] Tuchen, E. and Woodward, C. *Biochemistry*, **1987**, 26, 1918-1925

[41] Kitagawa, T.; Ondrias, M.R.; Rousseau, D.L.; Ikeda-Saito, M. and Yonetani, T. *Nature* **1982**, 26, 869-871

[42] (a) Smith, M.L.; Ohlsson, P.-I. and Paul, K.G. *FEBS Letters* **1983**, 163, 303-305

[43] Satterlee, J.D. and Erman, J.E. *J. Am. Chem. Soc.* **1984**, 106, 1139-1140

[44] For example see Chapter 8 in Peiffer, W.E., A. Ph.D. Dissertation, Michigan State University, **1992**

[45] (a) Oertling, W.A.; Kean, R.T.; Wever, R. and Babcock, G.T. *Inorg. Chem.*, **1989**, 29, 2633-2645 (b) Groves, J.T.; Huashalter, R.C.; Nakamura, M.; Nemo, T.E. and Evans, B.J. *J. Am. Chem. soc.*, **1981**, 103, 2884-2886 (c) Groves, J.T.; Nemo, T.E. and Myers, R.S. *J. Am. Chem. soc.*, **1979**, 101, 1032-1033 (d) Chang, C.K. and Kuo, M.-S. *J. Am. Chem. soc.*, **1979**, 101, 7613-7615

- [46] (a) Pettersen, R.C. and Alexander, L.E. *J. Am. Chem. soc.*, **1968**, **90**, 3873-3875 (b) Buchler, J.W.; Puppe, L.; Rohbock, K. and Schneehage, H.H. *Ann. N.Y. Acad. Sci.*, **1973**, **206** 116 (c) Su, O.Y.; Czernuscewicz, R.S.; Miller, L.A. and Spiro, T.G. *J. Am. Chem. Soc.* **1988**, **110**, 4150-4157
- [47] Procyk, A.D., Kim, Y., Schmidt, E., Fonda, H.N., Chang, C.K., Babcock, G.T. and Bocian, D.F. *J. Am. Chem. Soc.* **1992**, **114**, 6539-6549
- [48] Zhang, H.; Schmidt, E.; Wu, W.; Chang, G.T. and Babcock, G.T. *Chem. Phys. Lett.*, Submitted, **1994**
- [49] Fetter, J., Schmidt, E., Babcock, G.T. Fergusson-Miller, S. *Proc. Nat. Acad. Sci.*, Submitted **1994**

## CHAPTER 2

### **Preparation and Characterization of 5 and 6 Coordinated (CO)Co<sup>III</sup>OEP(ClO<sub>4</sub><sup>-</sup>) Complexes, Electron Absorption and Vibrational Spectroscopies and Normal Coordinate Analysis.**

#### **2.1 Overview**

When CO(g) was added to solutions of the cobaltous porphyrin  $\pi$  cation radical [Co(II)OEP<sup>•</sup>] $\text{ClO}_4$ , prepared from oxidation of CoOEP by  $\text{AgClO}_4$  in anhydrous  $\text{CH}_2\text{Cl}_2$ , room temperature binding at the metal center occurred. Two distinct products were formed, [(CO)Co(III)OEP] $\text{ClO}_4$  and [(CO)<sub>2</sub>Co(III)OEP] $\text{ClO}_4$ . These compounds exhibit Soret maxima at 366 and 414 nm, and form with  $P_{1/2}$  values of  $36 \pm 3$  and  $4000 \pm 300$  torr of CO, respectively. Isosbestic points in the optical absorption spectra occurred at 368 nm for binding of the first CO and at 385 nm during binding of the second ligand. FTIR and resonance Raman (RR) spectra of [(CO)Co(III)OEP] $\text{ClO}_4$  reveal vibrations at 2110 and 441  $\text{cm}^{-1}$  that shift to 2060 and 435  $\text{cm}^{-1}$  upon substitution of  $^{13}\text{CO}$  for the natural abundance CO. Isotope sensitive vibrations of [(CO)<sub>2</sub>Co(III)OEP] $\text{ClO}_4$  were measured at 2137 and 468  $\text{cm}^{-1}$ . These relatively high C-O stretching frequencies of 2137 and 2110  $\text{cm}^{-1}$  are suggestive of relatively weak metal  $d\pi$ -ligand  $\pi^*$  backbonding, resulting from the oxidation of Co(II) to Co(III). RR spectra before the addition of CO were used to characterize

the cobaltous porphyrin  $\pi$  cation radical, and after the addition of CO, RR spectra obtained by using 363.8 nm excitation were used to confirm the occurrence of the five-coordinate Co(III) porphyrin complex. This complex, along with halide ligated analogs, displays some structure sensitive frequencies that suggest that an unusual distortion of the porphyrin core occurs in  $\text{CH}_2\text{Cl}_2$  solution. RR spectra obtained by using 413.1 nm excitation after the addition of CO were used to identify the second product as a typical six-coordinate cobaltic porphyrin.

## 2.2 Introduction

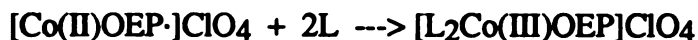
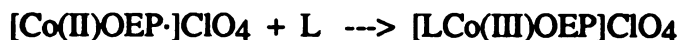
Synthetic cobalt porphyrin complexes have been used as models for oxygen transport proteins [1]. Low temperature binding of diatomics such as  $\text{O}_2$ , CO, and NO to conventional cobaltous porphyrins has been achieved [2], with ligation perhaps best established by vibrational spectroscopy [3]. Binding of dioxygen has received the most attention and matrix isolation techniques have been used to facilitate these studies [3]. As is typical of diatomic ligands, the O-O stretching frequency is modified by bonding to the metal and can usually be detected by IR [4,5], whereas resonance enhancement of the lower frequency Co-O<sub>2</sub> vibrations make these frequencies readily available from Raman measurements [6,7]. Thus, it is useful to use both techniques in order to establish all metal-ligand vibrational frequencies. Vibrational assignments are necessarily verified by isotopic substitutions on the ligand atoms, which affects the vibrational frequencies in these simple systems in a relatively straightforward manner [8]. Use of specialized protected porphyrins allow oxy cobaltous adducts in solution at room temperature to be studied by RR [9]. Possible protein interactions can be modeled and their effects on vibrational frequencies assessed in this manner [10]. Some interesting studies of vibrational coupling between bound dioxygen vibrations and vibrational modes of trans ligands and solvent

have been done with oxy cobalt porphyrins [11]. Cobalt porphyrins reconstituted into myoglobin and hemoglobin have been characterized by resonance Raman (RR) measurements [12]. Oxy derivatives of reconstituted cobalt myoglobin are stable at room temperature and RR measurements of these complexes originally revealed the O-O stretching frequency [6]; indeed, the O-O stretching vibration is not easily observed in oxy Fe myoglobin by Raman or IR [13] measurements. Thus, many RR studies of oxygen transport proteins have used these oxy cobaltous adducts [14].

Oxidized derivatives of cobalt porphyrins have been looked upon as models for intermediates in the enzymatic functions of catalases, peroxidases and cytochromes P450 [15]. During the catalysis cycle, the heme cofactors of these enzymes are oxidized by two electrons, usually at both the metal center and the porphyrin macrocycle to yielding an oxoferryl porphyrin  $\pi$  cation radical,  $[O=Fe(IV)P\cdot]^+$ . Like the heme cofactor, cobalt porphyrins readily lose one electron from each of the metal and the ring macrocycle. In particular, when cobaltous octaethylporphyrin CoOEP is oxidized by two electrons to  $[Co(III)OEP\cdot]^2+$ , two distinct species are possible, one grey and one green in color [16,17]. These two distinct uv-visible absorbance signatures were originally thought to be indicative of the electronic states,  $^2A_{1u}$  or  $^2A_{2u}$ , but later Raman [18], EPR and ENDOR [19,20] work by our group as well as NMR [21] and Raman [22] work by others, clearly showed that these two forms both have a  $^2A_{1u}$  ground electronic state. Rather, most likely differences in macrocycle conformation cause variations in the porphyrin nitrogen donation to the metal, which gives rise to the distinct spectral types [20].

Loss of one electron from CoOEP can result in a number of possible products, depending primarily on the presence of coordinating ligands. Salehi *et al.* [23] showed that one-electron oxidation of this compound by  $AgClO_4$  in

scrupulously dry  $\text{CH}_2\text{Cl}_2$  results in ring-centered oxidation yielding a pale, bluish-gray  $[\text{Co(II)OEP}]\text{ClO}_4$ . This complex is sensitive to the presence of even weakly ligating species (eg.  $\text{H}_2\text{O}$ ). Any ligand interactions with the  $\text{Co(II)}$  (a  $d^7$  complex) will cause an intramolecular electron transfer and "push" the odd electron in the metal  $d_{z^2}$  orbital into the electron deficient ring system. We have observed that reactions of the type



occur very easily. These adducts are at the same formal oxidation level, yet each has a distinct spectral signature. The cobaltous  $\pi$  cation radical has an absorbance maximum at 377 nm, quite different from either the grey or green cobaltic  $\pi$  cation radicals [16,24]. The five-coordinate cobaltic complex is easily made when L is a halide anion and exhibits two somewhat diffuse optical absorbances at ~373 and 546 nm, whereas the spectra of six coordinate complexes display sharper features at ~410, 525 and 558 nm for fairly weak ligands, with these features shifting to the red as the ligand strength increases [23,24]. It is not uncommon for samples of the one electron oxidized adduct to display heterogeneity and many spectra in the literature are due to a mixture of these species.

In contrast to the extensive investigation of dioxygen complexes of cobalt porphyrins described above, there are relatively few reports of carbon monoxy cobaltous complexes [2,3] and none at room temperature. Interestingly, Kadish and coworkers have recently presented evidence suggesting that CO will bind to cobalt porphyrins at room temperature when a one-electron oxidation of a cobaltous TPP (tetraphenylporphyrin) or OEP is carried out electrochemically under a CO atmosphere [25,26]. The result is a  $\text{COCO(III)}$  adduct. Preceding this work, there was only a single report of a cobaltic CO complex [27], and it is

considered somewhat odd for CO to bind metal ions in higher oxidation states due to the  $\pi$  acid nature of the ligand [28]. If oxidation of CoOEP under CO initially produces a cobaltous  $\pi$  cation radical with subsequent CO binding, then CO may simply serve as the ligand L in this case, analogous to the reactions depicted above. In the present work, we have prepared [Co(II)OEP·]ClO<sub>4</sub> and then introduced CO in a separate step. Here we report conclusive evidence of CO binding to Co(III), namely both Co-CO and CoC $\equiv$ O stretching frequencies, verified with isotopic substitution. Furthermore, we demonstrate that both five coordinate [(CO)Co(III)OEP]ClO<sub>4</sub> and six coordinate [(CO)<sub>2</sub>Co(III)OEP]ClO<sub>4</sub> can be formed, depending on CO pressure, and we measure formation equilibrium constants for these species. Our analysis reveals that the earlier work resulted in formation of predominantly the dicarbonmonoxy derivative, rather than the monocarbonmonoxy adduct, as was reported [26].

### 2.3 Experimental

Porphyrins were synthesized [29,30] and metals inserted according to established methods [31]. Oxidations were carried out by adding an excess of anhydrous AgClO<sub>4</sub>(s) to the cobalt porphyrin solution and stirring for 1 to 3 hours in an evacuated cell. CO(g) was typically bubbled into the sample through a syringe, while a second needle was used as a vent to expel excess gas.

For the CO titration, the sample was prepared in the usual way in dry CH<sub>2</sub>Cl<sub>2</sub>. CO was introduced with a calibrated gas tight syringe. Before each injection, the pressure within the gas tight syringe was allowed to equilibrate to atmospheric pressure, estimated at 760 Torr. The titration vessel was 135 mL capacity and the partial pressure of CO was calculated by starting under vacuum, then systematically injecting into the vessel a known volume of CO gas. Ideal

gas behavior was assumed and the partial pressure was calculated from  $(V_{\text{injected}}/V_{\text{vessel}})*760$  Torr.

FTIR requires highly concentrated samples. Due to the limited solubility of CoOEP in  $\text{CH}_2\text{Cl}_2$  these concentrations were unattainable. However, dimethyl-2,4,6,8-tetramethyl-3,7-dioctylporphine-1,5-dipropionate cobalt(II)porphyrin [30] (CoC<sub>8</sub>P) was sufficiently soluble in  $\text{CH}_2\text{Cl}_2$  so that FTIR samples could be made. To ensure that CoC<sub>8</sub>P had redox and ligation properties similar to those of CoOEP, we used optical absorption spectroscopy to follow the oxidation and CO titration of CoC<sub>8</sub>P. FTIR samples were prepared by placing 1 mg of cobalt porphyrin and anhydrous  $\text{AgClO}_4$  into a vial sealed with a rubber septum and flushed with  $\text{N}_2(\text{g})$ . Freshly distilled methylene chloride (1 mL) was injected into the vial with a Hamilton gas tight syringe. Deuterated solvent was used as supplied by Cambridge Isotope Laboratories. After oxidation was complete, the sample was transferred by a gas tight syringe into a 50  $\mu\text{m}$  NaCl cavity cell. The cavity cell was in a holder sealed with a rubber septum. Carbon monoxide was bubbled into the sample via a syringe needle inserted to the groove of the cavity cell. A second needle was used as a vent to expel excess CO. Solution infrared spectra were recorded on a Nicolet IR/42 FTIR spectrometer.

Raman spectra were obtained by using a  $90^\circ$  scattering geometry and were measured with either a Spex 1401 equipped with a PMT or a Spex 1877 monochromator equipped with an OMA III diode array detector. Laser emissions at 363.8 and 413.1 nm were from a Coherent Innova 200 argon ion laser and a Coherent Innova 90 krypton ion laser, respectively. Optical absorption spectra, obtained by using a Perkin-Elmer Lambda 5 spectrometer, were recorded prior to and following Raman studies to confirm sample integrity. Anaerobic quartz cuvettes were used for both the Raman and optical absorption measurements.

Normal coordinate calculations were carried out on an XS-ma 24, 4000 SGI machine using standard GF-matrix methods [32,33]. Initial force constants were chosen from Jones et al. [34]. Force constants were optimized by the method of McIntosh and Michaelan [33].

## **2.4 Results**

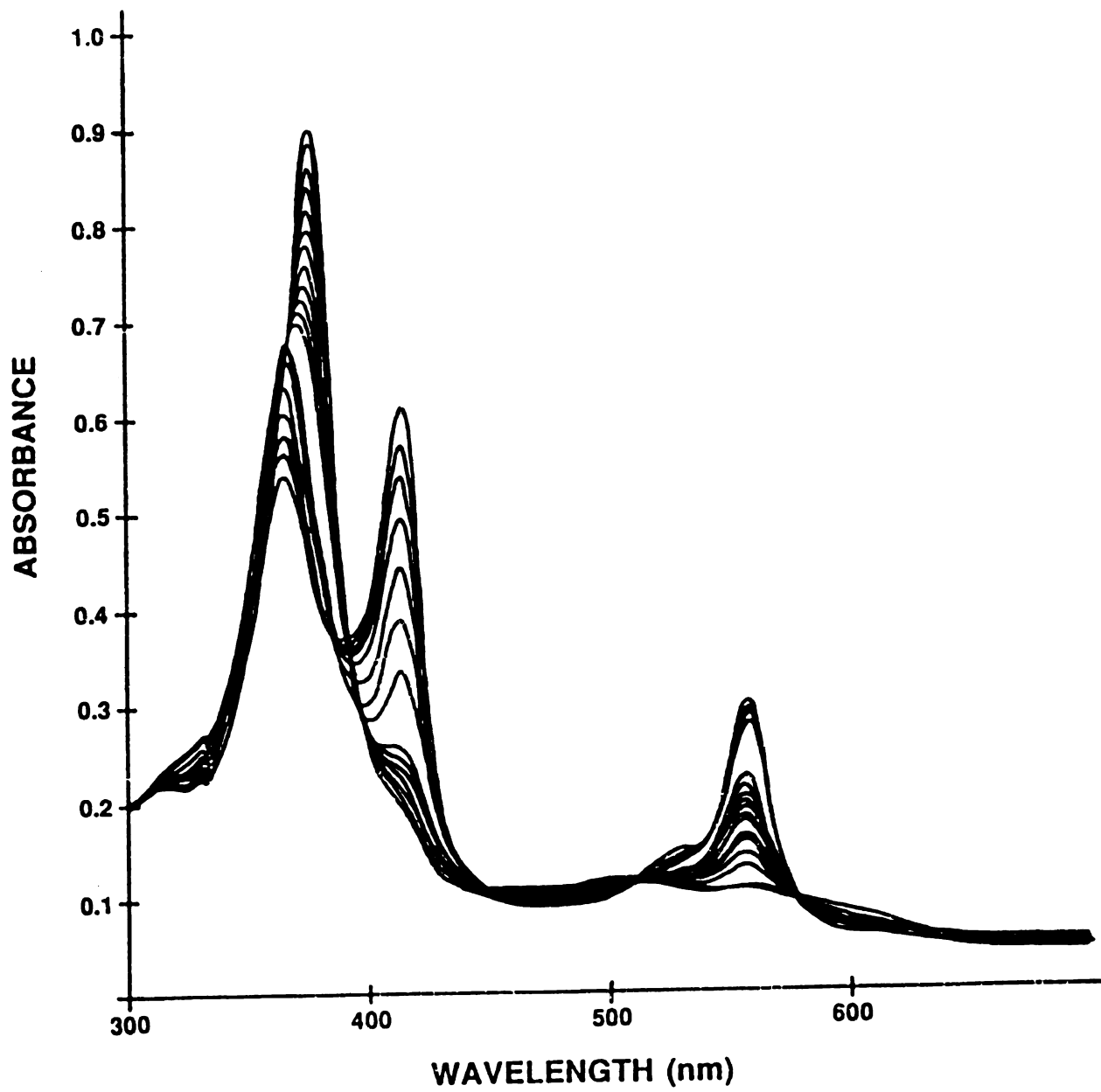
### **2.4.1 Optical Spectroscopy**

Uv-vis absorbance spectra depicting the sequential oxidation and ligand binding of CoOEP are shown in Figure 1. The starting material (solid line) is oxidized by one-electron in anhydrous  $\text{CH}_2\text{Cl}_2$  to give the cobaltous  $\pi$  cation radical  $[\text{Co(II)OEP}\cdot]\text{ClO}_4$  (dashed line). The spectrum of this species displays a Soret maxima at 377, as reported in earlier measurements [23,24]. When gaseous CO is introduced above the solution to a pressure of approximately 1 atm, a split Soret band with maxima at 366 and 414 nm develops, as in Figure 1c (dotted line). Also, typical Q-band absorptions at approximately 528 and 557 nm replace the broad of the  $\pi$  cation radical, suggesting that the porphyrin ring has been reduced by one electron to form the ring neutral species. The relative intensities of the two absorptions in the split Soret band of Figure 1c are dependent on CO pressure and titration with CO yields spectra with well defined isosbestic points (see below). This suggests that the bands at 366 and 414 nm arise from distinct complexes. Thus, initial oxidation results in a cobaltous  $\pi$  cation radical and subsequent introduction of CO seems to yield two distinct, possibly nonradical complexes.

### **2.4.2 Resonance Raman spectroscopy**

By using laser lines in resonance with each of the two absorbance maxima, Raman measurements can provide selective enhancement of vibrational spectra

**Figure 2.1** a) (—) Neutral  $\text{Co}^{\text{II}}\text{OEP}$  in  $\text{CH}_2\text{Cl}_2$  b) (---) One electron oxidized  $\text{Co}^{\text{II}}\text{OEP}^+\cdot(\text{ClO}_4^-)$  in  $\text{CH}_2\text{Cl}_2$  under an  $\text{N}_2$  atmosphere. c) (....) One electron oxidized  $\text{Co}^{\text{II}}\text{OEP}^+\cdot(\text{ClO}_4^-)$  in  $\text{CH}_2\text{Cl}_2$  under a  $\text{CO}$  atmosphere.



from each of the two species giving rise to the Soret absorptions in Figure 1c. Furthermore, RR spectra of metalloporphyrin  $\pi$  cation radicals are distinct from those of metalloporphyrins [18,22-24] and can be used to characterize the oxidation and ligation state of these species. The spectrum of [Co(II)OEP] $\cdot$ ClO<sub>4</sub>, obtained by using 363.8 nm excitation before CO is introduced, is shown in Figure 2a. By using this excitation wavelength after the introduction of CO, spectra characteristic of the 366 nm absorbing complex were obtained. These appear in Figure 2b. The 1300 - 1700 cm<sup>-1</sup> region contains several structure sensitive frequencies that can be used to characterize both the radical and nonradical species involved [18, 22-24,35]. Table I collects these vibrational frequencies and assigns normal modes according to earlier normal coordinate calculations [36,37]. The first column in the table gives characteristic frequencies for the starting material, Co(II)OEP (spectra not shown). The second column collects frequencies obtained from Figure 2a. These, together with the 377 absorbance maximum, are indicative of a "grey type" cobaltous  $\pi$  cation radical. The third column contains frequencies for the 366 nm absorbing species in the final mixture. The Raman spectrum in Figure 2b and the frequencies listed in Table I are remarkably similar to those of [BrCo(III)OEP] [24], a rather unique five-coordinate cobaltic compound that also displays a dramatically blue-shifted Soret absorbance (373 nm). This species is discussed in detail below. When the sample was made with isotopically labelled <sup>13</sup>CO, rather than natural abundance CO, spectrum 2c was obtained. There is some residual cobaltous  $\pi$  cation radical in this sample, evidenced by the feature at 1363 cm<sup>-1</sup>. Otherwise, all vibrations but one appear unaffected by the isotopic substitution: the low frequency feature at 441 cm<sup>-1</sup> is shifted to 435 cm<sup>-1</sup> in the <sup>13</sup>CO sample. This suggests that this feature is a cobalt-CO vibration, unambiguously establishing CO binding to the metal center.

**Figure 2.2** Resonance Raman spectra of one electron oxidized  $\text{Co}^{\text{II}}\text{OEP}^+\cdot(\text{ClO}_4^-)$  under a) an  $\text{N}_2$  atmosphere, b) a  $^{12}\text{CO}$  atmosphere, c) a  $^{13}\text{CO}$  atmosphere. The excitation wavelength in all spectra was 363.8nm at 5mW of power. The samples were prepared in dry  $\text{CH}_2\text{Cl}_2$ , UV-vis spectra were taken prior to and following the Raman spectroscopy to verify the integrity of the samples.

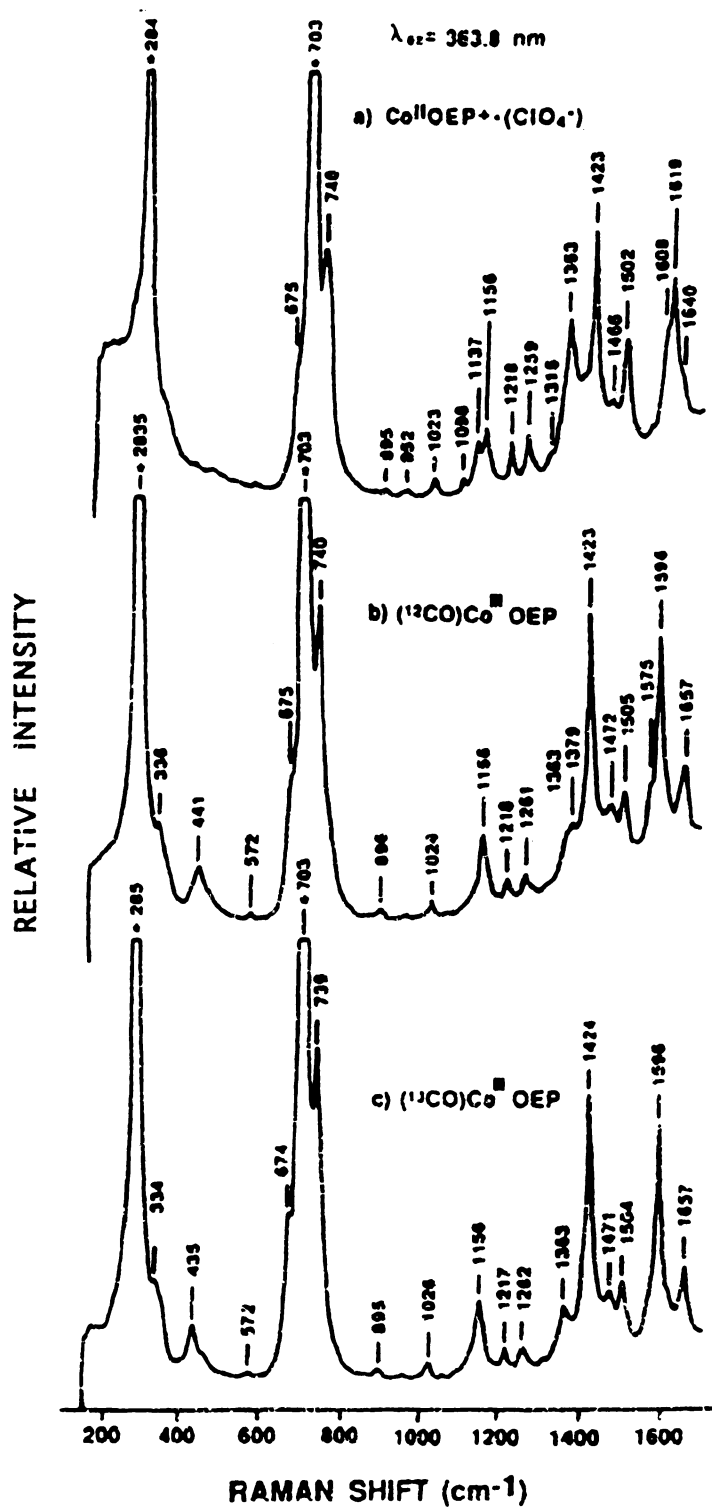
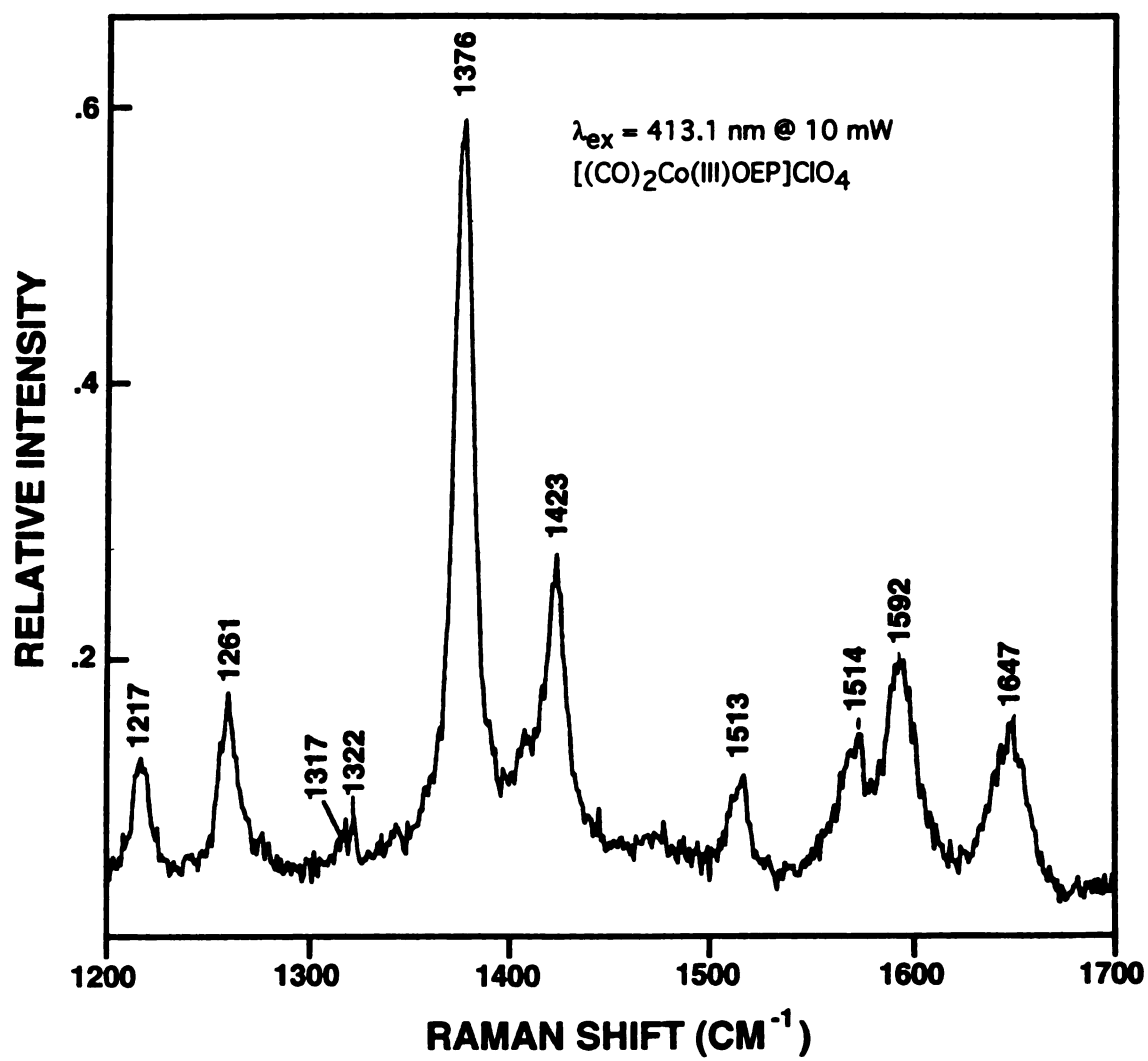


**Table I.** Structural sensitive vibrational frequencies ( $\text{cm}^{-1}$ ) observed in resonance Raman spectra obtained at the given excitation wavelengths (nm).

	Co <sup>II</sup> OEP	[Co <sup>II</sup> OEP·](ClO <sub>4</sub> )		
	[(CO) <sub>n</sub> Co <sup>III</sup> OEP](ClO <sub>4</sub> )			
Normal mode	363.8 nm	363.8 nm	363.8 nm	413.1 nm
			n=1	n=2
$\nu_4$ (C <sub>a</sub> N)	1379	1363	1379	1376
$\nu_3$ (C <sub>a</sub> C <sub>m</sub> )	1512	1502	1505	1514
$\nu_{11}$ (C <sub>b</sub> C <sub>b</sub> )	1575	1608	1575	1571
$\nu_2$ (C <sub>b</sub> C <sub>b</sub> )	1599	1619	1596	1593
$\nu_{10}$ (C <sub>a</sub> C <sub>m</sub> )	1647	1640	1657	1647

**Figure 2.3** High range resonance Raman spectra of one electron oxidized  $\text{Co}^{\text{II}}\text{OEP}^+$  under a CO atmosphere, The excitation wavelength in the spectra was prepared 413.1 nm at 5 mW of power. The sample in dry  $\text{CH}_2\text{Cl}_2$ , UV-vis spectra were taken prior to and following the Raman spectroscopy to verify the integrity of the sample.



RR spectra obtained by using 413.1 nm laser excitation appear in Figure 3 and give rise to the frequencies listed in the last column of Table I. These are very similar to those of the starting material, CoOEP. Together with the red-shifted Soret maximum at 414 nm, these are consistent with a six-coordinate cobaltic complex, (L)<sub>2</sub>Co(III)OEP [12,24]. The spectrum obtained by using  $\lambda_{\text{ex}} = 413.1$  nm in Figure 3 is distinct from those observed with  $\lambda_{\text{ex}} = 363.8$  nm (Figure 2b) indicating efficient spectral resolution of the two distinct species resulting from CO ligation.

The data presented thus far suggest that, upon introduction of CO to the cobaltous  $\pi$  cation radical, two species with optical absorption and RR spectra consistent with five and six-coordinate cobaltic complexes are formed. The five-coordinate complex appears to have CO bound to the metal center. To confirm this analysis we present below RR and IR spectra that reveal additional isotope sensitive vibrations from each of the two product species as well as optical absorption spectra that monitor titration of [Co(II)OEP]ClO<sub>4</sub> with CO.

If CO is bound to the complex absorbing at 366 nm, the RR spectrum may reveal a high frequency vibration corresponding to the  $\nu(\text{C}\equiv\text{O})$  stretch of the bound ligand. Figure 4 shows the high frequency region of Raman scattering enhanced at  $\lambda_{\text{ex}} = 363.8$  nm. There appears to be a feature at 2110 cm<sup>-1</sup> that shifts to 2059 cm<sup>-1</sup> when the isotopically labelled <sup>13</sup>CO is used. In search of an analogous isotope sensitive band from the other species, we scanned the 1800 - 2500 cm<sup>-1</sup> region of the scattering resulting from the 413.1 nm laser line, but could not detect such a feature. On the other hand, Figure 5 displays the low-frequency region of the resonance Raman spectrum obtained by using  $\lambda_{\text{ex}} = 413.1$  nm, and reveals a feature at 468 cm<sup>-1</sup> that shifts to 461 cm<sup>-1</sup> in the spectrum of the isotopically labeled adduct. This frequency is quite different from the

**Figure 2.4** High range resonance Raman spectra of one electron oxidized  $\text{Co}^{\text{II}}(\text{OEP})^+$  under a) a  $^{12}\text{CO}$  atmosphere, b) a  $^{13}\text{CO}$  atmosphere. The excitation wavelength in all spectra was 363.8nm at 5mW of power. The samples were prepared in dry  $\text{CH}_2\text{Cl}_2$ . UV-vis spectra were taken prior to and following the Raman spectroscopy to verify the integrity of the samples.

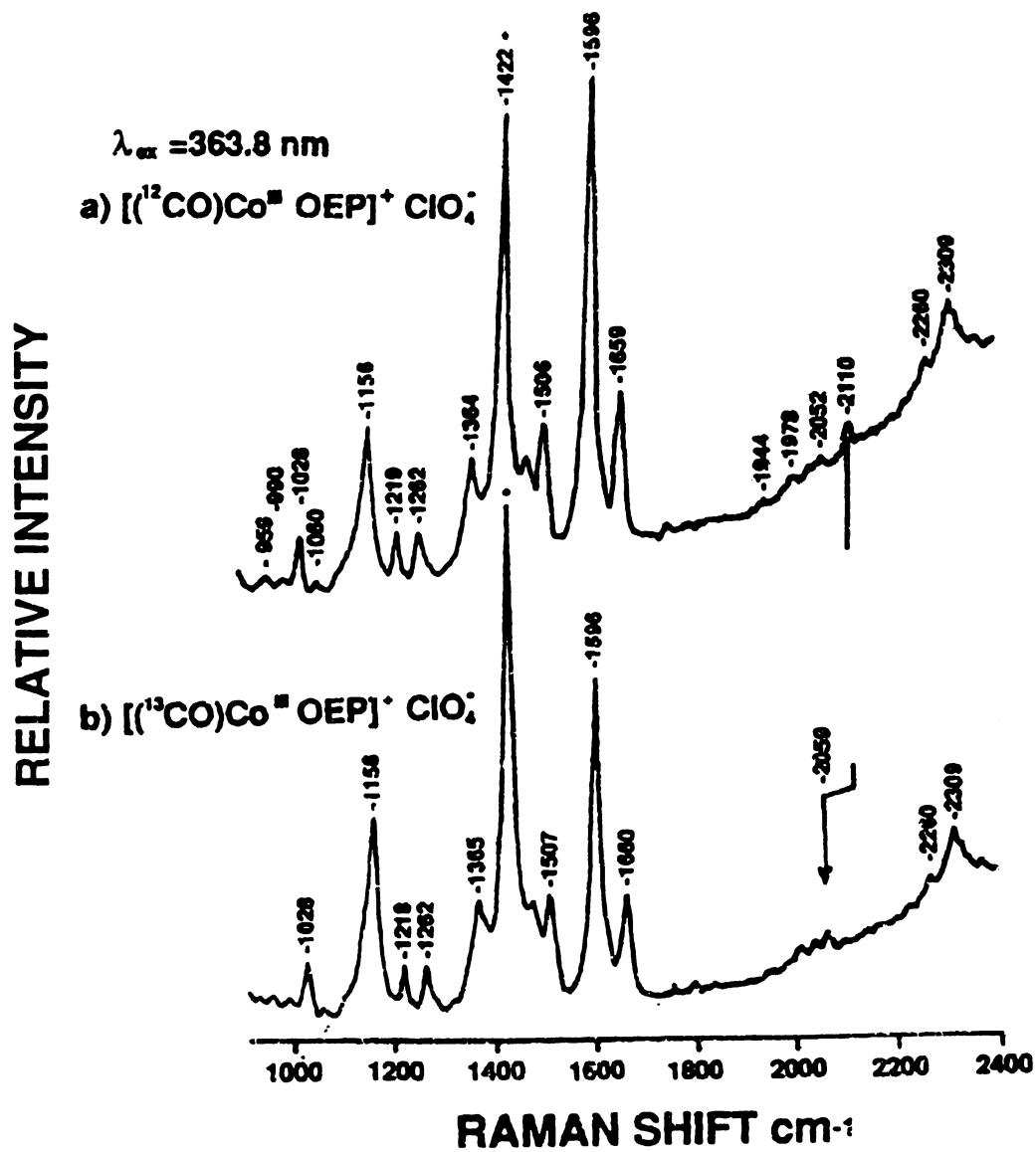
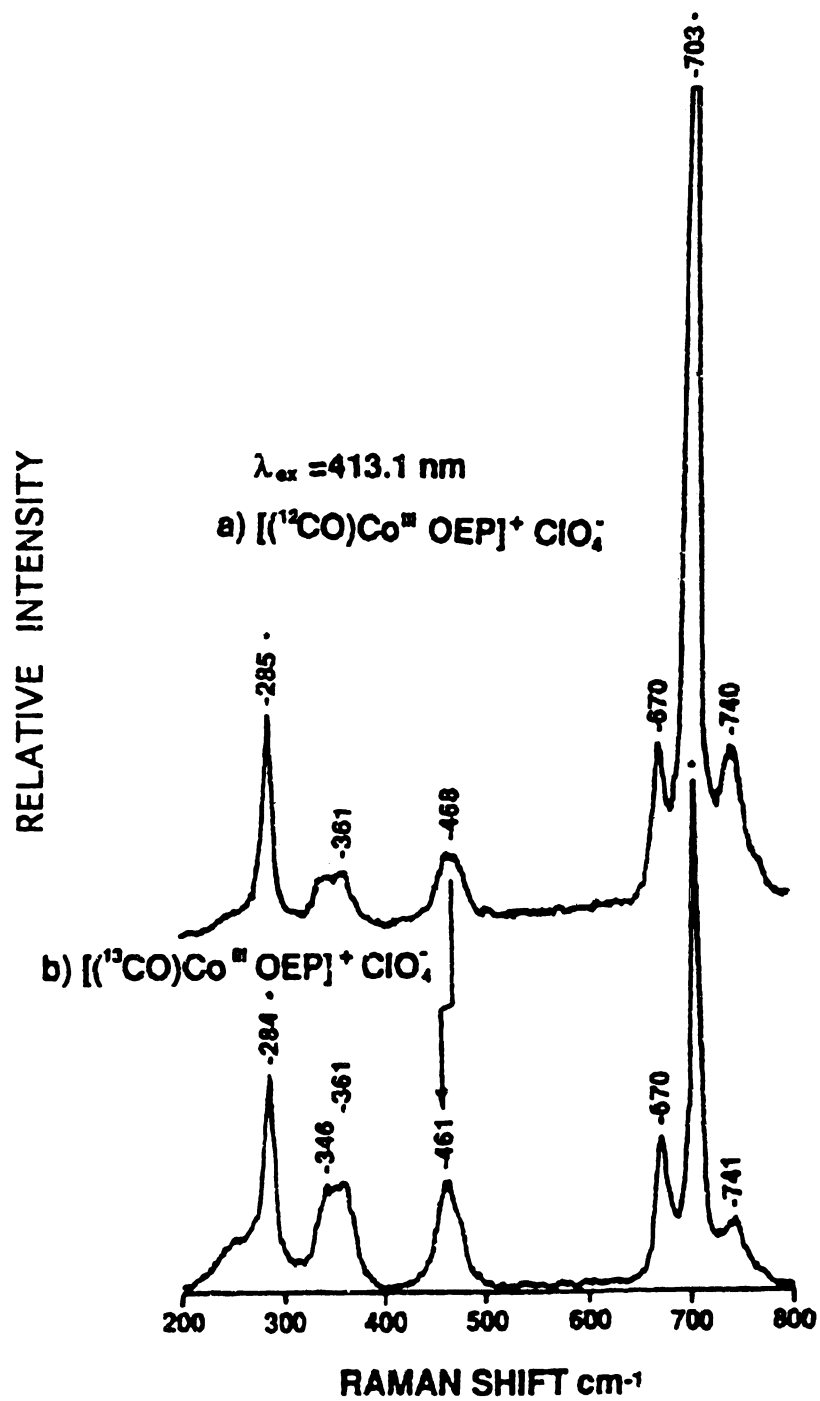


**Figure 2.5** Resonance Raman spectra of one electron oxidized  $\text{CoIIIOEP}^+(\text{ClO}_4^-)$  a) under an  $^{12}\text{CO}$  atmosphere, b) under an  $^{13}\text{CO}$  atmosphere. The excitation wavelength in all spectra was 413.1nm at 5mW of power. The samples were prepared in dry  $\text{CH}_2\text{Cl}_2$ , UV-vis spectra were taken prior to and following the Raman spectra to verify the integrity of the samples.



analogous one observed with  $\lambda_{\text{ex}} = 363.8 \text{ nm}$ , which occurs at  $441 \text{ cm}^{-1}$  and shifts to  $435 \text{ cm}^{-1}$  when  $^{13}\text{CO}$  is used (Figure 2b and c, above).

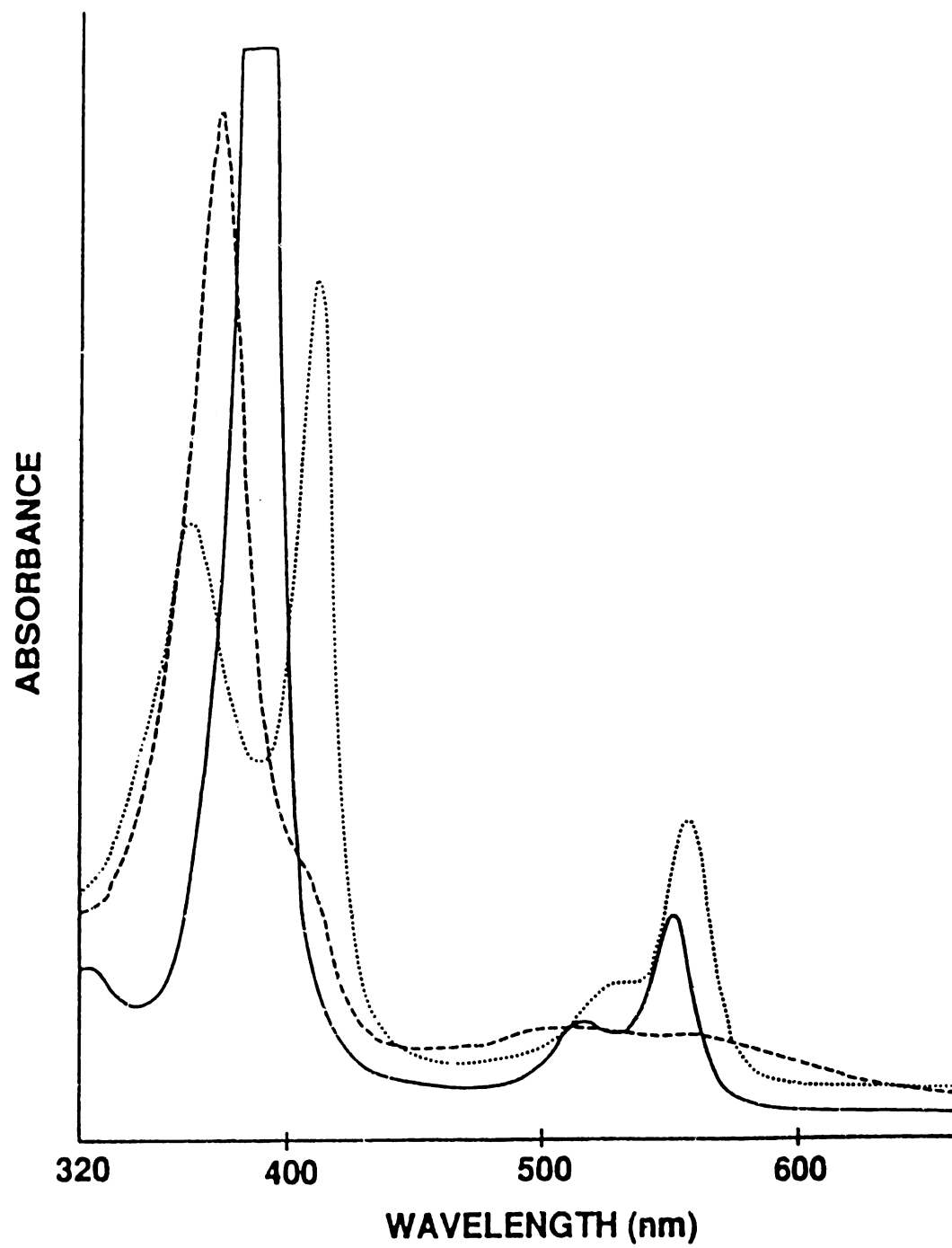
### 2.4.3 FTIR spectroscopy

Solution FTIR spectra (not shown) of concentrated samples (see Experimental for details of preparation) in both  $\text{CH}_2\text{Cl}_2$  and  $\text{CD}_2\text{Cl}_2$  detect two bands in the  $\nu(\text{C}\equiv\text{O})$  stretching region at  $2110$  and  $2137 \text{ cm}^{-1}$ . When the sample is prepared with  $^{13}\text{CO}$ , bands are observed at  $2061$  and  $2088 \text{ cm}^{-1}$ . The  $2110 \text{ cm}^{-1}$  feature, which shifts to  $2061 \text{ cm}^{-1}$  with  $^{13}\text{CO}$ , is in good agreement with the  $363.8 \text{ nm}$  Raman result and suggests that this feature arises from the five-coordinate complex. It is then reasonable to assume that the other feature,  $2137 \text{ cm}^{-1}$  which shifts to  $2088 \text{ cm}^{-1}$  upon isotopic substitution, arises from the labeled six-coordinate species. This assumption is consistent with more extensive vibrational analysis presented below.

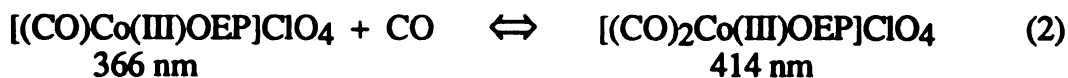
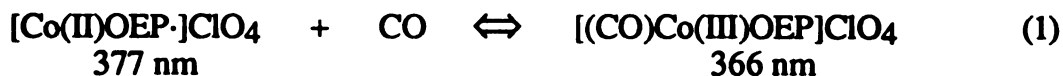
### 2.4.4 Carbon monoxide titration

Absorbance spectra that monitor the CO titration of  $[\text{Co}(\text{II})\text{OEP}]\text{ClO}_4$  are shown in Figure 6. The most intense feature in the Soret region ( $377 \text{ nm}$ ) originates from the cobaltous  $\pi$  cation radical. Initially, this band diminishes as the band at  $366 \text{ nm}$  grows, giving rise to an isosbestic point at approximately  $368 \text{ nm}$ . Concomitant with these changes, a band at  $555 \text{ nm}$  appears and intensifies along with the  $366 \text{ nm}$  absorbance. Eventually, with further addition of CO, a feature at  $414 \text{ nm}$  intensifies as the band at  $366 \text{ nm}$  diminishes, giving rise to an isosbestic point at about  $385 \text{ nm}$ . Changes in the Q-band region, which accompany the latter spectral change, are more subtle, but the band at  $555 \text{ nm}$  diminishes in intensity and red shifts slightly to  $558 \text{ nm}$  and the feature at  $527 \text{ nm}$

**Figure 2.6** Titration spectra of the  $\text{Co}^{\text{II}}\text{OEP}^+(\text{ClO}_4^-)$  with carbon monoxide gas. The sample was prepared in the usual way in dry  $\text{CH}_2\text{Cl}_2$ , the path length of the optical cell was 5mm. The titration vessel was 135ml capacity and the partial pressure of CO was calculated by starting under vacuum, then systematically injecting into the vessel a known volume of CO gas. Ideal gas law properties were assumed and the partial pressure was calculated from  $(V_{\text{inj}}/V_{\text{vessel}})*760\text{Torr}$ . The pressure within the gas tight syringe was allowed to equilibrate to atmospheric pressure, estimated at 760 Torr.



begins to resolve. The two clearly defined isosbestic points provide credibility for our suggestion of two ligation events. Thus, the pressure dependence of the absorbance spectra suggests the formation of two complexes that are in equilibrium as shown by the following:



We show below that we can neglect (3) for this system. Vibrational analysis of the cobalt-carbonmonoxy vibrations provides further evidence for this scheme and is also presented below, followed by determination of the equilibrium constants for (1) - (3).

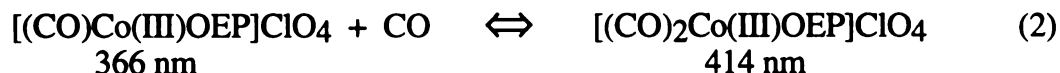
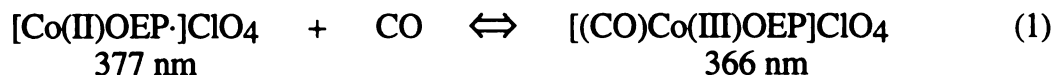
## 2.5 Discussion

### 2.5.1 Analysis of Cobalt-CO vibrations.

#### 2.5.1.1 Group theoretical analysis

The five-coordinate complex  $[(\text{CO})\text{Co(III)OEP}]\text{ClO}_4$  belongs to the  $C_{4v}$  point group and a linear  $\text{Co}-\text{C}\equiv\text{O}$  unit is expected to give rise to four vibrations given by:  $2A_1 + E$ . The two vibrations of  $A_1$  symmetry are totally symmetric stretching motions while the E vibrations are a degenerate pair of linear bends. All vibrations are expected to be both Raman and IR active [38]. The linear bends, being degenerate, should occur at the same frequency and give rise to a single feature in the  $200 - 600 \text{ cm}^{-1}$  region. One stretch is expected to be primarily  $\nu(\text{C}\equiv\text{O})$  occurring around  $2100 \text{ cm}^{-1}$  and the other  $\nu(\text{Co}-\text{C})$  at around  $300-600 \text{ cm}^{-1}$ . There is little mixing of these stretching coordinates because of the large difference in frequencies.

begins to resolve. The two clearly defined isosbestic points provide credibility for our suggestion of two ligation events. Thus, the pressure dependence of the absorbance spectra suggests the formation of two complexes that are in equilibrium as shown by the following:



We show below that we can neglect (3) for this system. Vibrational analysis of the cobalt-carbonmonoxy vibrations provides further evidence for this scheme and is also presented below, followed by determination of the equilibrium constants for (1) - (3).

## 2.5 Discussion

### 2.5.1 Analysis of Cobalt-CO vibrations.

#### 2.5.1.1 Group theoretical analysis

The five-coordinate complex  $[(\text{CO})\text{Co(III)OEP}]\text{ClO}_4$  belongs to the  $C_{4v}$  point group and a linear  $\text{Co}-\text{C}\equiv\text{O}$  unit is expected to give rise to four vibrations given by:  $2A_1 + E$ . The two vibrations of  $A_1$  symmetry are totally symmetric stretching motions while the E vibrations are a degenerate pair of linear bends. All vibrations are expected to be both Raman and IR active [38]. The linear bends, being degenerate, should occur at the same frequency and give rise to a single feature in the  $200 - 600 \text{ cm}^{-1}$  region. One stretch is expected to be primarily  $\nu(\text{C}\equiv\text{O})$  occurring around  $2100 \text{ cm}^{-1}$  and the other  $\nu(\text{Co}-\text{C})$  at around  $300-600 \text{ cm}^{-1}$ . There is little mixing of these stretching coordinates because of the large difference in frequencies.

The six-coordinate complex  $[(\text{CO})_2\text{Co(III)OEP}]\text{ClO}_4$  most likely belongs to the  $D_{4h}$  group. A linear  $\text{O}\equiv\text{C}-\text{Co}-\text{C}\equiv\text{O}$  unit is expected to generate ten vibrations given by:  $2A_{1g} + 2A_{2u} + 2E_g + E_u$ . The A type modes are stretches and the E type modes are degenerate linear bends. Gerade vibrations are Raman active and ungerade vibrations are IR active [38]. The frequency regions in which the vibrations are expected are similar to the  $C_{4v}$  case above. For example, a totally symmetric ( $A_{1g}$ ) Raman active mode  $\langle\text{--O}\equiv\text{CCoC}\equiv\text{O--}\rangle$  is expected around  $2100\text{ cm}^{-1}$ , while another, corresponding to symmetric stretching of the metal-carbon bonds  $\langle\text{--OC-Co-CO--}\rangle$ , is expected in the low frequencies. The situation is similar for IR active  $A_{2u}$  antisymmetric stretching modes.

### 2.5.1.2 Vibrational spectroscopy

Table II collects the observed metal-ligand vibrational frequencies, calculated frequencies obtained by using FG matrix methods, and our vibrational normal mode assignments for both the five and six-coordinate complexes. The appearance of the  $2110\text{ cm}^{-1}$  vibration in both the RR and IR data is strong support for a five-coordinate  $C_{4v}$  complex. The assignment of the other high frequency IR feature to the asymmetric coupled  $\text{C}\equiv\text{O}$  stretch of the six-coordinate complex is reasonable. Our analysis predicts the presence of another Raman active high frequency mode  $\sim 2300\text{ cm}^{-1}$  corresponding to the symmetric coupled  $\text{C}\equiv\text{O}$  stretch for this six-coordinate species, but we did not observe it by using  $413.1\text{ nm}$  excitation. This is not surprising because the resonance enhancement of these modes is typically weak, and, because Raman intensity is proportional to the fourth power of the absolute scattered frequency, detection of this mode by using  $413.1\text{ nm}$  excitation is expected to be more difficult than by using  $363.8\text{ nm}$  excitation (Figure 4).

Based on the number of d electrons in the metal (6) and the number of  $\pi^*$  electrons in the ligand (0), the geometry of the Co(III)-C-O is expected to be linear [8]. Yu *et al.* [39] report no RR enhancement of metal-ligand bending vibrations for complexes known to have linear M-C-O geometries. Similarly, we observed no bending motions in the RR spectra. In the course of doing our normal coordinate calculations, we were able to fit our observed frequencies only when linear Co-C-O geometries were input. Thus, CO most likely binds to Co in a linear fashion in these complexes.

The C-O stretching frequencies observed,  $2137\text{ cm}^{-1}$  for the six-coordinate and  $2110\text{ cm}^{-1}$  for the five coordinate complex, reflect relatively weak metal  $d\pi$ -ligand  $\pi^*$  backbonding. This reflects the decreased electron density at the Co(III) due to the high oxidation state. Metals in lower oxidation states are able to more strongly donate electrons back into the  $\pi^*$  orbital of the ligand, causing a greater decrease in the C-O stretching frequency [40]. For example, C-O frequencies ( $\text{cm}^{-1}$ ) observed for some M(II) porphyrin complexes include:  $(\text{CO})_2\text{CoTPP}$ , 2077;  $(\text{CO})_2\text{FeTPP}$ , 2042;  $(\text{CO})_2\text{RuTPP}$ , 2005 [3]. The  $2137\text{ cm}^{-1}$  that we observe for  $[\text{CO})_2\text{Co(III)OEP}]\text{ClO}_4$  is hardly lowered from the frequency of free CO  $\sim 2155\text{ cm}^{-1}$ , indicating that the bonding interaction is dominated by  $\sigma$  donation from the ligand to the metal in this M(III) complex. Judging from our observed frequencies, the backbonding in the six-coordinate complex is even weaker than in the five-coordinate complex because in the six-coordinate complex the metal donation must be split between two ligands. Comparison of the C-O frequency for  $(\text{CO})_2\text{FeTPP}$ ,  $2042\text{ cm}^{-1}$ , to that of  $(\text{CO})\text{FeTPP}$ ,  $1973\text{ cm}^{-1}$ , illustrates the same trend [2c].

### 2.5.2 Calculation of equilibrium constants and $P_{1/2}$ values for reactions (1) - (3).

Assuming that the system follows Henry's law, relating the partial pressure of a gas above a solution to its solution concentration, we can write equilibrium constant expressions for (1) and (2):

$$K_1 = \frac{[(CO)Co(III)OEP]^+}{[Co(II)OEP]^+ P_{\infty}}$$

$$K_2 = \frac{[(CO)_2Co(III)OEP]^+}{[(CO)Co(III)OEP]^+ P_{\infty}}$$

The true concentration equilibrium constants can be obtained by multiplication of  $K_1$  and  $K_2$  by the appropriate Henry's constant for CO in  $CH_2Cl_2$ .  $K_3$  (for the third reaction) is the product  $K_1K_2$  and is negligible for this system.  $K_1$  and  $K_2$  can be determined from Figure 6 by using the following [41]:

$$\frac{1}{A - A_0} = \frac{1}{K_i(A_{\infty} - A_0)} * \frac{1}{P_{CO}} + \frac{1}{(A_{\infty} - A_0)}$$

where  $A$  represents the absorbance of the system at a particular partial pressure of CO,  $A_0$  is the initial absorbance of the reactant species,  $K_i$  is  $K_1$  or  $K_2$ ,  $A_{\infty}$  is the final absorbance of pure product species, and  $P_{CO}$  is the partial pressure of CO. Thus, a plot of  $1/(A - A_0)$  vs.  $1/P_{CO}$  will give a line.  $A_{\infty}$  is determined from the intercept and  $K_i$  from the slope. Because only negligible formation of the six-coordinate complex occurs before reaction (1) has gone to completion, we can use the expression above to determine either  $K_1$  or  $K_2$  [42]. Figures 7 and 8 show such plots for reactions (1) and (2), respectively.  $P_{1/2}$ , represents the pressure of CO when the reaction has proceeded halfway, is given by the

reciprocal of the equilibrium constant,  $P_{1/2} = (K_i)^{-1}$ . From Figures 7 and 8 we obtain  $P_{1/2}$  estimates of  $36 \pm 3$  and  $4000 \pm 300$  torr for reactions (1) and (2), respectively.

### 2.5.2 Comparison of [(CO)Co(III)OEP]ClO<sub>4</sub> to BrCo(III)OEP and other complexes.

The optical absorbance spectrum of [(CO)Co(III)OEP]ClO<sub>4</sub> is similar to that of BrCo(III)OEP [24]. Both display dramatically blue-shifted Soret absorbances (366 and 373 nm, respectively, in CH<sub>2</sub>Cl<sub>2</sub>) compared to that of typical metalloporphyrin complexes. ClCo(III)OEP and ICo(III)OEP also display this blue-shifted Soret maximum [43]; however, we are aware of few other metalloporphyrins with this peculiar spectral signature. The ~370 nm Soret band is odd in two regards. First, oxidation of Co(II) to Co(III) normally causes a red-shift in porphyrin compounds [44]. (This is of course different for iron porphyrin complexes, which are not germane to the discussion of this topic.) Thus, the Soret maximum of cobaltic OEP compounds are expected to be red-shifted relative to that of Co(II)OEP (391 nm), as are the Soret absorbances of the six-coordinate adducts. In the absence of spin or oxidation-state changes,<sup>45</sup> ligation of a single axial ligand normally causes a red-shift in the spectrum of the metalloporphyrin, with a second ligand simply causing an additional red-shift. For example, spectral changes of Cu(II) porphyrins [46] upon ligation display the typical red-shifted trend. Indeed, this is what Kadish and coworkers[27] observed for Co(III)TPP<sup>+</sup> (TPP = tetraphenylporphyrin) complexes upon sequential ligation of CH<sub>3</sub>CN. Thus, the formation of this five-coordinate complex displaying the blue-shifted Soret band appears to be unique to cobaltic complexes of specific porphyrins in solution. Interestingly, (CN)Co(III)OEP is reported to exhibit distinct Soret maxima at 372 and 421 nm [47], while (CN)Co(III)protoporphyrin IX reconstituted in horseradish peroxidase displays a

Soret maximum at 436 nm [48]. The 372 and 421 nm maxima most likely represent two different conformations of the five-coordinate cobaltic cyano complex. The 372 nm band most likely arises from this rather unique configuration and the 421 nm band from a more conventional geometry. The 436 nm maximum represents the effect of a sixth ligand (histidine, and possibly other influences) from the protein.

It is well known that RR frequencies are much more informative of structural properties of metalloporphyrins [35] than optical absorbance maxima. Spaulding *et al.* [49] first recognized the linear correlation between the frequency of  $\nu_{19}$ , an anomalously polarized (ap) mode, and the porphyrin center to nitrogen distance. Similar correlations were demonstrated for virtually all high frequency vibrations [50-52]. Metalloporphyrins exhibiting ruffled or domed geometries, for example ferrous complexes, were shown to display  $\nu_{10}$  and  $\nu_{19}$  frequencies which were significantly lower than expected based on their core sizes [49-52]. Not surprisingly, BrCoOEP was noted to display Raman frequencies that uniquely deviated from these correlations. The BrCoOEP frequencies most sensitive to core-size are: 1657 ( $\nu_{10}$ ), 1599 ( $\nu_2$ ), 1575 ( $\nu_{11}$ ), 1572 ( $\nu_{19}$ ) and 1514 ( $\nu_3$ ). In particular, the difference in the  $\nu_{10}$  (dp) and  $\nu_{10}$  (dp) and  $\nu_{19}$  frequency of metalloporphyrins is typically  $54 \pm 4 \text{ cm}^{-1}$ , whereas in BrCoOEP it is  $82 \text{ cm}^{-1}$  [49]. Comparison of the spectra of Co(II)OEP and BrCo(III)OEP and [(MeOH)Co(III)OEP]Br [24] reveals that all of the RR frequencies between 1300 -  $1700 \text{ cm}^{-1}$  are essentially identical for the three complexes, with the exception of  $\nu_{10}$  and  $\nu_{19}$ . In the spectra of BrCo(III)OEP the  $\nu_{10}$  frequency is elevated and the  $\nu_{19}$  frequency lowered from typical values. We have speculated that this results from a severe structural perturbation in solution [24], and doming of the porphyrin with the metal ion significantly out of the plane has been suggested [49,53]. The elevation of  $\nu_{10}$  is puzzling, however, as both ruffling and doming

distortions are expected lower both of these frequencies by  $\sim 15\text{ cm}^{-1}$  [52]. We have not been able to obtain crystals of this compound suitable for x-ray crystallography.

Although the  $\nu_3$  frequency for  $[(\text{CO})\text{Co}(\text{III})\text{OEP}]\text{ClO}_4$  is somewhat less than that of  $\text{BrCoOEP}$ , the similarity of the other vibrational frequencies and the Soret maxima of these two complexes attests to shared structural features. We have noted [24] that a  $\mu$ -nitrido dimer  $(\text{OEPFe})_2\text{N}$  displays some similar spectral features [54] to the bromide complex and have speculated that the severely ruffled porphyrin core of this Fe complex [55] may model the  $\text{Co}(\text{III})$  complexes studied here. Shelnutt *et al.* [56] have pointed out that aggregates of some metallouroporphyrins display similarly blue-shifted Soret absorbances. Our dilution studies show no concentration dependence of the Soret absorbance of  $\text{BrCoOEP}$ , as would be expected for a dimer or aggregate. At any rate, the solution structure of these five-coordinate  $\text{Co}(\text{III})$  complexes most likely involves some distorted porphyrin conformation. This conformation perhaps makes the ligation of the sixth ligand more difficult, keeping the equilibrium constant  $K_2$  relatively low.

## REFERENCES

- [1] (a) Stynes, D.V., Stynes, H. C., James, B. R. and Ibers, J. A. *J. Am. Chem. Soc.* **1973**, *95*, 1796-1801. (b) Collman, J. P., Brauman, T. R. H. and Suslick, K. S. *Proc. Natl. Acad. Sci. USA*, **1976**, *73*, 3333-3337 (b) Jones, R. D., Summerville, D. A. and Basolo, F. *Chemical Reviews* **1979**, *79*, 139-179 (c) Liu, H. -Y., Abdalmuhdi, I., Chang, C. K. and Anson, F. C. *J. Phys. Chem.* **1985**, *89*, 665-670
- [2] (a) Wayland, B. B. and Mohajer, D. *J. Am. Chem. Soc.* **1971**, *93*, 5295-5296 (b) Wayland, B. B., Minkiewicz, J. V. and Abd-Elmageed, M. E. *J. Am. Chem. Soc.* **1974**, *96*, 2795-2801 (c) Wayland, B.B.; Mehne, L. F. and Swartz, J. *J. Am. Chem. Soc.* **1978**, *100*, 2379-2149
- [3] Kozuka, M. and Nakamoto, K. *J. Am. Chem. Soc.* **1981**, *103*, 2162-2168
- [4] Urban, M. W., Nakamoto, K. and Kincaid, J. *Inorganica Chim. Acta* **1982**, *61*, 77-81
- [5] Nakamoto, K. Paeng, I. R., Kuroii, T., Isobe, T. and Oshio, H. *J. Mol. Struc.* **1988**, *189*, 293-300
- [6] Tsubaki, M. and Yu, N.-T. *Proc. Natl. Acad. Sci. USA* **1981**, *78*, 3581-3585
- [7] Bajdor, K., Nakamoto, K and Kincaid, J. *J. Am. Chem. Soc.* **1983**, *105*, 678-679
- [8] for a review see: Yu, N. -T., & Kerr, E. A. in *Biological Applications of Raman Spectroscopy*, vol 3, **1988** Spiro, T. G., Ed., p39-95
- [9] Mackin, H. C., Tsubaki, M. and Yu, N. -T. *Biophys. J.* **1983**, *41*, 349-357
- [10] (a) Odo, J., Imai, H., Kyuno, E. and Nakamoto, K. *J. Am. Chem. Soc.* **1988**, *110*, 742-748 (b) Proniewicz, L. M., Odo, J., Góbral, J., Chang, C. K. and Nakamoto, K. *J. Am. Chem. Soc.* **1989**, *111*, 2105-2110 (c) Proniewicz, L. M., Bruha, A., Nakamoto, K., Kyuno, E. and Kincaid, J. R. *J. Am. Chem. Soc.* **1989**, *111*, 7050-7056
- [11] (a) Bajdor, K., Kincaid, J. R. and Nakamoto, K. *J. Am. Chem. Soc.* **1984**, *106*, 7741-7747 (b) Kincaid, J. R., Proniewicz, L. M., Bajdor, K., Bruha, A. and

Nakamoto, K. *J. Am. Chem. Soc.* **1985**, 107, 6775-6781 (c) Proniewicz, L. M. and Kincaid, J. *J. Am. Chem. Soc.* **1990**, 112, 675-681

[12] (a) Woodruff, W. H., Spiro, T. G. and Yonetani, T. *Proc. Natl. Acad. Sci. USA* **1974**, 71, 1065-1069 (b) Woodruff, W. H., Adams, D. H., Spiro, T. G. and Yonetani, T. *J. Am. Chem. Soc.* **1975**, 97, 1695-1698

[13] (a) Barlow, C. H.; Maxwell, J. C., Wallace, W. J. and Caughey, W. S. *Biochem. Biophys. Res. Commun.* **1973**, 55, 91-95 (b) Potter, W. T., Tucker, M. P., Houtchens, R. A. and Caughey, W. S. *Biochemistry* **1987**, 26, 4699-4707

[14] (a) Kitagawa, T., Ondrias, M. R., Rousseau, D. L., Ikeda-Saito, M. and Yonetani, T. *Nature* **1982**, 298, 869-871 (b) Thompson, H. M., Yu, N.-T. and Gersonde, K. *Biophys. J.* **1987**, 87, 289-295 (c) Bruha, A. and Kincaid, J. R. *J. Am. Chem. Soc.* **1988**, 110, 6006-6014

[15] (a) Frew, J. E. and Jones, P. In *Advances in Inorganic and Bioinorganic Mechanism*; Academic Press: New York, **1984**; Vol. 3, pp175-212 (b) Groves, J. T. In *Cytochrome P-450: Structure, Mechanism and Biochemistry*; Ortiz de Montellano, P., Ed.; Plenum Press: New York, **1986**; Chapter 1

[16] Dolphin, D., Forman, A., Borg, D. C., Fajer, J. and Felton, R. H. *Proc. Natl. Acad. Sci. USA* **1971**, 68, 614-618

[17] Fuhrhop, J.-H., Kadish, K. M. and Davis, D. G. *J. Am. Chem. Soc.* **1973**, 95, 5140-5147

[18] Oertling, W. A., Salehi, A., Chang, C. K. and Babcock, G. T. *J. Phys. Chem.* **1989**, 93, 1311-1319

[19] Sandusky, P. O., Salehi, A., Chang, C. K. and Babcock, G. T. *J. Am. Chem. Soc.* **1989**, 111, 6431-6439

[20] Sandusky, P. O., Oertling, W. A., Chang, C. K. and Babcock, G. T. *J. Phys. Chem.* **1991**, 95, 4300-4307

[21] (a) Morishima, I., Takamuki, Y. and Shiro, Y. *J. Am. Chem. Soc.* **1984**, 106, 7666-7672 (b) Godziela, G. M. and Goff, H. M. *J. Am. Chem. Soc.* **1986**, 108, 2237-2243

[22] Czernuszewicz, R. S., Macor, K. A., Li, X. Y., Kincaid, J. R. and Spiro, T. G. *J. Am. Chem. Soc.* **1989**, 111, 3860-3869

[23] Salehi, A., Oertling, W. A., Babcock, G. T. and Chang, C. K. *J. Am. Chem. Soc.* **1986**, 108, 5630-5631

[24] Oertling, W. A., Salehi, A., Chung, Y. C., Leroi, G. E., Chang, C. K. and Babcock, G. T. *J. Phys. Chem.* **1987**, 91, 5887-5898

- [25] Mu, X. H. and Kadish, K. M. *Inorg. Chem.* **1989**, 28, 3743-3747
- [26] Hu, Y., Han, B. C., Bao, L. Y., Mu, X. H. and Kadish, K. M. *Inorg. Chem.* **1991**, 30, 2444-2446
- [27] Herlinger, A. W. and Brown, T. L. *J. Am. Chem. Soc.* **1971**, 93, 1790-1791
- [28] Jones, L. H., McDowell, R. S. and Goldblatt, M. *Inorg. Chem.* **1969**, 11, 2349-2363
- [29] Wang, C. B. and Chang, C. K. *Synthesis* **1979**, 548-459
- [30] Eaton, S. S.; Eaton, G. R. and Chang, C. K. *J. Am. Chem. Soc.* **1985**, 107, 3177-3184
- [31] Falk, J. E. in *Porphyrins and Metalloporphyrins*; Elsevier: New York, **1964**, p798
- [32] Wilson, W. E. B., Jr.; Decius, J. C. and Cross, P. C. in *Molecular Vibrations*, McGraw-Hill: New York, **1955**; Chapter 4
- [33] McIntosh, D. F. and Michaelan, K. H. *Canadian J. Spectr.*, **1979**, 24, 1-10; 35-40; 65-74
- [34] Jones, L. H.; McDowell, R. S. and Goldblatt, M. *Inorg. Chem.*, **1968**, 8, 2350-2363
- [35] Spiro, T. G., Czernuszewicz, R. S. and Li, X. -Y. *Coord. Chem. Rev.* **1990**, 100, 541-571
- [36] Abe, M., Kitagawa, T., and Kyogoku, Y. *J. Chem. Phys.* **1978**, 69, 4526-4534
- [37] (a) Li, X. -Y., Czernuszewicz, R. S., Kincaid, J. R., & Spiro, T. G. *J. Am. Chem. Soc.* **1989**, 111, 7012-7023 b) Li, X. -Y., Czernuszewicz, R. S., Kincaid, J. R., Stein, P., & Spiro, T. G. *J. Phys. Chem.* **1990**, 94, 47-61
- [38] Harris, D. C. and Bertolucci, M. D. in *Symmetry and Spectroscopy*, Dover, **1989**, p93-224
- [39] Yu, N. -T., Kerr, E. A., Ward, B. and Chang, C. K. *Biochemistry*, **1983**, 22, 4534-4540
- [40] Nakamoto, K. in *Infrared and Raman Spectra of Inorganic and Coordination Compounds*, 4th ed., Wiley, 1986, p291-308
- [41] Neya, S., Morishima, I. and Yonezawa, T. *Biochemistry*, **1981**, 20, 2610-1614

- [42] (a) Antonini, E. and Brunori, M. *Hemoglobin and Myoglobin in their Reactions with Ligands*, Neuberger, A. and Tatum, E. L. (Eds.) North-Holland Publishing Company, Frontiers of Biology Vol. 21, 1971 (b) James, B. in *The Porphyrins*, Dolphin, D. (Ed.); Academic: New York, Chapter 6, Vol. V
- [43] Salehi, A. Ph.D. Dissertation, Michigan State University, 1988, p143-155
- [44] (a) Tsutsui, M., Velapoldi, R. A., Hoffman, L., Suzuki, K. and Ferrari, A. *J. Am. Chem. Soc.* 1969, 91, 3337-3341 (b) Whitten, D. G., Baker, E. W. and Corwin, A. *H. J. Org. Chem.* 1963, 28, 2363-2368
- [45] Kim, D., Su, O. Y. and Spiro, T. G. *Inorg. Chem.* 1986, 25, 3988-3993
- [46] Shelnutt, J. A., Straub, K. D., Rentzepis, P. M., Gouterman, M. and Davidson, E. R. *Biochemistry*, 1984, 23, 3946-3954
- [47] Tait, C. D., Holten, D. and Gouterman, M. *J. Am. Chem. Soc.* 1984, 106, 6653-6659
- [48] Wang, M. -Y. R. and Hoffman, B. M. *J. Am. Chem. Soc.* 1984, 106, 4235-4240
- [49] Spaulding, L. D., Chang, C. C., Yu, N. -T., & Felton, R. H. *J. Am. Chem. Soc.* 1975, 97, 2517-2525
- [50] Parthasarathi, N., Hansen, C., Yamaguchi, S. and Spiro, T. G. *J. Am. Chem. Soc.* 1987, 109, 3856-3871
- [51] Sarma, Y. A. *Spectrochimica Acta*, 1989, 45A, 649-652
- [52] Prendergast, K. and Spiro, T. G. *J. Am. Chem. Soc.* 1992, 114, 3793-3801
- [53] Felton, R. H., Yu, N. -T., O'Shea, D. C. and Shelnutt, J. A. *J. Am. Chem. Soc.* 1974, 96, 3675-3676
- [54] Hofmann, J. A. and Bocian, D. F. *J. Phys. Chem.* 1984, 88, 1472-1479
- [55] Scheidt, W. R., Summerville, D. A. and Cohen, I. A. *J. Am. Chem. Soc.* 1976, 96, 6623-6628
- [56] Shelnutt, J. A., Dobry, M. M. and Satterlee, J. D. *J. Phys. Chem.* 1984, 88, 4980-4987

## CHAPTER 3

### Optical and Vibrational Spectroscopies of Oxovanadyl Porphyrin Compounds, Evidence of Hydrogen Bonding to the Oxo Ligand

#### 3.1 Introduction

Heme proteins are involved in a wide range of functions in nature. The oxygen ( $O_2$ ) transporting and storing proteins hemoglobin and myoglobin reversibly bind  $O_2$  with an  $Fe^{2+}$  protoporphyrin active site. Iron protoporphyrins are also found at the active sites of catalytic heme proteins. Catalytic heme proteins initially bind  $O_2$  with iron in the ferrous state. The reaction cycle, however, involves a sequence of steps that change the oxidation states of both the iron and the oxygen. The active intermediates of many catalytic heme proteins are either known or postulated to go through oxoferryl complexes. Oxoferryls are known as intermediates in catalases and peroxidases [1], cytochrome d [2], cytochrome c oxidase [3-5] and the P-450 enzyme [6].

The reported vibrational frequencies for  $\nu(O=Fe^{IV})$  in proteins ranges from  $745\text{ cm}^{-1}$  in lactoperoxidase compound II [7] to  $804\text{ cm}^{-1}$  in cytochrome c oxidase [3-5]. In previously reported oxoferryl model compounds  $\nu(O=Fe^{IV})$  ranged from  $807\text{ cm}^{-1}$  [8] to  $841\text{ cm}^{-1}$  [9] in six coordinate complexes while five

coordinate complexes ranged from  $841\text{ cm}^{-1}$  [10] to  $852\text{ cm}^{-1}$  [11-12]. The large range of observed vibrational frequencies for  $\nu(\text{O}=\text{Fe}^{\text{IV}})$  has been attributed to the strength of the trans ligand [13] and hydrogen bonding to the oxo ligand [14-15]. The large range of vibrational frequencies seen in oxoferryl complexes is not seen in vibrational frequencies of Oxy- $\text{Fe}^{\text{II}}$  complexes. Reported frequencies of  $\nu(\text{O}_2\text{-Fe}^{\text{II}})$  ranged from  $559\text{ cm}^{-1}$  in horse radish peroxidase III [16] to  $572\text{ cm}^{-1}$  in myoglobin [17]. In heme model compounds the reported range of frequencies for  $\nu(\text{O}_2\text{-Fe}^{\text{II}})$  in  $\text{T}_{\text{pivPP}}$  is  $562\text{ cm}^{-1}$  and  $573\text{ cm}^{-1}$  in protoporphyrin. The reported  $\nu(\text{O}_2\text{-Fe}^{\text{II}})$  frequencies for the heme models is essentially the same as the frequencies for heme proteins.

Free oxoiron(IV) porphyrin species are unstable above  $-30^\circ\text{C}$  [8-13]. Therefore, other oxometals such as chromium [18-20], manganese [21-24], ruthenium [25] and vanadium [26, 33] have been used to gain an understanding of oxoferryl intermediates in the reduction of oxygen.

In nature, examples of vanadium are, for the most part, restricted to marine organisms [27-29]. However, the use of vanadium substituted proteins, owing to their stability has proved a useful method in understanding biological functionality [30-31]. To probe environmental effects on oxovanadyl systems Su et al.[26] have carried out detailed studies of solvent effects on oxovanadyl porphyrin systems. They have shown that a linear correlation occurs between  $\nu(\text{V-O})$  and the solvent acceptor number established by Gutmann [32]. The results they obtained on the oxovanadyl porphyrins were correlated with reported  $\nu(\text{Fe-O})$  of oxoferryl porphyrins. Although hydrogen bonding to the oxo ligand was implied in their work, no direct spectroscopic evidence was given.

In this work we show direct evidence for both intermolecular and intramolecular hydrogen bonding to oxovanadyl porphyrins. Intermolecular hydrogen bonding was verified by the deuterium isotope effect. In the

intramolecular hydrogen bonding case, we have established the hydrogen bonding ability of the model compound, naphthyl Kemp's acid porphyrin. Hydrogen bonding from the Kemp's porphyrin is seen in both the acid (NKAP) and amide (NKAmP) forms. The NKAP has a much stronger effect on the oxovanadyl vibration which is consistent with the acid form being a better proton donor than the amide form.

## 3.2 Experimental

### 3.2.1 Oxo[5-(8-Kempacid-1-Naphthyl)-2,8,13,17-Tetraethyl-3,7,12,18-Tetramethyl Porphine]vanadium (1)

The naphthyl Kemp porphyrin derivatives were all synthesized by Ying Liang. A detailed description of the synthetic process will be given in her thesis and corresponding publications. Ten mg (0.01 mmol) NKAP, 15ml acetic acid, 450 mg sodium acetate and 100 mg VO(acac)<sub>2</sub> (Aldrich, 95%) were placed in a round-bottomed flask fitted with a ground glass joint connected to a reflux condenser. The mixture was refluxed under argon and the progress of the reaction was monitored by UV-vis spectroscopy. When a sample, withdrawn with a pipette, indicated that no more complex was being formed (>95% conversion), the reaction was quenched by adding 15 ml of water. The mixture was allowed to stand overnight to form the crystal. The product was collected by filtration and washed with water until the filtrate was colorless. The crude compound was purified by running it over a short column of silica gel with methylene chloride as eluant. This gave the pure product which is red in color. Yield: 9.9 mg (92%). FABMS: m/e, 920. UV-vis:  $\lambda_{\text{max}}$  at 417.5 nm is identified as the porphyrin Soret band. The IR spectra show a strong absorption band at 978 cm<sup>-1</sup> characteristic of an oxovanadyl vibration.

Methylene chloride was freshly distilled before use. VO(acac)<sub>2</sub> (vanadyl acetyl acetate, 95%) and DBN (1,5-diazabicyclo[4,3,0]non-5-ene, 95%) were

purchased from Alderich and used as received. Acetic acid-d (98 atom%D) was purchased from Alderich. HOAc (glacial) was from EM science and NaOAc (anhydrous) were purchased from J. T. Baker.

### 3.2.2 Instrumentation

UV-vis spectral measurements were carried out on a Perkin-Elmer lambda-5 spectrophotometer. Infrared spectra were obtained by layering the porphyrin complex (1) on a NaCl plate, spectra were then recorded on a Nicolet IR/42 spectrometer. FABMS (fast atom bombardment mass spectra) were recorded on a JEOL HX-110 HF double focusing spectrometer operating in the positive ion detection mode. Resonance Raman spectra were recorded on a computer-controlled Spex 1401 double monochromator equipped with photo-counting electronics. Laser excitation at 406.7nm and 413.1nm was provided by a Coherent-Innova Model 90K krypton ion laser. Excitation at 441.7nm was from a He-Cd laser. Preparation conditions for individual samples is given with each spectrum. The integrity of all RR samples was monitored before and after laser excitation by absorption spectroscopy.

### 3.3 Results

Figure 3.1 shows the structures of naphthyl Kemp's acid porphyrin(NKAP) in (a) the free base and (b) the oxovanadyl forms. The crystal structure of the oxovanadyl amide form shows that the proton of the amide is oriented so that the vanadyl, oxo, and acidic protons are at 180°. This orientation is set for maximum hydrogen bonding to the axial oxo ligand. The crystal structure of the free base NKAP reveals that a water molecule is oriented into the "pocket" such that hydrogen bonding occurs between the acid proton and the oxygen of water. Correspondingly, a water proton and the carbonyl oxygen are also hydrogen bonded.

**Figure 3-1** (a) The Structure of free base naphthyl Kemp's acid porphyrin showing the acid proton coordinated over the center of the porphyrin ring. (b) The structure of oxovanadyl naphthyl Kemp's acid porphyrin showing the potential for hydrogen bonding between the acid proton and the oxo ligand.

### 3.3.1 Optical Properties

Figure 3.2 shows the optical absorption spectra of oxovanadyl naphthyl Kemp's acid porphyrin {NKAP(VO)} in the protonated (solid line) and deprotonated (dashed line) forms. In the deprotonated compared to the protonated acid we observe a 4nm blue shift in the Soret band from 417.5nm to 413.5nm. This blue shift is accompanied by a 30% increase in the extinction coefficient. If, however, we calculate the oscillator strength from:

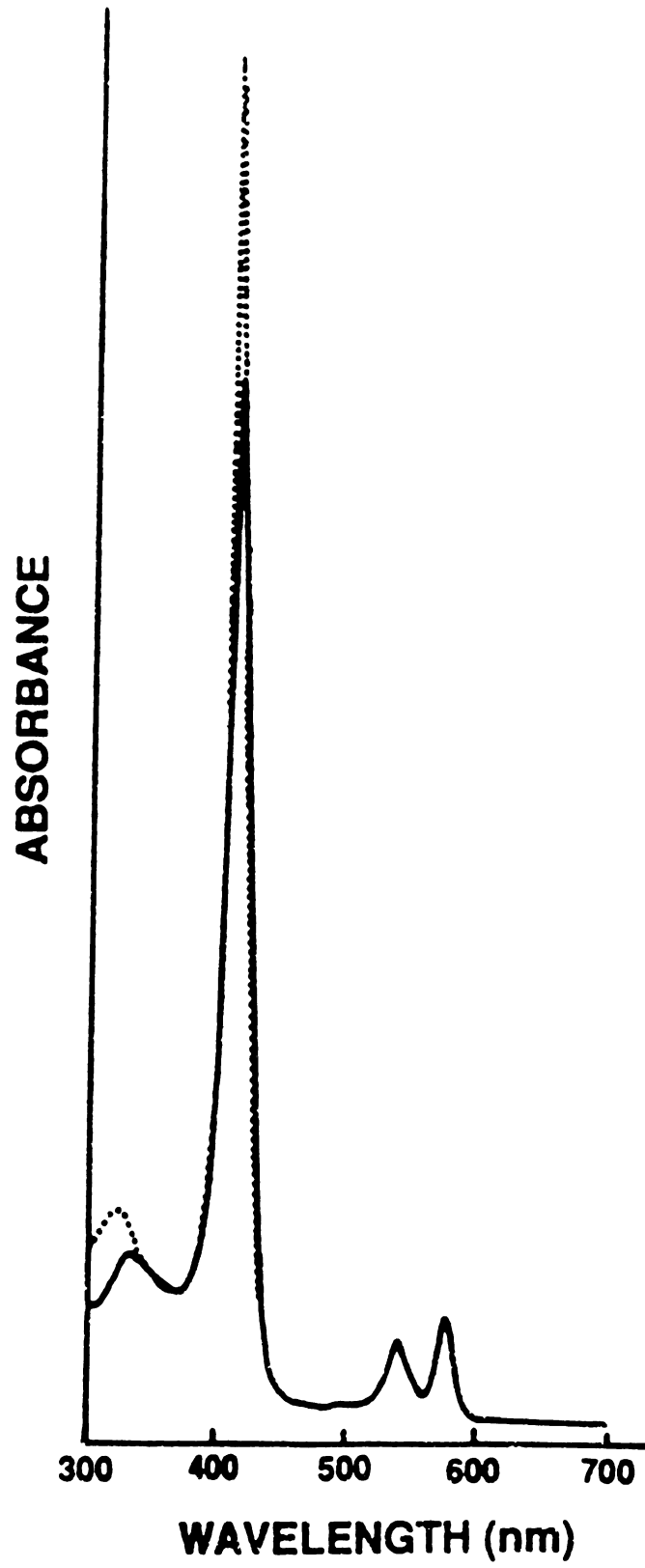
$$f = 4.33 \times 10^{-9} \int_0^{\infty} \epsilon(\bar{\nu}) d\bar{\nu} \quad \text{eq. 1}$$

we find that it remains unchanged. Since the Soret band arises from the allowed  $\pi$  to  $\pi^*$  transition of the porphyrin system the relatively small shift of the Soret band implies that the hydrogen bond interaction effects are localized to the VO portion of the molecule.

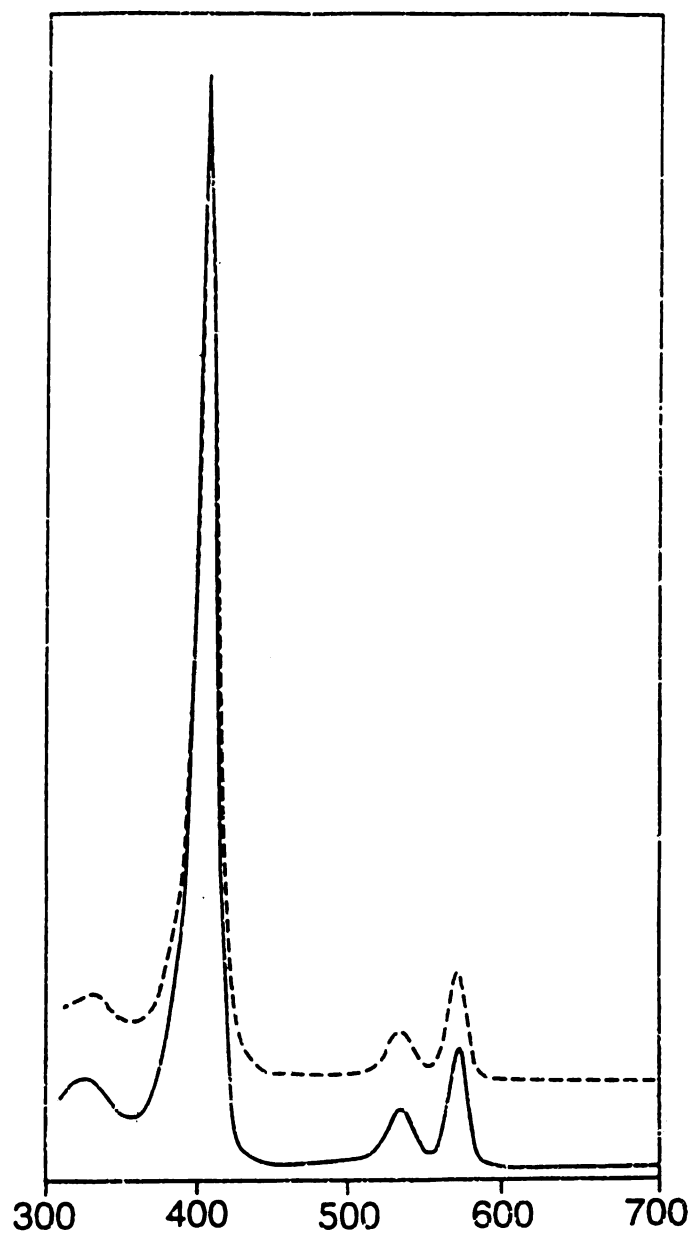
The Q bands in the visible region of the absorption spectrum show no apparent effect from the removal of the acidic proton. This implies that the energy levels and subsequent orbital interactions are only slightly affected by hydrogen bonding to the axial ligand.

Figure 3.3 shows the optical spectra of oxovanadyl octaethyl porphyrin {OEP(VO)} in pure methylene chloride (solid line) and a 1:1 mixture of methylene chloride and acetic acid. The optical spectra of six-coordinated MPs, when compared to five-coordinated MPs, all have characteristic red shifted Soret bands. The bands of OEP(VO) in methylene chloride and acetic acid show no change in the position of the Soret band. Thus, there is no indication of axial coordination by acetic acid to the vanadyl to give a six-coordinate compound. We also tested the coordinating properties of tetra butyl ammonium acetate. The acetate ion,

**Figure 3.2** The optical absorption spectra of oxovanadyl naphthyl Kemp's acid porphyrin, (a) (—) in pure methylene chloride and (b) (....) in methylene chlorided with 1-2% 1,5-diazabicyclo[4,3,0]one-5ene.



**Figure 3..3** The optical absorption spectra of oxovanadyl octaethyl porphyrin (—) in pure methylene chlorided and (....) in a mixture of 50% methylene chlorided and 50% acetic acid.



with

ac-

Th

co

io

C

b

f

a

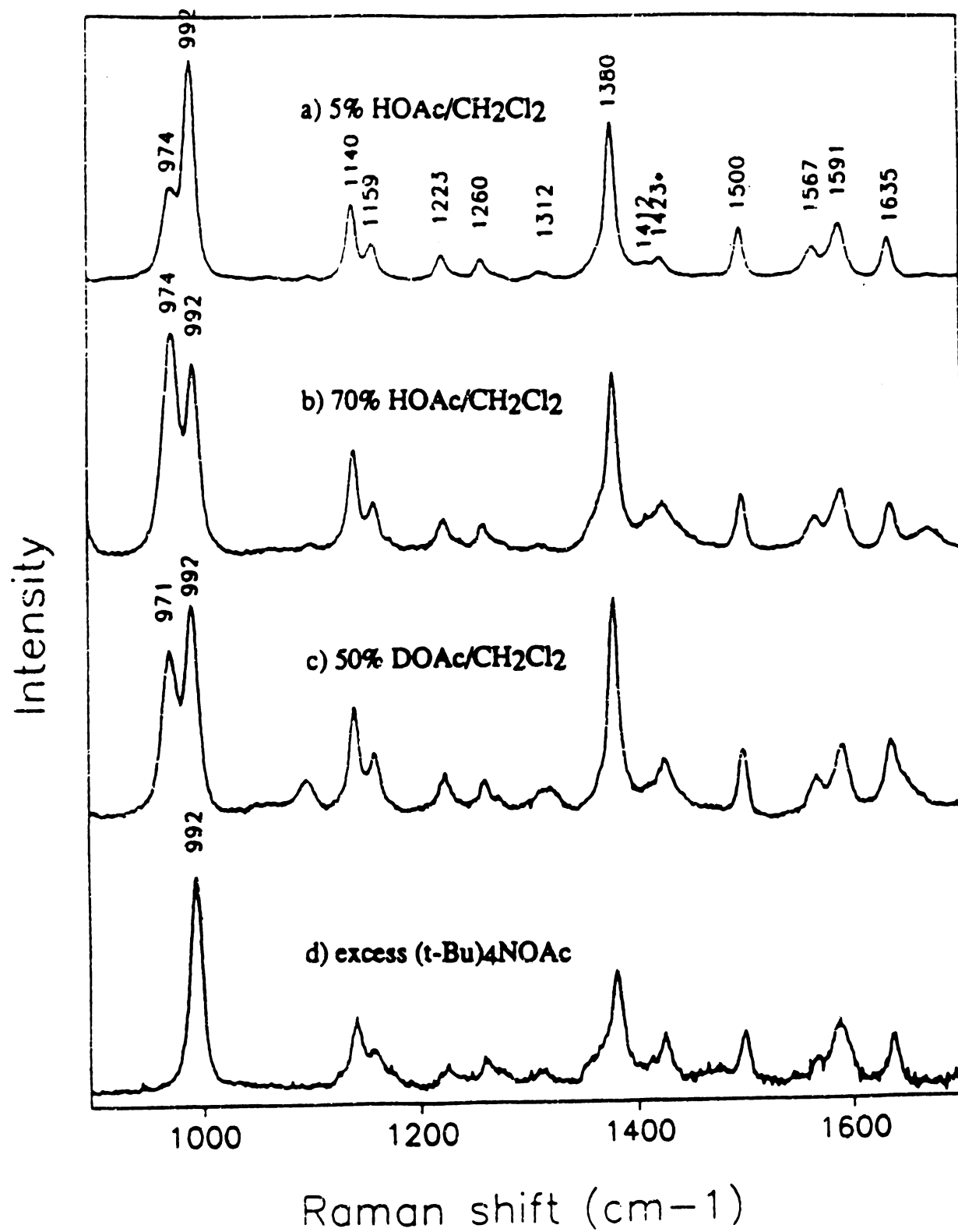
c

with its full negative charge should be a better coordinating ligand than acetic acid. However, we found that the acetate ion does not coordinate to OEP(VO). The optical results are verified by resonance Raman spectra that show no six-coordinate character for OEP(VO) in the presence of acetic acid or the acetate ion.

### 3.3.2 Resonance Raman

Figures 3.4a and 3.4b show the RR spectra, with  $\lambda_{ex} = 413.1$  nm, of OEP(VO) in  $\text{CH}_2\text{Cl}_2$  with various concentrations of acetic acid (HOAc) or tetra butyl ammonium acetate. Figure 3.4c is the RR spectra of OEP(VO) in DOAc and figure 3.4d is the RR spectrum of OEP(VO) in  $\text{CH}_2\text{Cl}_2$  with tetra butyl ammonium acetate. In spectrum 4a with OEP(VO) in  $\text{CH}_2\text{Cl}_2$  and 5% HOAc the OEP carbon-nitrogen skeletal modes are unaffected by the addition of HOAc. Previous studies of oxovanadyl porphyrins have established that the VO stretching frequency is in the  $1000\text{ cm}^{-1}$  region, thus, we can assign the peak at  $991\text{ cm}^{-1}$  to stretching of the VO bond. In addition to the VO vibrational mode at  $991\text{ cm}^{-1}$  the appearance of an additional band at  $974\text{ cm}^{-1}$  is detected. The intensity of this band is dependent on the concentration of acetic acid present in the sample. This intensity dependence is evident in spectrum 3.4b where we have OEP(VO) in 75% acetic acid and 25% methylene chloride solvent. In spectrum 3.4c we used deuterated acetic acid at a 1:1 ratio with methylene chloride. Spectrum 3.4c is the first reported evidence that the oxovanadyl bond is sensitive to direct hydrogen bonding. Hydrogen bonding is a factor in the acceptor number calculated by Gutmann [31]. However, there are no previously reported cases of a deuterium isotope effect to verify the presence of hydrogen bonded (VO)porphyrins. The three wavenumber shift to lower energy for  $\nu(\text{VO})$  is consistent with an increased mass for the  $(\text{H}\cdots\text{O})\text{-V}$  oscillator system. To verify

**Figure 3.4** Resonance Raman spectra obtained from 413.1 nm excitation of OEP(VO) in (a) 95% methylene chloride and 5% acetic acid (b) 25% methylene chloride and 75% acetic acid (c) in 50% methylene chloride and 50% deuterated acetic acid (d) in methylene chloride and an excess of tetrabutyl ammonium acetate. Optical absorption spectra were taken before and after the Raman spectra to ensure the integrity of the sample.



that this is indeed hydrogen bonding and not a six-coordinate complex we used an excess of tetra butyl ammonium acetate. In spectrum 4d we can see that  $\nu(\text{VO})$  is located at  $991\text{ cm}^{-1}$  or in the same position as  $\nu(\text{VO})$  in pure  $\text{CH}_2\text{Cl}_2$ . According to Gutmann's calculations acetic acid has a high coordination number. From our results, however, we conclude that the major effect of acidic acid on OEP(VO) is the formation of a hydrogen bond between oxovanadyl and the acid proton.

Figure 3.5b is the RR spectrum of NKAP(VO) in pure methylene chloride. Using the assignments of Abe et. al. [34] we can establish that the vibrational modes between  $1000$  and  $1700\text{ cm}^{-1}$  are all identified as etio porphyrin vibrations. The vibrational mode at  $978\text{ cm}^{-1}$  we assign as the VO stretch of the intramolecular hydrogen bonded NKAP(VO) complex. Evidence that the vibrational mode at  $978\text{ cm}^{-1}$  is due to intramolecular hydrogen bonded oxovanadyl comes from Figure 3.5a. Figure 3.5a is the RR spectrum of NKAP(VO) in methylene chloride and 1-2% DBN. Although the porphyrin core vibrations are unaffected by the addition of DBN, the peak at  $978\text{ cm}^{-1}$  is shifted  $13\text{ cm}^{-1}$  to higher energy. This shows an increase in the VO bond strength. We interpret this as a removal of the acidic proton and the corresponding hydrogen bond. Removal of the hydrogen bond allows the electron density of the hydrogen bond to localize into the VO bond.

Figure 3.6a is the RR spectrum of OEP(VO) in pure methylene chloride. We can identify the usual porphyrin core vibrations; the additional peak at  $991\text{ cm}^{-1}$  is identified as the VO stretching vibration. Figure 3.6b is the RR spectrum of OEP(VO) in methylene chloride and excess DBN. We detect no signs of peak shifts from Fig. 3.6a and conclude that DBN, at the concentrations that we are using, does not act as a sixth ligand to the vanadyl.

**Figure 3.5** Resonance Raman spectra obtained from the 413.1 nm excitation of oxovanadyl naphthyl Kemp's acid porphyrin, (a) in pure methylene chloride and (b) in methylene chlorided with 1-2% 1,5-diazabicyclo[4.3.0]one-5-ene. Optical absorption spectra were taken before and after the Raman spectra to ensure the integrity of the sample.

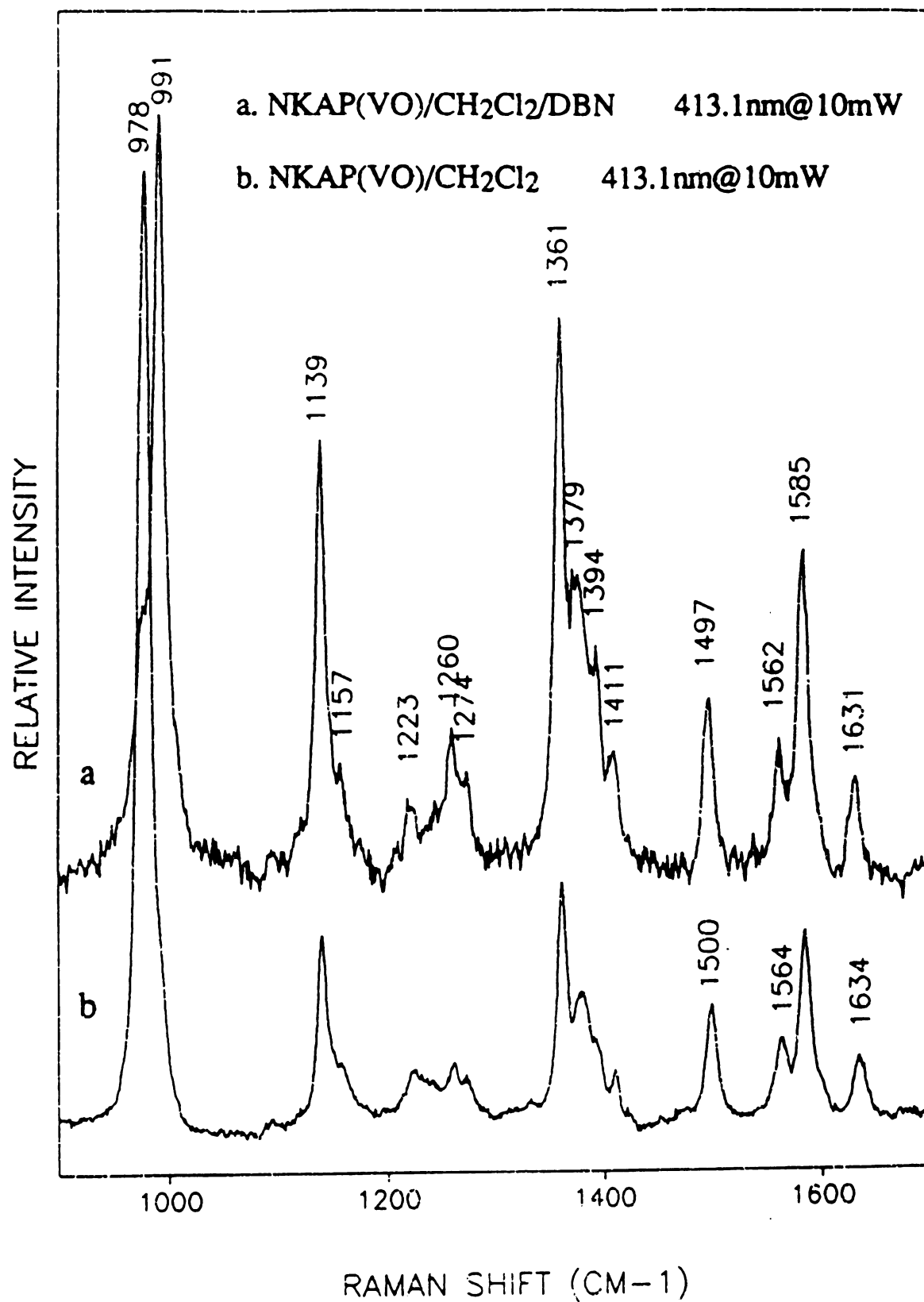


**Figure 3.6** Resonance Raman spectra obtained from 413.1 nm excitation of OEP(VO) in (a) in pure methylene chloride and (b) in methylene chlorided with an excess of 1,5-diazabicyclo [4,3,0]one-5-ene. Optical absorption spectra were taken before and after the Raman spectra to ensure the integrity of the sample.

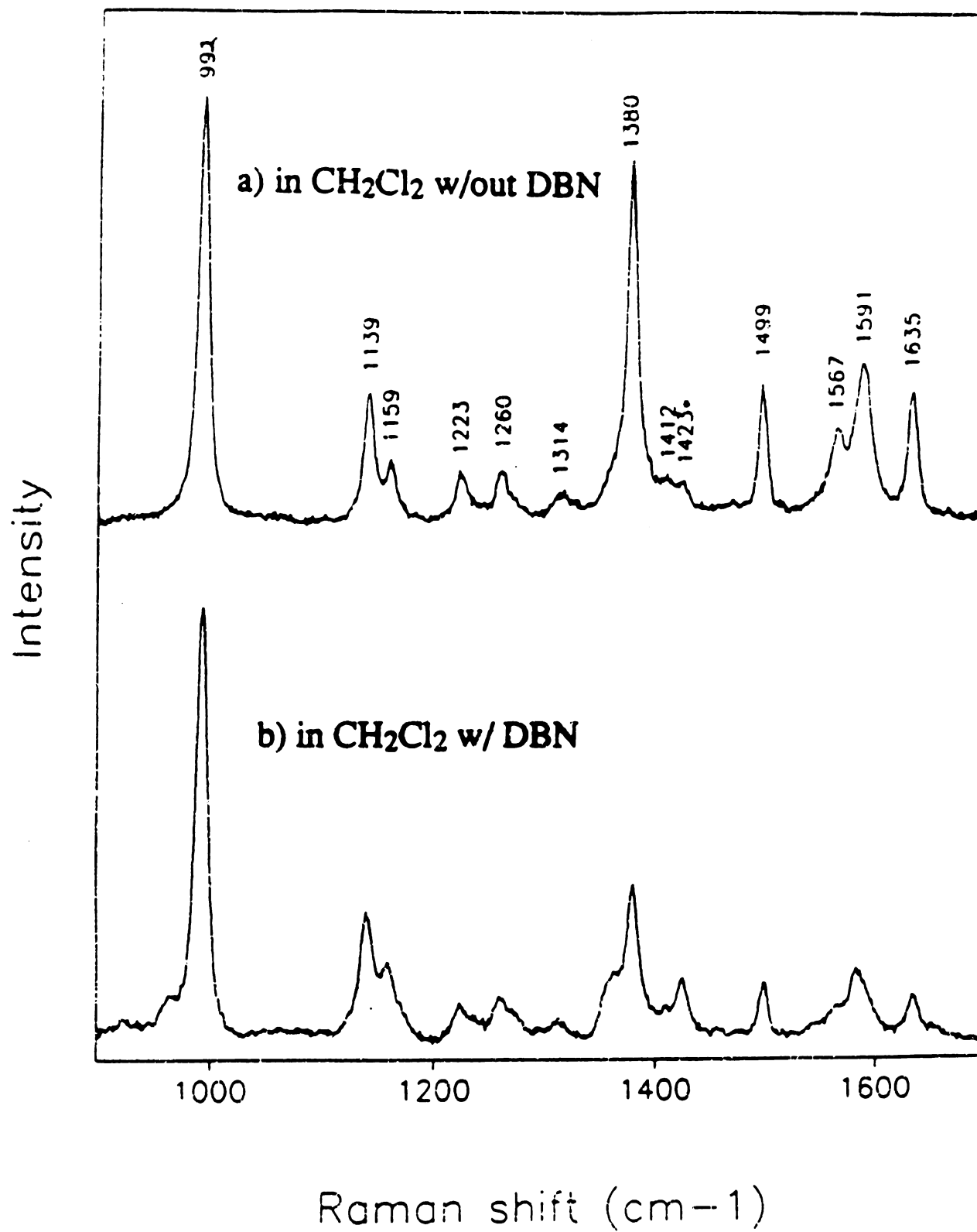
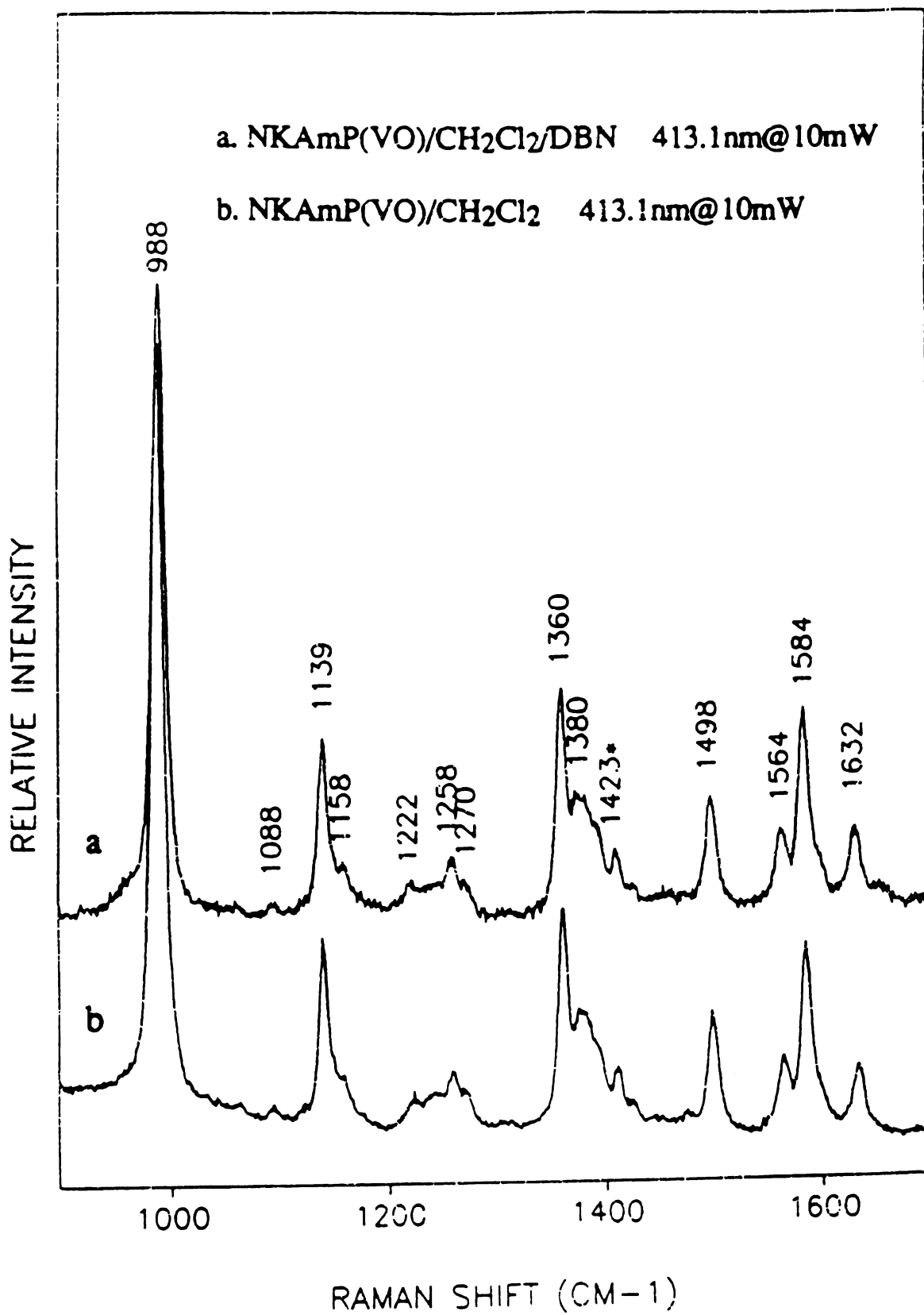


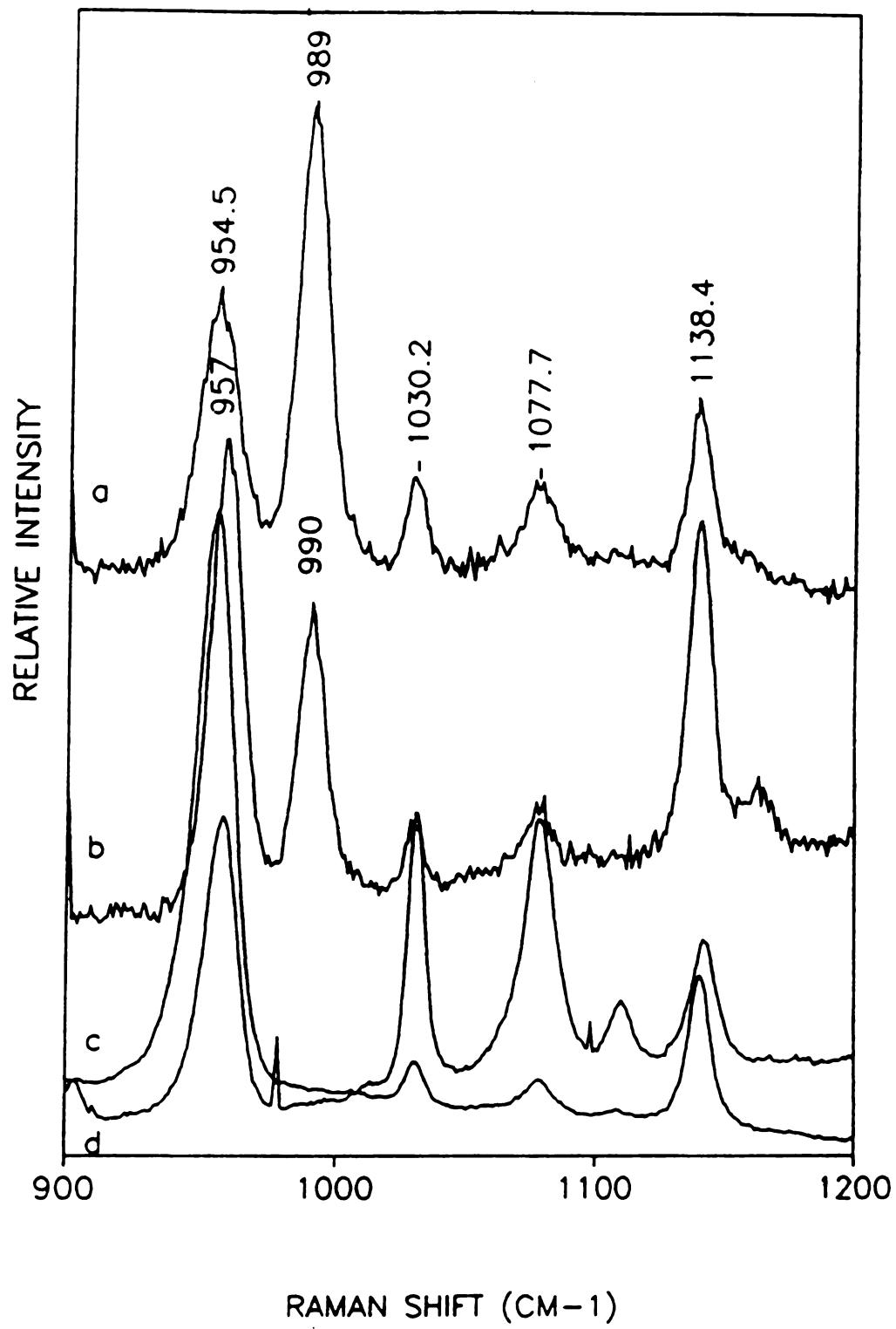
Figure 3.7 is the RR spectra of oxovanadyl naphthyl Kemp's amide porphyrin (NKAmP(VO)) in methylene chloride (a) with DBN and (b) without DBN. DBN is a relatively weak base compared to amide and we expect the amide to remain fully protonated in the presence of DBN. Comparison of 3.7a with 3.7b shows that no effect from DBN is detectable. We established above that DBN does not coordinate to the vanadyl. Since DBN does not coordinate and it is a relatively weak base compared to amide we can predict that the frequency of VO will not be affected in the presence of DBN. The results seen in Figs. 3.7a and 3.7b verify that no effect from DBN is seen.

Figure 3.8 is the RR spectra of OEP(VO) and NKAmP(VO) N-methyl Imidazole at either 406.7 nm or 441.1 nm laser excitation. At these wavelengths we can selectively excite the six-coordinate complex (441.1 nm) or a mixture of the five and six-coordinate complexes (406.7 nm). In both the five and six-coordinated NKAmP(VO) forms we see a  $3\text{ cm}^{-1}$  shift of  $\nu(\text{VO})$  relative to the  $\nu(\text{VO})$  of OEP(VO). From these results it is evident that the effect on  $\nu(\text{VO})$  can not be accounted for simply in terms of solvent to metal interactions. The properties of N-methyl imidazole are similar to those of pyridine and we expect similar interactions from these solvents. The VO vibration in the five-coordinate OEP(VO) complex is at  $989\text{ cm}^{-1}$  and at  $957\text{ cm}^{-1}$  for the six-coordinate complex. The VO vibration of NKAmP(VO) is  $988\text{ cm}^{-1}$  for the five-coordinate compound and  $954\text{ cm}^{-1}$  for the six-coordinate compound. The six-coordinate compound for both NKAmP(VO) and OEP(VO) have the same  $3\text{ cm}^{-1}$  difference for  $\nu(\text{VO})$  in N-methyl imidazole as is seen in methylene chloride. In the five-coordinate compounds, in N-methyl imidazole,  $\nu(\text{VO})$  for NKAmP(VO) is unaffected relative to methylene chloride while  $\nu(\text{VO})$  for OEP(VO) is down shifted  $2\text{ cm}^{-1}$  relative to  $\nu(\text{VO})$  in methylene chloride. This implies that the solvent effects on the five-coordinate compounds that changes  $\nu(\text{VO})$  are oriented to the oxo side of the

**Figure 3.7** Resonance Raman spectra obtained from the 413.1 nm excitation of oxovanadyl naphthyl Kemp's amide porphyrin, (a) in pure methylene chloride and (b) in methylene chlorided with 1,5-diazabicyclo[4,3,0]one-5-ene. Optical absorption spectra were taken before and after the Raman spectra to ensure the integrity of the sample.



**Figure 3.8** (a) Resonance Raman spectra obtained from the 406.7 nm excitation of oxovanadyl naphthyl Kemp's amide porphyrin, in N-Methyl Imidazole. (b) Resonance Raman spectra obtained from the 406.7 nm excitation of oxovanadyl octaethy porphyrin, in N-Methyl Imidazole. (c) Resonance Raman spectra obtained from the 441.8 nm excitation of oxovanadyl naphthyl Kemp's amide porphyrin, in N-Methyl Imidazole. (d) Resonance Raman spectra obtained from the 441.8 nm excitation of oxovanadyl octaethy porphyrin, in N-Methyl Imidazole.



porphyrin. That is to say, the vanadyl side is unrestricted and if solvent effects are oriented solely to the vanadyl, then solvents should effect both NKAmP(VO) and OEP(VO) vibrations equivalently.

### 3.4 Conclusions

We have presented proof for both intramolecular and intermolecular hydrogen bonding effects on oxovanadyl porphyrin systems. In the intermolecular case we have presented the first deuterium isotope effect on the vanadyl-oxo vibration. The shift to a lower energy when DOAc is used in place of HOAc has the predicted effect since there is an effective mass increase in (D $\cdots$ O)-VOEP versus (H $\cdots$ O)-VOEP oscillators.

Results from Yan and Czernuszewicz [35] working with vanadyl protoporphyrin IX and different alcohols as solvents they report a deuterium isotope effect that was previously undetected [26]. The deuterium isotope effect that they see has the  $\nu(\text{V}=\text{O})$  vibration shifting to a higher energy than the proton effect.

To explain this difference we need to consider the proton releasing ability of the donor solvent. The PKa of acidic acid is 0.7 while the Pka of methanol is 17 [36]. The H-OAc bond is considerably weaker than the H-OCH<sub>3</sub> bond. The effect that this has is that the hydrogen bond of V=O $\cdots$ H-OAc is considerable stronger than the hydrogen bond of V=O $\cdots$ H-OCH<sub>3</sub> in other words the V=O $\cdots$ H of the acid is more of an individual unit, therefor, more prone to the effects of the increased mass of the deuterium substitution.

We have demonstrated the intramolecular hydrogen bonding ability of the recently synthesized Naphthoic Kemp's acid porphyrin and its derivatives. The hydrogen bonding ability was clearly demonstrated by removal of the acidic proton with the demonstrated non-coordinating base DBN. The resulting effects

were manifested in the oxo-vanadyl vibration. The likelihood that steric effects, not hydrogen bonding, is the cause of this interaction seems highly unlikely since the amide form would be equally, if not more, hindering than the acid form of naphthoic Kemp's porphyrin. Furthermore, we rule out the possibility of purely ionic interactions, since removal of the acidic proton of NKAP causes  $\nu(\text{O-V})$  to shift back to the same frequency as  $\nu(\text{O-VOEP})$ . The addition of DBN to NKAmP has no effect on  $\nu(\text{O-V})$ , this implies that some factor is still present to influence  $\nu(\text{O-V})$  and we conclude this factor to be hydrogen bonding to the oxo ligand.

## REFERENCES

- [1] Hewson, W.O. and Hager, L.P. in *The Porphyrins*; Dolphin, D.; Ed.; Academic: New York, 1979, Vol. VII, Chapter 6
- [2] Lochr, T. *Biochem.* **1991**, 30, 11485-11489
- [3] (a) Varotsis, C. and Babcock, G.T. *Biochem* **1990**, 29, 7357-7362  
 (b) Varotsis, C.; Woodruff, W.H. and Babcock, G.T. *J. Biol. Chem* **1990**, 265, 11131-  
 (c) Varotsis, C.; Woodruff, W.H. and Babcock, G.T. *J. Am. Chem. Soc.* **1989**, 111, 6439-  
 (d) Varotsis, C.; Zhang, Y.; Appelman, E.H. and Babcock, G.T. *Proc. Natl. Acad. Sci., U.S.A.* **1992**, 90, 237-241
- [4] (a) Han, S.; Ching, Y.-c. and Rousseau, D.L. *Biochemistry*, **1990**, 29, 1380- (b) Han, S.; Ching, Y.-c. and Rousseau, D.L. *Proc. Natl. Acad. Sci., U.S.A.* **1990**, 87, 2491- (c) Han, S.; Ching, Y.-c. and Rousseau, D.L. *Proc. Natl. Acad. Sci., U.S.A.* **1990**, 87, 8404-
- [5] (a) Ogura, T.; Takahashi, S.; Shinzawa-Itoh, K; Yoshikawa, S. and Kitagawa, J. *J. Biol. Chem.* **1990**, 265, 14721-14723 (b) Ogura, T.; Takahashi, S.; Hirota, S; Shinzawa-Itoh, K; Yoshikawa, S.; Appelman, E.H. and Kitagawa, J. *J. Am. Chem. Soc.* **1993**, 115, 8527-8536
- [6] Watanabe, Y. and Groves, J.T. in *The Enzymes*, Chap. 9, Academic Press, Inc., New York, **1992**
- [7] Reczek, C.M.; Sitter, A.J. and Turner, J. *J. Mol. Spec.*, **1985**?6?,
- [8] Schappacher, M.; Chottard, G. and Weiss, R. *J. Chem. Soc., Chem. Commun.*, **1986**, 93-94
- [9] Gold, A.; Jayaraj, K.; Doppelt, P.; Weiss, K.; Chottard, G.; Bill, E.; Ding, X and Trautwein, A.X. *J. Am. Chem. Soc.*, **1988**, 110, 5756-5761
- [10] Czernuszewicz, R.S. and Macor, K.A. *Raman spectrosc.*, **1988**, 19, 553-557
- [11] Bajdor, K. and Nakamoto, K. *J. Am. Chem. Soc.*, **1984**, 106, 3045-3046

- [12] Proniewicz, Z.L.; Bajdor, K. and Nakamoto, K. *J. Phys. Chem.*, **1986**, *90*, 1760-1766
- [13] Oertling, W.A.; Kean, R.T.; Wever, R. and Babcock, G.T. *Inorg. Chem*, **1989**, *29*, 2633-2645
- [14] Sitter, A.J. Reczek, C.M. and Turner, J. *J. Biol. Chem.*, **1985**, *260*, 7515-7522
- [15] Hashimoto, S.; Tatsuno, Y. and Kitagawa, T. *Proc. Natl. Acad. Sci.*, **1986**, *83*, 2417-2421
- [16] VanWart, H.E. and Zimmer, J. *J. Biol. Chem.*, **1985**, *260*, 8372-8377
- [17] Tsubaki, M.; Nagai, K. and Kitagawa, T. *Biochemistry*, **1980**, *19*, 379-385
- [18] Groves, J.T. and Kruper, W.J.Jr. *J. Am. Chem. Soc.* **1979**, *101*, 3413-3415
- [19] Nill, K.H.; Wasgestian, F. and Pfeil, A. *Inorg. Chem*, **1979**, *18*, 564-567
- [20] Groves, J.T. and Kruper, W.J.Jr. and Nemo, T.E. *J. Mol. Catal.* **1980**, *7*, 169-177
- [21] Tabushi, I. and Koga, N. *J. Am. Chem. Soc.* **1979**, *101*, 6456-6458
- [22] Hill, C.L. and Schardt, B.C. *J. Am. Chem. Soc.* **1980**, *102*, 6374-6375
- [23] Groves, J.T. and Kruper, W.J.Jr. and Haushalter, R.C. *J. Am. Chem. Soc.* **1980**, *102*, 6375-6377
- [24] Willner, I.; Otvos, J.W. and Calvin, M.J. *J. Chem. Soc. Chem Commun.* **1980**, 964-965
- [25] Groves, J.T. and Ahn, K.-H. *Inorg. Chem.* **1987**, *26*, 3833-3835
- [26] Su, O.Y.; Czernuscewicz, R.S.; Miller, L.A. and Spiro, T.G. *J. Am. Chem. Soc.* **1988**, *110*, 4150-4157
- [27] Vilter, H. *Phytochemistry* **1984**, *23*, 1387-1390
- [28] Carlson, R.M.K. *Proc. Nat. Acad. Sci. USA* **1975**, *72*, 2217-2221
- [29] Carlisle, D.B. *Proc. Roy. Soc. London Ser. B.* **1968**, *171*, 31
- [30] Buchler, J.W.; Puppe, L.; Rohbock, K. and Schneehage, H.H. *Ann. N. Y. Acad. Sci.* **1973**, *206*, 116-
- [31] Pettersen, R.C. and Alexander, L.E. *J. Am. Chem. Soc.* **1968**, *90*, 3873-3875

- [32] (a) Mayer, U.; Gutmann, V. and Gerger, W. *Monatash. Chem.*, **1975**, 106, 1235-1257 (b) Gutmann, V. *Electrochem. Acta.*, **1976**, 21, 661-670 (c) Gutmann, V. *The donor-Acceptor Approach to Molecular Interactions*, Plenum: New York, **1978**
- [33] Lin, M.; Lee, M.; Yue, K.T. and Marzilli, L.G. *Inorg. Chem.* **1993**, 32, 3217-3226
- [34] Abe, M.; Kitagawa, T. and Kyogoku, Y. *J. Chem. Phys.* **1979**, 69, 4526-4534
- [35] Yan, Qing and Crenuszewicz, Roman S. Presented at the International Conference on Raman Spectroscopy in Hong Kong
- [36] March, Jerry *Advanced Organic Chemistry* John Wiley & Sons, Inc.: New York 3rd Ed. **1995**

## **CHAPTER 4**

### **Cyanide Titrations of (Cl<sup>-</sup>)Fe(III)porphyrins Followed by Optical Spectroscopy**

#### **4.1 Introduction**

##### **4.1.1 Sol-gel systems**

Sol-gel processes involve the mixing of two liquids that react to give a uniformly mixed material. The concept of mixing liquids allows for complete interactions at the molecular level. If the liquids, once mixed, undergo a chemical reaction, a polymer-like material results. The reaction may occur by itself or it may, in fact, require a catalyst. The reaction proceeds with an increase in viscosity of the liquids; when it reaches a solid state it is known as a solid gel or sol-gel.

Ninety-five percent of the sol-gel processes being used today involve inorganic oxides. To explain this process an example, such as, barium-oxygen and titanium-oxygen will be helpful. In the barium-titanate crystal, barium is next to an oxygen that is next to a titanium, and so on. This leads to a very ordered array within the crystal structure. However, in the sol-gel process, polymerization of these compounds are, indeed, crystalline like in the short range; but, due to the continuous molecular exchange that occurs in liquids the overall product is amorphous and very porous. Trapped within the pores are the solvents that were used; indeed, the sol-gel product, in this respect, resembles a sponge. The product

or sponges, if you will, may be treated with acid, base or whatever appropriate agent will preferentially remove the trapped solvent leaving behind a porous oxide that is somewhat disordered. If you heat the material to evaporate the solvent you end up with a very dense porous material. The more you heat the compound the denser it gets. This density factor comes about from the large surface area created by the pores. In the heating process the system reduces the amount of free energy present and it does so by collapsing in on itself, thus, becoming denser and denser.

Now we have a method of making dense oxide materials at relatively low temperatures. In the case of the gel the viscosity increases as the gel starts to form. At a certain point in the gel's formation, the viscosity is expected to be such to allow for molding of the material into specific shapes such as drawn fibers, shaped blocks, thin films and many more [1].

#### **4.1.2 Cyanide detection systems**

If we consider the sponge like nature of sol-gel materials, in the dried form we have a product with interconnecting pores that are approximately 100 Angstroms in diameter. With controlled heating, the pore size can be adjusted to smaller sizes. The pores may be impregnated with organic molecules with any of a variety of properties. In our case, we were looking for a suitable material to act as a cyanide detector.

The optical properties of iron porphyrins are well established [2]. Likewise the strong propensity of cyanide anions for ferric porphyrins is well known [3]. It then seems reasonable to make thin film sol-gel sheets and impregnate these with a ferric porphyrin to act as a cyanide ligand trapping agent. The optical

properties of the unligated and the ligated forms could be used to establish the concentration of cyanide present in the test solution.

#### **4.1.3 Properties of substituted phenyl tetraphenyl porphyrins**

The spin state of an  $\text{Fe}^{\text{III}}$ porphyrin is dependent on the ligand field strength of the equatorial [4-7] and axial [8-10] ligands. The more electron withdrawing the macrocycle is, the higher the spin multiplicity[11]. Thus, it is possible to control the spin state by varying the electron withdrawing nature of the peripheral substituents around the porphyrin macrocycle.

To understand the environmental influences, various model complexes have been synthesized and studied. Substituents on the phenyl ring of tetraphenyl porphyrin (TPP) significantly alter the redox potential and subsequent binding properties of the metal center. The redox potentials of  $\sigma$ -bonded perfluoroaryl $\text{Fe}^{\text{III}}$ porphyrins and alkyl $\text{Fe}^{\text{III}}$ porphyrins have been reported by Kadish and coworkers [11-15]. The work of Kadish et al. showed that the redox potentials for  $\text{Fe}^{\text{III}}$ tetraphenyl porphyrins was significantly affected by axial coordinated ligands with differing electron withdrawing properties. The more electron withdrawing the axial ligand is the the higher the oxidation potential of the iron porphyrin.

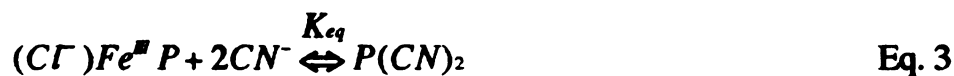
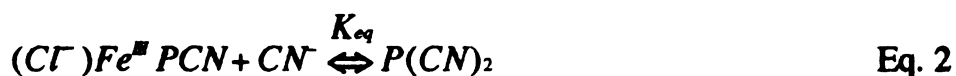
#### **4.2 Experimental**

All samples were prepared in freshly distilled acetonitrile as solvent. Tetrabutyl ammonium cyanide was used as purchased from Fluka chemicals. Stock solutions were freshly prepared at the beginning of each series of titration's. Titrations were followed by electron absorption spectroscopy on a Cary 214 spectrophotometer. A one centimeter path length quartz curette fitted

with an extended neck was used as the titration vessel. Tetrabutyl ammonium cyanide samples were prepared by weighing out tetrabutyl ammonium cyanide and dissolving in a known volume of freshly distilled  $\text{CH}_3\text{CN}$ .

### 4.3 Results

Analysis of the coordination of cyanide to the different porphyrins used in this study can be made through the following equations:



In all the titration curves of the various porphyrins there is only one observable isosbestic point. This leads to the conclusion that only one of the equations above is valid for our studies. Equation 2 can be ruled out as the binding scheme since it has two stepwise additions of cyanide to the porphyrins. Equation 3 is unlikely since bis coordinated cyanide porphyrins require significantly higher concentrations of cyanide than those with which we are working with [17]. The likely conclusion then, is that eq. 1 accounts for the binding scheme of cyanide to the various fluoro-substituted phenyl tetraphenyl porphyrins.

From eq. 1 we define  $K_{eq}$  as:

$$K_{eq} = \frac{[\text{NCFe}^{\text{III}}\text{P}]}{[\text{Fe}^{\text{III}}\text{P}][\text{CN}]} \quad \text{eq. 4}$$

Experimental binding data are often analyzed with the fractional saturation term  $\bar{Y}$  [3a], so,

$$K_{eq} = \frac{\bar{Y}}{(1 - \bar{Y})[L]} \quad \text{eq. 5}$$

where  $[L]$  represents the concentration of the binding ligand. Ligand binding titrations can be followed quantitatively by optical spectroscopy by using the following relationships:

$$\bar{Y} = (A - A_0) / (A_\infty - A_0) \quad \text{eq. 6}$$

or

$$\bar{Y} / (1 - \bar{Y}) = (A - A_0) / (A_\infty - A) \quad \text{eq. 7}$$

where  $A_0$  is the optical absorbance at a given wavelength  $\lambda$  with no ligand present.  $A_\infty$  is the optical absorbance at  $\lambda$  for the fully ligated compound and  $A$  is the optical absorbance at  $\lambda$  at any time during the titration. If we combine eqs. 4-7 we have [16]:

$$\frac{1}{A - A_0} = \frac{1}{K_{eq}(A_\infty - A_0)[CN^-]} + \frac{1}{A_\infty - A_0} \quad \text{eq. 8}$$

Equation 8 can be used so that a plot of  $1/(A - A_0)$  versus  $1/[CN^-]$  gives a straight line and an equilibrium constant can be calculated from the slope and intercept values. The titration curves are shown in Figure 1 through Figure 6 on the following pages.

Table 4.1 below is a tabulation of the calculated equilibrium constants for the ferric porphyrin chlorides in Figure 1 through Figure 6. The calculated values reflect the average of 2 to 4 calculations.

Table 4.1. Equilibrium constants for the room temperature binding of the cyanide anion the Fe(III) porphyrins.

compound	$K_{eq}$
$Fe^{III}T(pentaFP)P-Cl$	$3.61 \cdot 10^{-7} M^{-1}$
$Fe^{III}T(PFP)P-Cl$	$2.59 \cdot 10^{-7} M^{-1}$
$Fe^{III}TPP-Cl$	$1.12 \cdot 10^{-7} M^{-1}$
$Fe^{III}T(PMP)P-Cl$	$4.59 \cdot 10^{-8} M^{-1}$
$Fe^{III}OEP-Cl$	$5.01 \cdot 10^{-8} M^{-1}$
$Fe^{III}Porphycene$	$1.02 \cdot 10^{-7} M^{-1}$

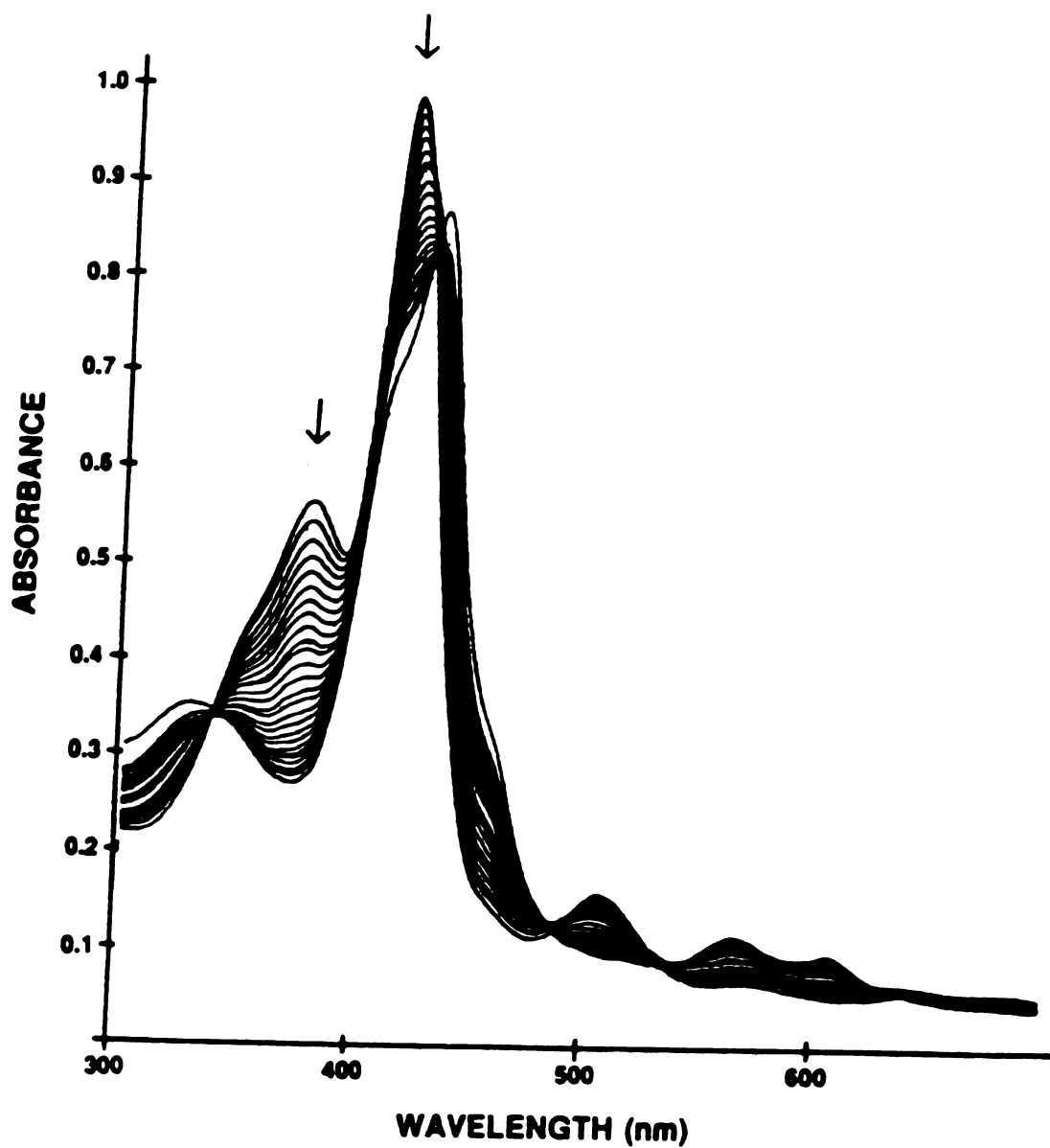


Figure 4.1 Titration curve of (para-fluoro) tetraphenyl porphyrin (Fe<sup>III</sup>)chloride (Fe<sup>III</sup>(P-F)TPPCl) in acetonitrile (CH<sub>3</sub>CN) titrated with tetrabutyl ammonium cyanide in CH<sub>3</sub>CN.

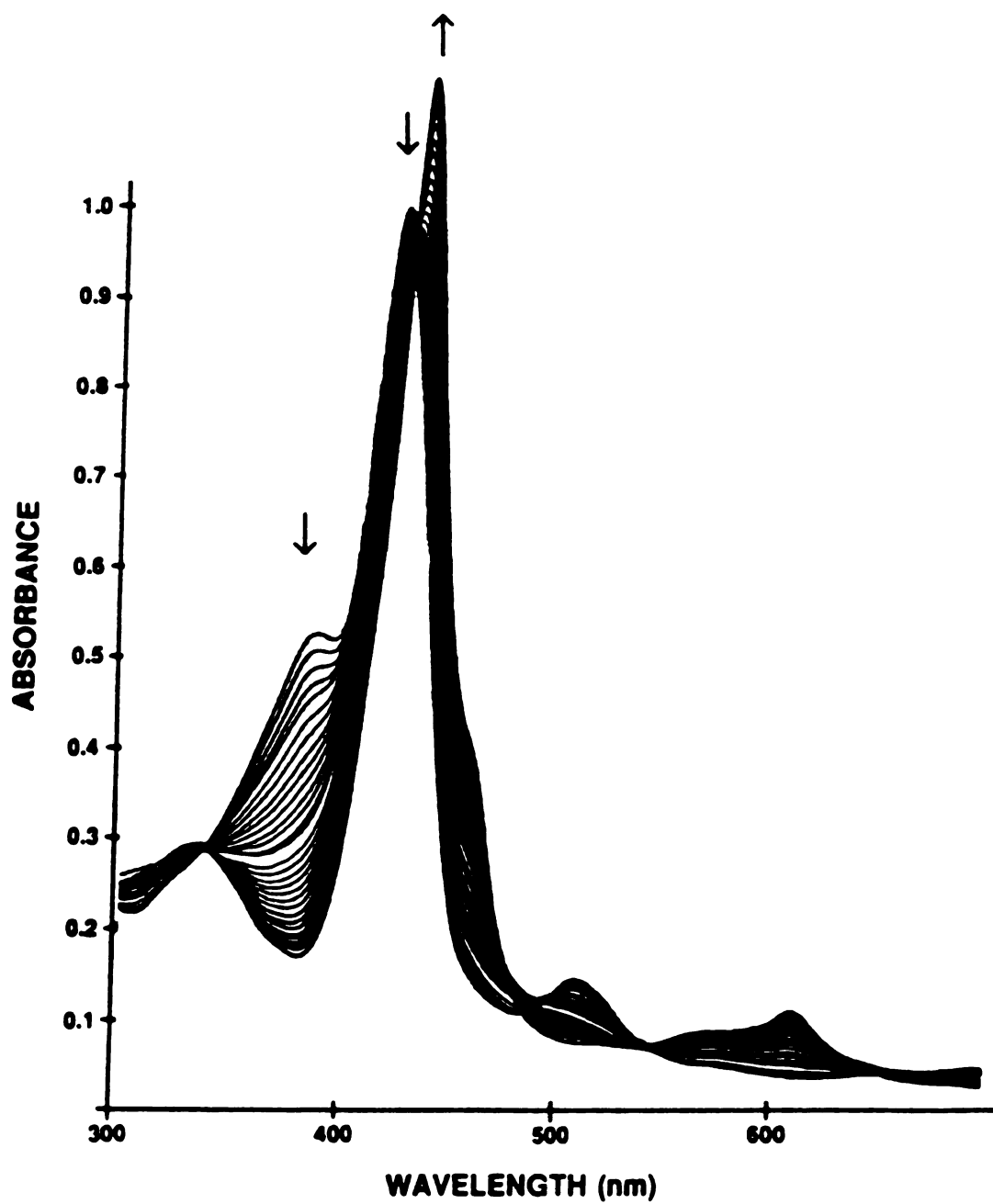


Figure 4.2 Titration curve of tetraphenyl porphyrin (Fe<sup>III</sup>)chloride (Fe<sup>III</sup>TPTMPCl) in acetonitrile (CH<sub>3</sub>CN) titrated with tetrabutyl ammonium cyanide in CH<sub>3</sub>CN.

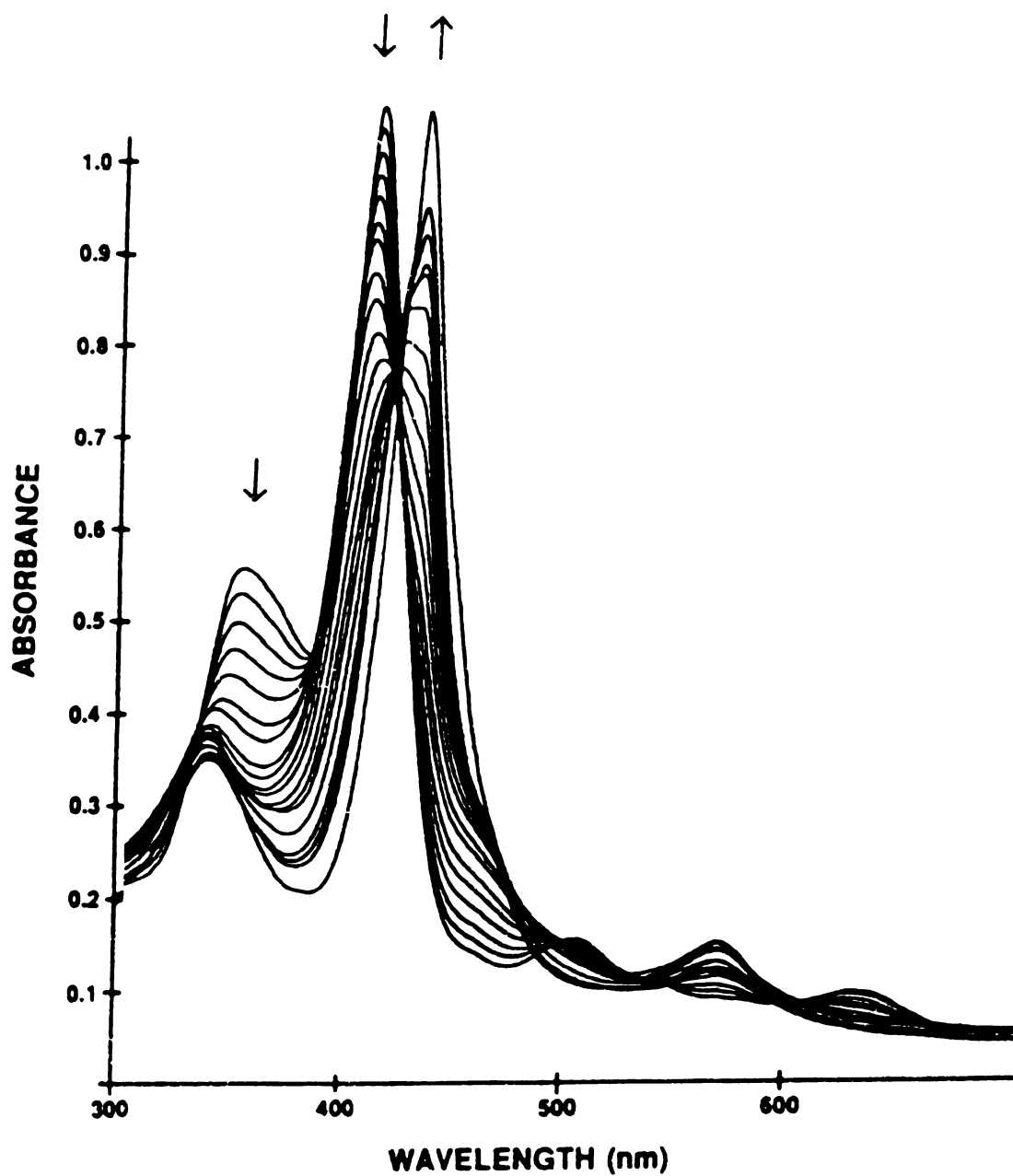


Figure 4.3 Titration curve of (pentafluoro) tetraphenyl porphyrin ( $\text{Fe}^{\text{III}}$ )chloride ( $\text{Fe}^{\text{III}}(\text{PentaF})\text{TPPCl}$ ) in acetonitrile ( $\text{CH}_3\text{CN}$ ) titrated with tetrabutyl ammonium cyanide in  $\text{CH}_3\text{CN}$ .

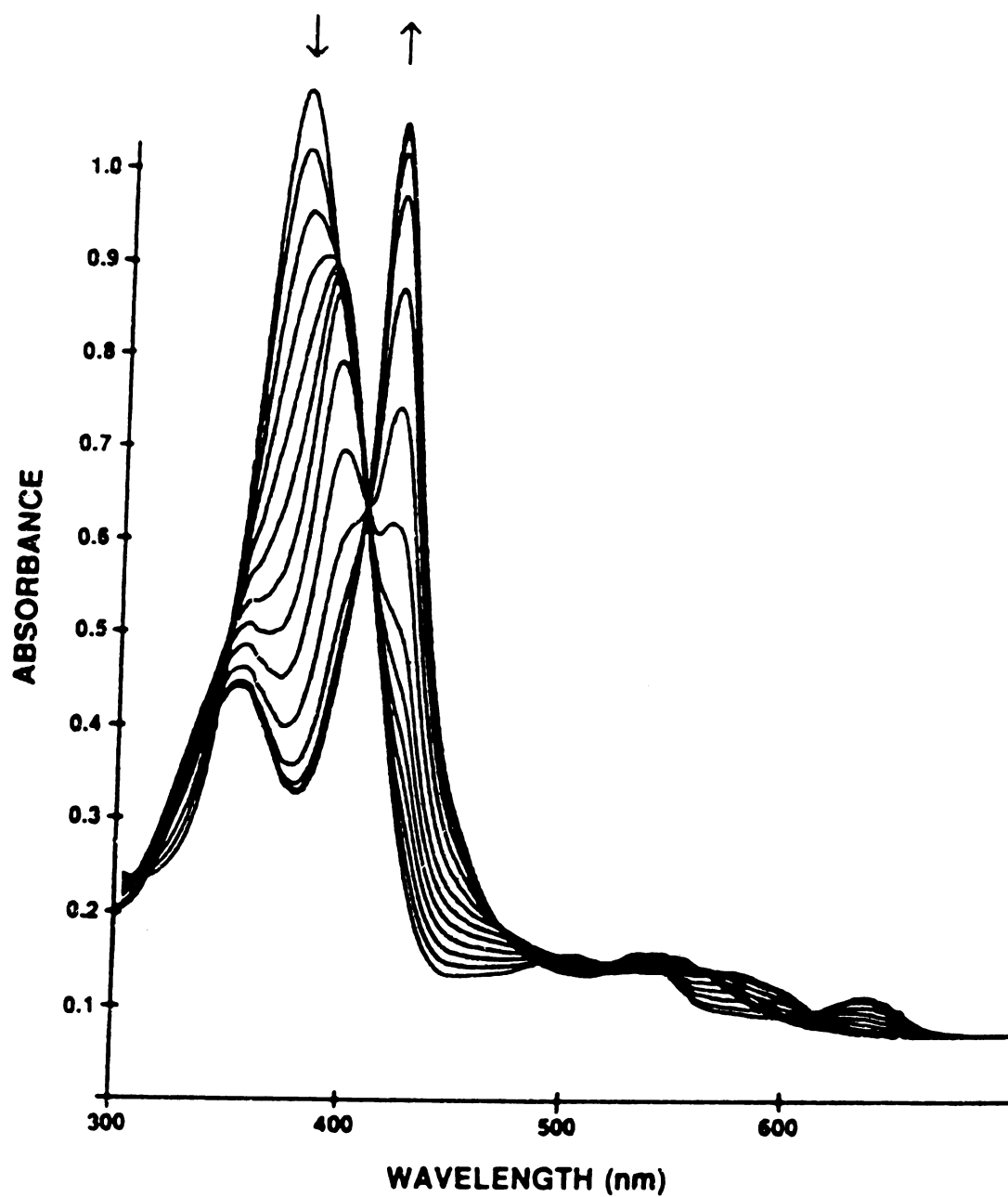


Figure 4.4 Titration curve of Octaethyl porphyrin (Fe<sup>III</sup>)chloride (Fe<sup>III</sup>OEPCI) in acetonitrile (CH<sub>3</sub>CN) titrated with tetrabutyl ammonium cyanide in CH<sub>3</sub>CN.

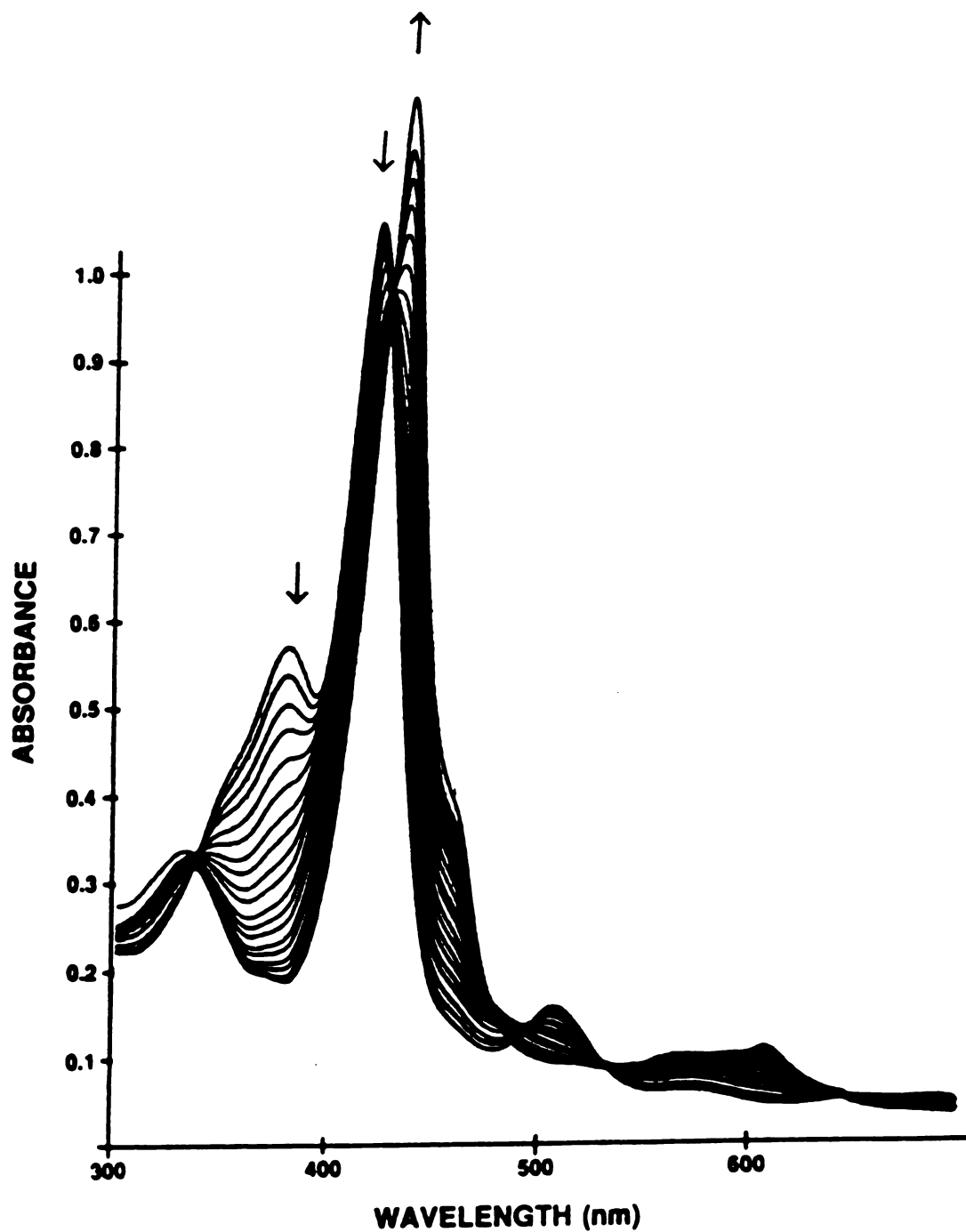


Figure 4.5 Titration curve of tetraphenyl porphyrin (Fe<sup>III</sup>)chloride (Fe<sup>III</sup>TPPCL) in acetonitrile (CH<sub>3</sub>CN) titrated with tetrabutyl ammonium cyanide in CH<sub>3</sub>CN.

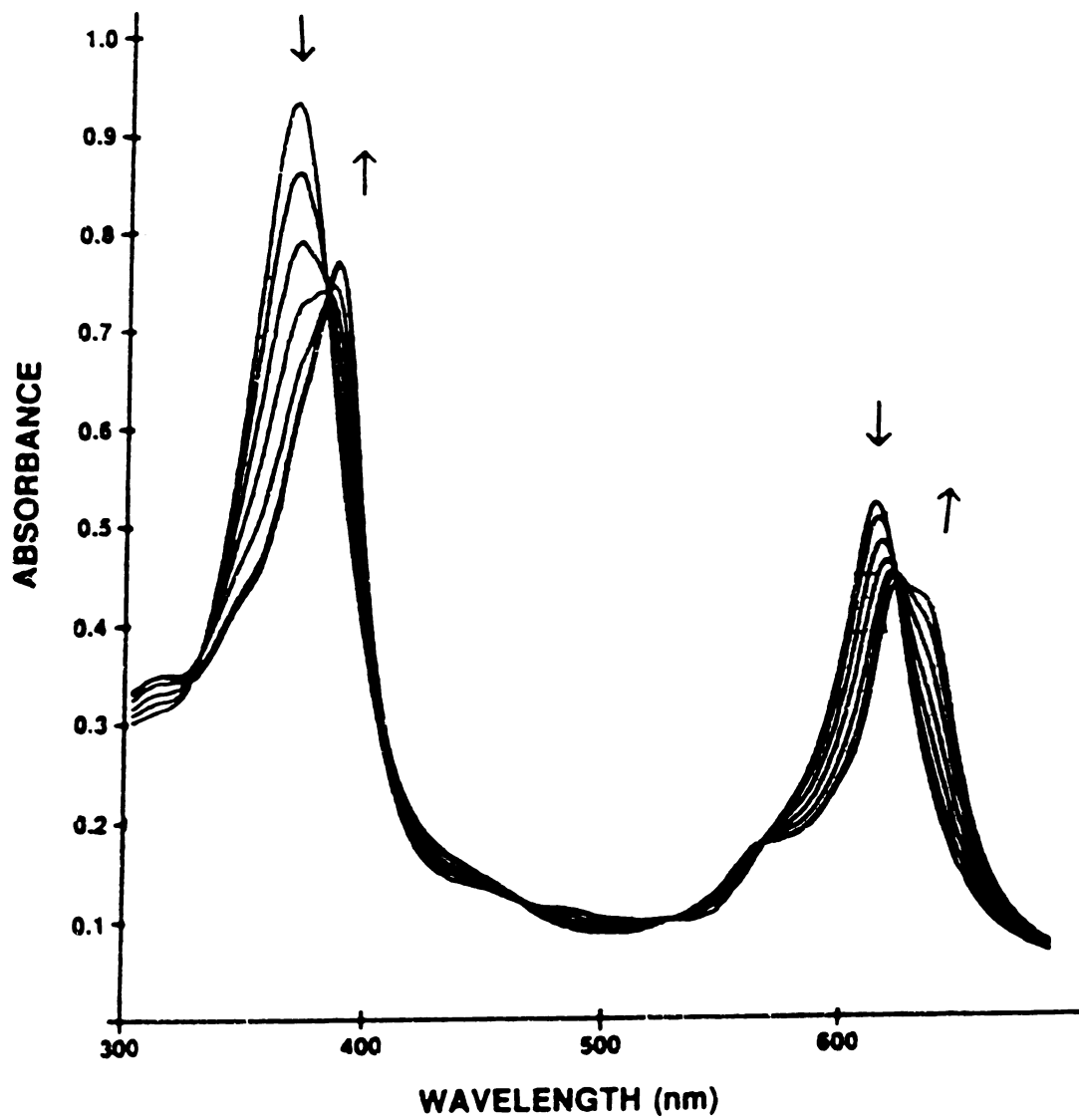


Figure 4.6 Titration curve of porphycene ( $\text{Fe}^{\text{III}}$ )chloride ( $\text{Fe}^{\text{III}}$ Por) in acetonitrile ( $\text{CH}_3\text{CN}$ ) titrated with tetrabutyl ammonium cyanide in  $\text{CH}_3\text{CN}$ .

## 4.4 Discussion

The binding constants of cyanide to the electron withdrawing properties of the peripheral substituents show a direct correlation. The binding constants increase with an increase in electron withdrawing ability of the substituents. This correlation holds true with the exception of porphycene, which we will address later.

Table 2 is a summary of redox potentials, measured by Kadish and coworkers, for  $\sigma$ -bonded perfluoroarylFe<sup>III</sup>porphyrins or  $\sigma$ -bonded chloroFe<sup>III</sup>porphyrins. The properties of these compounds show a direct correlation with the electron withdrawing ability of the axial ligand. First, we can see that the axial ligand is significant in determining the spin state of the metal. If the ligand is more electron withdrawing (better  $\pi$ -acid) then the core iron is more likely to be high spin. Second, it is apparent that the axial ligand is highly significant factor in the redox potential in that, the more electron withdrawing the axial ligand is, the higher the oxidation potential. Third, and more significant to the present work, is that the peripheral substituents of the ring are also a major factor in the redox potential of the iron core. The peripheral substituents, like the axial ligand, increase the oxidation potential when they are electron withdrawing.

In our binding studies the cyanide anion is strongly nucleophilic so it would be intuitive that the higher the oxidation potential of the iron, the easier the anion would be to bind. If we look at our binding constants in table 1 this is exactly the trend we see. The binding constant for Fe<sup>III</sup>OEP-Cl, which has electron donating peripheral substituents, is almost an order of magnitude less than the binding constant for Fe<sup>III</sup>T(pentaFP)P-Cl, which is highly electron withdrawing.

**Table 2 . Half-wave potentials of different (P)Fe(R) and (P)Fe(Cl) complexes in PhCN (0.1) M (TBA)PF<sub>6</sub>). Reproduced from reference 11.**

Porphyrin (P)	axial ligand	spin state	Oxidation		reduction		
			2nd	1st	1st	2nd	3rd
OEP	Cl	r.t. hs		1.08	-0.54	-1.26	-1.95
	C6F5	hs	1.18	0.87	-0.59	-1.3	
	C6F4H	hs	1.14	0.79	-0.64	-1.28	
	C6H5	ls	1.3	0.48	-0.93		
TPP	Cl	hs		1.14	-0.39	-1.09	-1.71
	C6F5	hs	1.38	0.94	-0.42	-1.06	-1.72
	C6F4H	hs	1.32	0.86	-0.45	-1.06	-1.71
	C6H5	ls	1.43	0.61	-0.7		
(m-Me)-TPP	Cl	hs	1.57	1.18	-0.33	-1.08	-1.73
	C6F5	hs	1.36	0.92	-0.42	-1.08	-1.76
	C6F4H	hs	1.31	0.84	-0.46	-1.06	-1.74
(p-Me)-TPP	Cl	hs	1.56	1.13	-0.34	-1.09	-1.77
	C6F5	hs	1.33	0.89	-0.45	-1.09	-1.77
	C6F4H	hs	1.28	0.82	-0.49	-1.07	-1.74
(CN)4TPP	Cl	hs		1.42	0.16	-0.43	-0.85
	C6H5	ls		1.03	-0.03	-0.96	
(p-Et <sub>2</sub> N)-TPP	Cl	hs	0.73	0.59	-0.48	-1.17	
	C6H5	ls	0.58	0.47	-0.83		

In the iron porphycene (Fig. 4.7) we have a molecule that apparently does not follow the trend of the porphyrins in our study. The  $\beta$  and meso carbons of the porphycene molecule are all covalently bound to a hydrogen. Hydrogen would conceptually place porphycene somewhere between Fe<sup>III</sup>T(PMP)P-Cl and Fe<sup>III</sup>TPP-Cl in our cyanide binding study. However, the core of porphycene is larger than the core of regular porphyrins. In all of the porphyrins and the porphycene the fifth ligand is a chloride ion. We know from previous studies that five coordinated metalloporphyrin complexes have the metal out of the plane formed by the four pyrrole nitrogens. The further the metal is pulled out-of-the plane the harder it is to bind a sixth ligand. A possible explanation for the cyanide binding difference of the porphycene, compared to the porphyrins, is that

the iron of the porphycene is not pulled out of the plane as far as the iron of the porphyrins.

The sol-gel systems discussed in the introduction lend themselves well to the introduction of porphyrins, in particular tetraphenyl porphyrins. Keeping in mind that the emphasis of this study was to find a suitable system to prepare cyanide detectors the porphyrin chosen for this purpose was PFPP. The detection system developed from the implementation of PFPP into a sol-gel derived titanium carboxylate thin film was found to be stable over a long period of time, with the properties necessary for accurate detection of cyanide ions over a wide range of concentrations [17].

## REFERENCES

- [1] Mackenzie, J.D. *OE Reports*, **1990**
- [2] Gouterman, M. *The Porphyrins*, Dolphin, D., Ed., Academic: New York Vol. III Chapter 1
- [3] (a) Antonini, E. and Brunori, M. *Hemoglobin and Myoglobin in their Reactions with Ligands*, Neuberger, A. and Tatum, E. L. (Eds.) North-Holland Publishing Company, *Frontiers of Biology* Vol. 21, **1971** (b) James, B. in *The Porphyrins*, Dolphin, D. (Ed.); Academic: New York, Chapter 6, Vol. V
- [4] Scheidt, W.R. and Reed, C.A. *Chem. Rev.*, **1981**, 81, 543
- [5] Scheidt, W.R.; Geiger, D.K. and Haller, K.J. *J. Am. Chem. Soc.*, **1982**, 104, 495
- [6] Scheidt, W.R.; Geiger, D.K.; Hayes, R.G. and Lang, G. *J. Am. Chem. Soc.*, **1983**, 105, 2625
- [7] Behere, D.V.; Birdy, R. and Mitra, S. *Inorg. Chem.*, **1984**, 23, 1978
- [8] Mitra, S. In *Iron Porphyrins*, Lever, A.B.P. and Gray, H.B., Eds.; Addison-Wesley: Reading, MA, **1983**, Part II, Chapter 1
- [9] Scheidt, W.R.; Lee, J.Y. Geiger, D.K.; Taylor, K. and Hantano, K. *J. Am. Chem. Soc.*, **1982**, 104, 3367
- [10] Geiger, D.K. and Scheidt, W.R. *Inorg. Chem.*, **1984**, 23, 1970
- [11] Guillard, R.; Boisselier-Cocolio, B; Tabard, A. Cocolios, P.; Simonet, B. and Kadish, K.M. *Inorg. Chem.*, **1985**, 24, 2509-2520
- [12] Lancon, D.; Cocolios, P.; Guillard, R. and Kadish, K.M. *J. Am. Chem. Soc.*, **1984**, 106, 4472

- [13] Lancon, D.; Cocolios, P.; Guillard, R. and Kadish, K.M. *Organometallics*, **1984**, *3*, 1164
- [14] Kadish, K.M.; Tabard, A.; Lee, W.; Liu, Y.H.; Ratti, C. and Guillard, R. *Inorg. Chem.*, **1991**, *30*, 1542-1549
- [15] Kadish, K.M.; D'Souza, F.; Caemelbecke, E.V.; Villard, A.; Lee, J.-D.; Tabard, A.; and Guillard, R. *Inorg. Chem.*, **1993**, *32*, 4179-4185
- [16] Neya, S., Morishima, I. and Yonezawa, T. *Biochemistry*, **1981**, *20*, 2610-1614
- [17] Bunuwilla, D.D.; Torgerson, B.A.; Chang, C.K. and Berglund, K. A. *Anal. Chem.* **1994**, *66*, 2739-2744

## **CHAPTER 5**

### **Resonance Raman Evidence of the Hydrogen Bonding Effect on $\nu(\text{M-CO})$ where $\text{M} = \text{Fe(II)}$ or $\text{Ru(II)}$ .**

#### **5.1 Background**

Hemoglobin and myoglobin work in tandem to transport and store oxygen in vertebrates. Hemoglobin is found in high concentrations in red blood cells and myoglobin is found in aerobic muscle tissue. Hemoglobin is an  $\alpha_2\beta_2$  heterotetramer that cooperatively binds  $\text{O}_2$  in areas of high oxygen concentration, such as the lungs. The cooperative binding properties allow hemoglobin to become saturated with  $\text{O}_2$ . The  $\text{O}_2$  saturated hemoglobin is transported, in the blood stream, to areas of lower oxygen concentration, such as respiring tissue, where the  $\text{O}_2$  is released and delivered to myoglobin. The structural and functional makeup of the individual  $\alpha$  and  $\beta$  subunits are comparable to myoglobin [1]. Myoglobin, a single polypeptide, is a small globular, oxygen storing protein, made up of eight  $\alpha$ -helices (known as A-H) that form a pocket that constitutes the active site of the protein.

The active site of these proteins contains an iron protoporphyrin IX with iron in the reduced ( $\text{Fe(II)}$ ) oxidation state [2-5]. The iron atom is coordinated to the protein moiety through a histidine at position 8 along the F helix. The

porphyrin through the four pyrrole nitrogens. The remaining binding site of the iron is known as the distal site and this is where exogenous ligand coordination to the iron takes place.

In the reduced state iron, in addition to binding oxygen, is subject to binding by a variety of ligands such as CO, NO, nitroso compounds and alkyl isocyanides [6,7]. Although NO is an important ligand in itself, and the nitroso compounds and alkyl isocyanides are pollutants that we are subject to on an increasing basis, CO is the major competing ligand of O<sub>2</sub> for binding to the reduced iron.

Unhindered model heme compounds are known to favor CO binding over O<sub>2</sub> binding by as much as five orders of magnitude [8-13]. However, when the heme is contained within the protein structure, the CO binding affinity is dropped to less than 200 fold over the O<sub>2</sub> binding. Thus, the proteins are extremely efficient at ligand discrimination, which translates into preservation of the life form since CO is an endogenously produced molecule [14,15].

For hemoglobin and myoglobin to function efficiently as oxygen transport and storage proteins, they must have appropriate kinetic and thermodynamic properties with respect to oxygen binding. The affinity for oxygen, by hemoglobin, must be on the order of  $P_{1/2} = 20$  to  $50 \mu\text{M}$  which is sufficiently low enough to release oxygen in the muscle tissue. In addition to the binding affinity, the association ( $k'_{\text{o}_2}$ ) and dissociation ( $k_{\text{o}_2}$ ) rate constants must be on the order of  $k'_{\text{o}_2} > 10^6 \text{ M}^{-1}\text{s}^{-1}$  and  $k_{\text{o}_2} > 10 \text{ s}^{-1}$  so that rapid release and uptake may occur in muscle tissue and capillary beds [16,17]. The proteins must also be slow to autooxidize to the ferric state and be resistant to denaturing.

### 5.1.1 Proposed ligand discriminations

In 1970 Perutz proposed that the oxygen binding energy differences in various hemoglobins and myoglobins was due to steric hindrance induced by the proximal histidine [18]. The reasoning was that the proximal histidine formed a five-coordinate complex that forced the iron out of the plane of the porphyrin ring. The "pocket" left on the distal side, where ligand binding occurs, makes it difficult for oxygen to bind. The more out plane the iron is, the more difficult it is to bind oxygen. This explanation for the differences in oxygen binding energy works for the case of oxygen but does not explain the protein's ability to discriminate between different ligands.

The question of distal effects as ligand binding mediators in heme proteins has resulted in efforts to discern the role of the E7 distal histidine of the primary amino acid sequence [19-30]. In hemoglobin the E7 histidine is situated closest to the ligand binding site [19,24]. Two possible effects of histidine E7 have been used to explain the phenomenon of ligand discrimination in hemoglobin and myoglobin. One school of thought is that the primary effect of histidine E7 is that it exerts its effect through steric hindrance [14,31] and the other school of thought invokes the hydrogen bonding effect. The argument for the steric hindrance effect arises from the fact that CO is at its maximum binding efficiency when it can bind end on in a linear conformation of Fe-C-O with CO perpendicular to the porphyrin plane. In this orientation the orbital overlap, in the  $\pi$ -back-bonding model of transition metal carbonyl complexes, is at a maximum. Oxygen, in contrast to CO, binds end on in a bent conformation. The bent orientation of Fe-O<sub>2</sub> would not be subject to steric effects of E7 since its hinderance effects would decrease .

The crystal structure of the CO-pyridine-tetraphenylporphyrin complex shows that the CO and pyridine ligands are bound to the metal center in a linear orientation [32]. Recently, however, Gerothanassis et al. [33] have suggested

that the Fe-CO binding orientation of an unhindered "picket fence" model is actually bent. The basis for the bent assignment was the calculated  $^{13}\text{C}$  shielding tensor, which is sensitive to the Fe-CO binding geometry. The calculations were carried out by using data from  $^{13}\text{C}$  CP MAS NMR spectroscopy. X-ray and neutron diffraction studies of CO bound hemoglobin and myoglobin show various orientations of the Fe-CO system; some are bent, others are tilted, while others are bent and tilted [34-39]. This variety of Fe-CO binding orientations would imply that hindrance is not the only factor that can effect the ligand binding discrimination in heme proteins. Kim and Ibers have recently presented crystallographic data on a CO bound "capped" porphyrin. Their study showed that the Fe-C-O bond angle was as much as  $7^\circ$  from linearity, yet there was no detectable effect on the CO binding affinity [40]. Kim et al. have shown results with model compounds that have reduced CO affinity while retaining a linear configuration [41].

## **5.2 Mutagenesis of HisE7 and the effect on CO affinity**

Site directed mutagenesis studies of histidine E7 have given no compelling evidence that steric hindrance is the key factor in ligand binding discrimination. The argument for steric hindrance centers on the concept that larger residues would have a greater hindrance while smaller residues would have a lessened hindrance effect. However, the results to date have not shown these effects. The HisE7Leu mutant has a 30-fold increase in CO affinity over  $\text{O}_2$  affinity [42-44]. This is an exceptionally "high" CO affinity since the norm for other E7 mutants is 2 to 5-fold. In the Gly, Ala and Val mutants, which are considerably smaller side chains than Leu, the CO affinity is at most 5-fold over that of  $\text{O}_2$ . The HisE7Tyr mutant effectively decreases CO affinity by 6-fold [45]. It has been shown that in the mutation HisE7Tyr, in metmyoglobin, that the tyrosine side chain chelates

directly to the ferric iron atom [45,46]. Table 1 is a summary of the reported CO and O<sub>2</sub> affinities of HisE7 mutants.

From the mutagenesis studies presented above, it would appear that steric hindrance is not the major factor of reduced CO affinity in myoglobin. It would seem most likely that the remaining determining factors are the need to displace distal water molecules and/or direct unfavorable electrostatic effects between the ligand and the adjacent amino acid residues. It has been suggested by Rohlfs et al. [47] that a major kinetic barrier to O<sub>2</sub> and CO binding involves the disruption of hydrogen bonding between HisE7 and an adjacent water molecule found in approximately 80 percent of the crystal structures of native or wild type deoxymyoglobins [43]. It is proposed by Quillin et al. that mutation of HisE7 with large apolar residues' results in loss of the water molecule and the resulting effect would be enhanced binding rates of both CO and O<sub>2</sub> [43]. The Fe-CO complex is relatively apolar compared to the Fe-O<sub>2</sub> complex. As a consequence, replacement of HisE7 with aliphatic residues should increase K<sub>CO</sub> by eliminating the need for water displacement. In contrast, the Fe-O<sub>2</sub> complex is highly polar and strongly stabilized by direct hydrogen bonding to HisE7 [13]. Apolar substitution at position E7 prevents this interaction and the net result is a notable decrease in O<sub>2</sub> affinity.

### **5.2.1 CO ligated myoglobin and vibrational spectroscopy**

A large variety of CO ligated heme proteins and model compounds, studied by resonance Raman (RR) and infrared (IR) spectroscopies, have shown an inverse correlation between  $\nu(\text{C-O})$  and  $\nu(\text{M-CO})$  [48-52]. The inverse correlation has been interpreted as resulting from back-bonding from the metal atom to the anti-bonding orbital of CO. Li and Spiro have suggested that a proton donor source near the oxygen atom of the bound ligand may enhance the degree of

protein	$k'_{\text{co}}$ ( $\mu\text{M}^{-1}\text{s}^{-1}$ )	$k_{\text{co}}$ ( $\text{s}^{-1}$ )	$K_{\text{co}}$ ( $\mu\text{M}^{-1}$ )	$k'_{\text{O}_2}$ ( $\mu\text{M}^{-1}\text{s}^{-1}$ )	$k_{\text{O}_2}$ ( $\text{s}^{-1}$ )	$K_{\text{O}_2}$ ( $\mu\text{M}^{-1}$ )	$K_{\text{co}}/K_{\text{O}_2}$
A. Wild-Type							
<i>sperm whale</i> (SW)	0.51	0.019	27	17	15	1.1	25
<i>pig</i>	0.78	0.019	41	17	14	1.2	34
human	0.76	0.022	35	19	22	0.86	41
B. HisE7 Mutants							
<i>E7Gln</i> (SW)	1.0	0.012	82	24	130	0.180	460
<i>E7Gly</i> (SW)	5.8	0.038	150	140	1 600	0.090	1 700
<i>E7Gly</i> (human)	4.1	0.041	100	63	1 200	0.053	1 900
<i>E7Ala</i> (SW)	4.2	0.061	69	53	2 300	0.023	2 800
<i>E7Ala</i> (human)	2.9	0.055	53	46	2 200	0.021	2 500
<i>E7Val</i> (SW)	7.0	0.048	150	110	10 000	0.011	14 000
<i>E7Val</i> (pig)	6.4	0.050	130	110	14 000	0.0077	17 000
<i>E7Val</i> (human)	5.4	0.051	100	84	7 700	0.011	9 100
<i>E7Thr</i> (SW)	6.9	0.045	150	110	6 400	0.017	8 800
<i>E7Leu</i> (SW)	26	0.024	1 100	98	4 100	0.023	48 000
<i>E7Leu</i> (human)	24	0.029	830	120	5 400	0.022	38 000
<i>E7Ile</i> (SW)	8.0	0.047	170	90	6 400	0.014	12 000
<i>E7Ile</i> (human)	5.6	0.044	130	79	11 000	0.0072	18 000
<i>E7Met</i> (SW)	4.6	0.023	200	75	1 700	0.045	4 400
<i>E7Phe</i> (SW)	4.5	0.054	83	75	10 000	0.075	11 000
<i>E7Tyr</i> (SW)	0.50	0.092	5.4	6.7	3 200	0.0021	2 600
<i>E7Trp</i> (SW)	0.65	0.023	28	6.2	87	0.071	390
<i>E7Arg</i> (SW)	5.7	0.014	400	79	880	0.090	4 400
<i>E7Asp</i> (SW)	4.4	0.052	85	d	d	d	d

Table 1. Rate and equilibrium constants for O<sub>2</sub> and CO binding for Mb wild type and mutants. (Reproduced from Springer, B. A.; Sligar, S. G.; Olson, J. S. and Phillips, G. N., Jr. *Chem. Rev.*, 1994, 94, 699-714)

back-bonding [50]. The increased back-bonding would also increase the carbon to metal bonding and the net result would resemble  $M^{\delta(+)}=C=O^{\delta(-)}$  which would manifest itself in an increased  $\nu(M-CO)$  energy and a decreased  $\nu(C-O)$  energy. Although mutations of HisE7 resulted in large increases (Table 1) in CO affinity, the IR spectra of all these mutants have  $\nu(C-O)$  bands in the 1960 to 1970  $cm^{-1}$  region. The mutation of ValE11 with threonine in porcine myoglobin decreased CO affinity 4-5 fold but shifted  $\nu(C-O)$  from 1945 to 1961  $cm^{-1}$  [54] while the replacement of ValE11 with Asn also decreased CO affinity but shifted  $\nu(C-O)$  from 1954 to 1916  $cm^{-1}$  [50,53]. These results, as the previous results, suggest that there is little or no correlation between CO affinity,  $\nu(C-O)$  and Fe-C-O geometry.

### 5.3 Oxygen binding and hydrogen bonding

As mentioned above  $O_2$  binds as an end on bent molecule, therefore, it is largely unaffected by steric hindrance. The iron- $O_2$  complex, unlike the iron-CO complex, is highly polar which makes it subject to stabilization by hydrogen bonding. Evidence for  $O_2$  being hydrogen bonded to HisE7 was reported in cobalt substituted proteins [55-58]. Evidence for the hydrogen bond comes from neutron diffraction and spectral studies including a deuterium isotope effect from vibrational spectroscopy. Studies with "hanging basket" model compounds, show that if the ether linkage is replaced by a proton donating amide linkage, the oxygen binding affinity increases by an order of magnitude while the CO binding affinity remains unaffected [27,59]. Confirmation of a hydrogen bond between the amide and the oxygen was provided by NMR studies [60,61]. Similar reports of enhanced  $O_2$  binding affinities have been reported for model hemes with distal alcohol or secondary amines [62] and phenyl urea substituents [63].

Table 1 lists the CO and oxygen binding parameters for some myoglobin HisE7 mutants. The tabulated results show a strong effect of hydrogen bond donors in the distal pocket. When the strong hydrogen donating histidine ligand is replaced with any of the other listed ligands the oxygen affinity is decreased from one to three orders of magnitude.

Many synthetic model compounds have been prepared that affect the CO and O<sub>2</sub> binding affinities and subsequent spectroscopic properties. However, until recently there has not been a model that is ideally suited to studying the effects of hydrogen bonding to axial ligands.

In chapter 3, using the stable oxovanadyl forms, we established the intramolecular hydrogen bonding of naphthyl Kemp acid porphyrin (NKAP). The usefulness of using stable molecules, as templates, for less stable system is well established [64-70]. In this chapter we will show the effects of hydrogen bonding on the vibrational modes of  $\nu(\text{M-CO})$ , where  $\text{M} = \text{Fe(II)}$  or  $\text{Ru(II)}$ .

## 5.4 Experimental

Raman spectra for the carbon monoxide bound complexes were obtained by using a 90° scattering geometry and were measured with a Spex 1877 monochromator equipped with a CCD detector. Laser emission at 406.7 nm was from a Coherent Innova 90 krypton ion laser. Optical absorption spectra, obtained by using a Perkin-Elmer Lambda 5 spectrometer, were recorded prior to and following Raman studies to confirm sample integrity. Anaerobic quartz cuvettes were used for both the Raman and optical absorption measurements for the carbon monoxide complexes.

Raman spectra of the oxygen bound complexes were obtained by using a 180° scattering geometry on the detector described above. The sample was prepared by dissolving Co(III)KNAP or Co(III)NKAmP in methylene chloride

under an argon atmosphere. To the methylene chloride sample mixture was added an excess of water saturated with sodium dithionite. The dithionite concentration within the mixture was sufficiently high so that any free oxygen that might have been present was reduced to water. At the same time the Co(III)KNAP or Co(III)NKAmP compounds were reduced to Co(II)KNAP or Co(II)NKAmP, respectively. The aqueous and organic layers remained separated. The organic layer, consisting of methylene chloride and Co(II)KNAP or Co(II)NKAmP, was transferred via gas tight syringe into a specially prepared bulb that was attached, with heat shrink tubing, to a removable epr tube [71]. Prior to adding the sample dimethyl formamide (DMF) was placed into the bulb and was carried through several freeze-pump-thaw cycles to remove any oxygen from the DMF. After placing the sample into the bulb we opened the system to vacuum which evaporated the methylene chloride but not the DMF. In this way we were able to degas and reduce the sample while maintaining an aqueous free DMF solvent. Once prepared in DMF the Co(II)KNAP or Co(II)NKAmP sample can be transferred into the epr tube that could be sealed with the heat shrink. A sample holder for the epr tube was previously designed by Tony Oertling [71,72] so that a stream of nitrogen gas could be blown through a dewar of liquid nitrogen and on to the sample. The flow rate of the nitrogen gas stream is used to regulate the temperature of the sample. In this way it was possible to reach temperatures as low as -120°C.

## **5.5 Results**

### **5.5.1 Carbon monoxide bound RuNKAP**

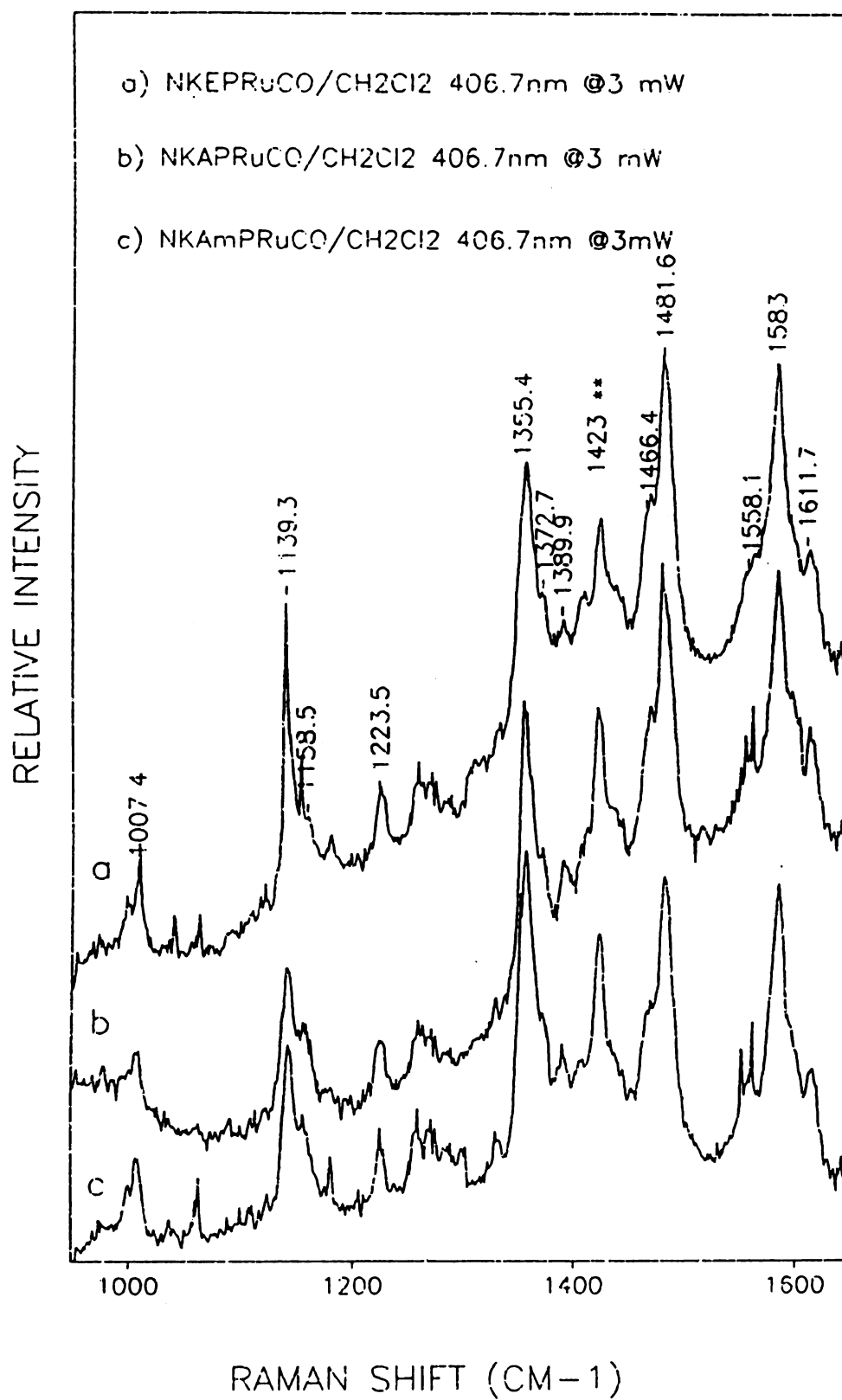
Figure 5.1 a represents the high frequency RR spectrum of CO bound ruthenium naphthoic Kemp's esterporphyrin. Figure 5.1 b represents the high frequency RR spectra of CO bound ruthenium naphthoic Kemp's acidporphyrin.

Figure 5.1 c represents the high range RR spectra of CO bound ruthenium naphthyl Kemp's amideporphyrin. In all of these spectra we identify the usual porphyrin core vibrational modes. These modes are all insensitive to the structure of the Kemp's functional group. Figure 5.2 represents the corresponding low frequency RR spectra of these compounds. In the low frequency spectra we see a vibrational mode in the  $560\text{ cm}^{-1}$  region that is sensitive to the Kemp's functional group. We identify this vibrational mode as the carbon-ruthenium vibration of the CO bound ruthenium Kemp's porphyrin complex. Comparison of the metal-carbon vibrational frequency shows that the acid form of the Kemp porphyrin has the lowest energy while the ester form has the highest energy. This suggests that the CO ligand is more linear in the ester case than in the acid. If steric hindrance is the major factor controlling CO binding discrimination than we expect the opposite results since a methyl group is much bulkier than a proton.

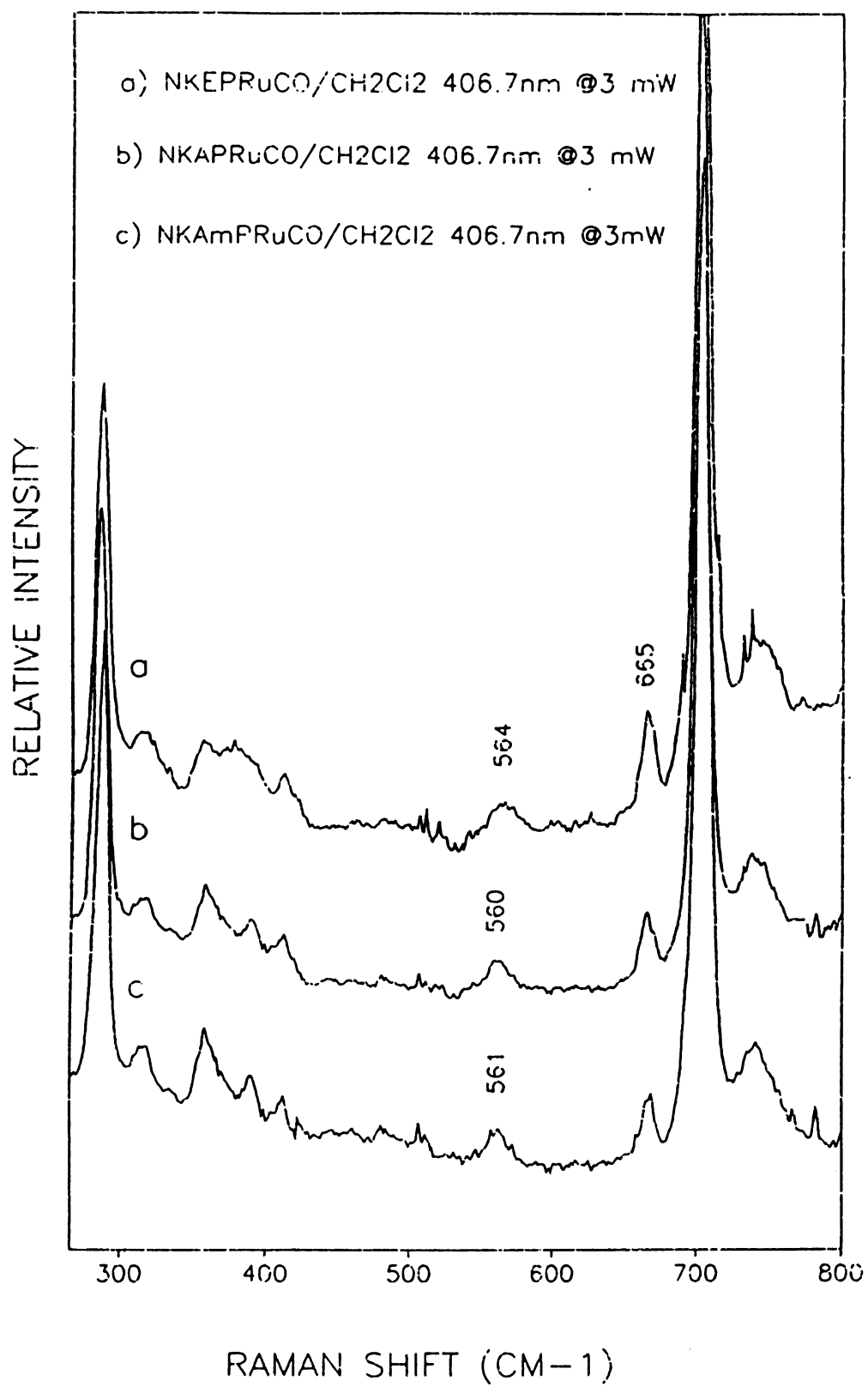
### 5.3.2 Carbon monoxide bound FeNKAP

Figure 5-3 represents the high frequency region RR spectra of CO bound iron(II)porphyrins. In Fig. 5-3a we can identify the usual vibrational modes that are associated with five-coordinated Fe(II) octaalkylporphyrins [73]. Figures 5-3 b, c and d represent the the high frequency region RR spectra of CO bound iron(II) Kemp's ester, amide and acid porphyrins, respectively. The naphthyl substituted meso carbon lowers the  $D_{4h}$  symmetry of the porphyrin with a notable effect on the totally symmetric  $\nu_4$  and  $\nu_5$  vibrations. The  $\nu_5$  mode is shifted to lower energy while  $\nu_4$  becomes split into multiple components. The  $\nu_{10}$  frequency of all four CO ligated Fe(II) porphyrins is located at  $1635\text{ cm}^{-1}$  which is shifted down from the  $1655\text{ cm}^{-1}$  region for typical planar porphyrins. This down shift is consistent with previously reported domed or ruffled

**Figure 5-1** The high frequency resonance Raman spectra obtained with  $\lambda_{\text{ex}} = 406.7$  nm of (a) carbon monoxide bound ruthenium naphthly Kemp's esterporphyrin (b) carbon monoxide bound ruthenium naphthly Kemp's acidporphyrin (c) carbon monoxide bound ruthenium naphthly Kemp's amideporphyrin.



**Figure 5-2** The low frequency resonance Raman spectra obtained with  $\lambda_{\text{ex}} = 406.7$  nm of (a) carbon monoxide bound ruthenium naphthly Kemp's esterporphyrin (b) carbon monoxide bound ruthenium naphthly Kemp's acidporphyrin (c) carbon monoxide bound ruthenium naphthly Kemp's amideporphyrin.



**Figure 5-3** The high frequency resonance Raman spectra obtained with  $\lambda_{\text{ex}} = 406.7$  nm of (a) carbon monoxide bound iron(II) octaethylporphyrin in  $\text{CH}_2\text{Cl}_2$  (b) carbon monoxide bound iron(II) naphthly Kemp's esterporphyrin (c) carbon monoxide bound iron(II) naphthly Kemp's amideporphyrin (d) carbon monoxide bound iron(II) naphthly Kemp's acidporphyrin.

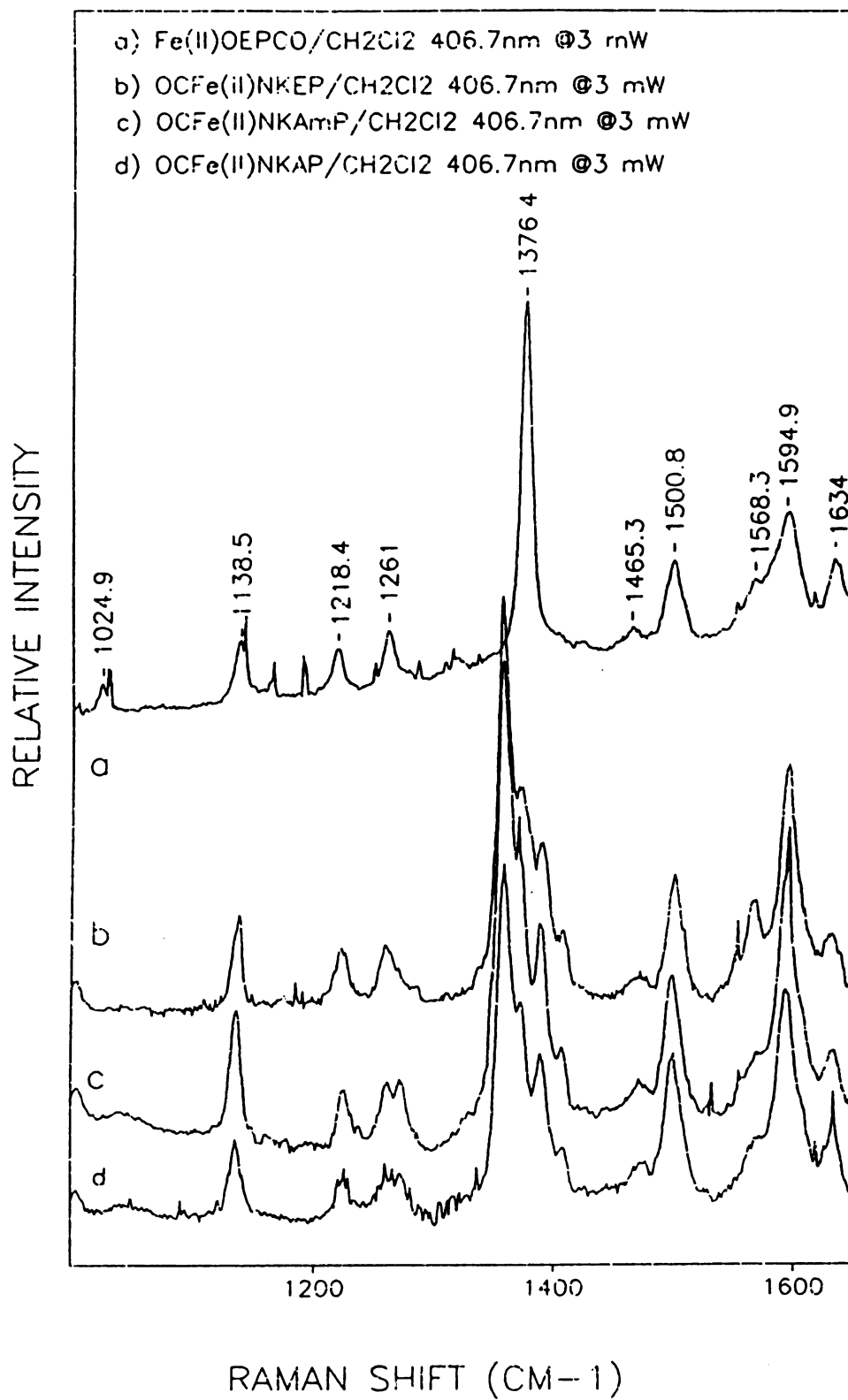


**Figure 5-4** The low frequency resonance Raman spectra obtained with  $\lambda_{\text{ex}} = 406.7$  nm of (a) carbon monoxide bound iron(II) octaethylporphyrin in  $\text{CH}_2\text{Cl}_2$  (b) carbon monoxide bound iron(II) naphthly Kemp's esterporphyrin (c) carbon monoxide bound iron(II) naphthly Kemp's amideporphyrin (d) carbon monoxide bound iron(II) naphthly Kemp's acidporphyrin.

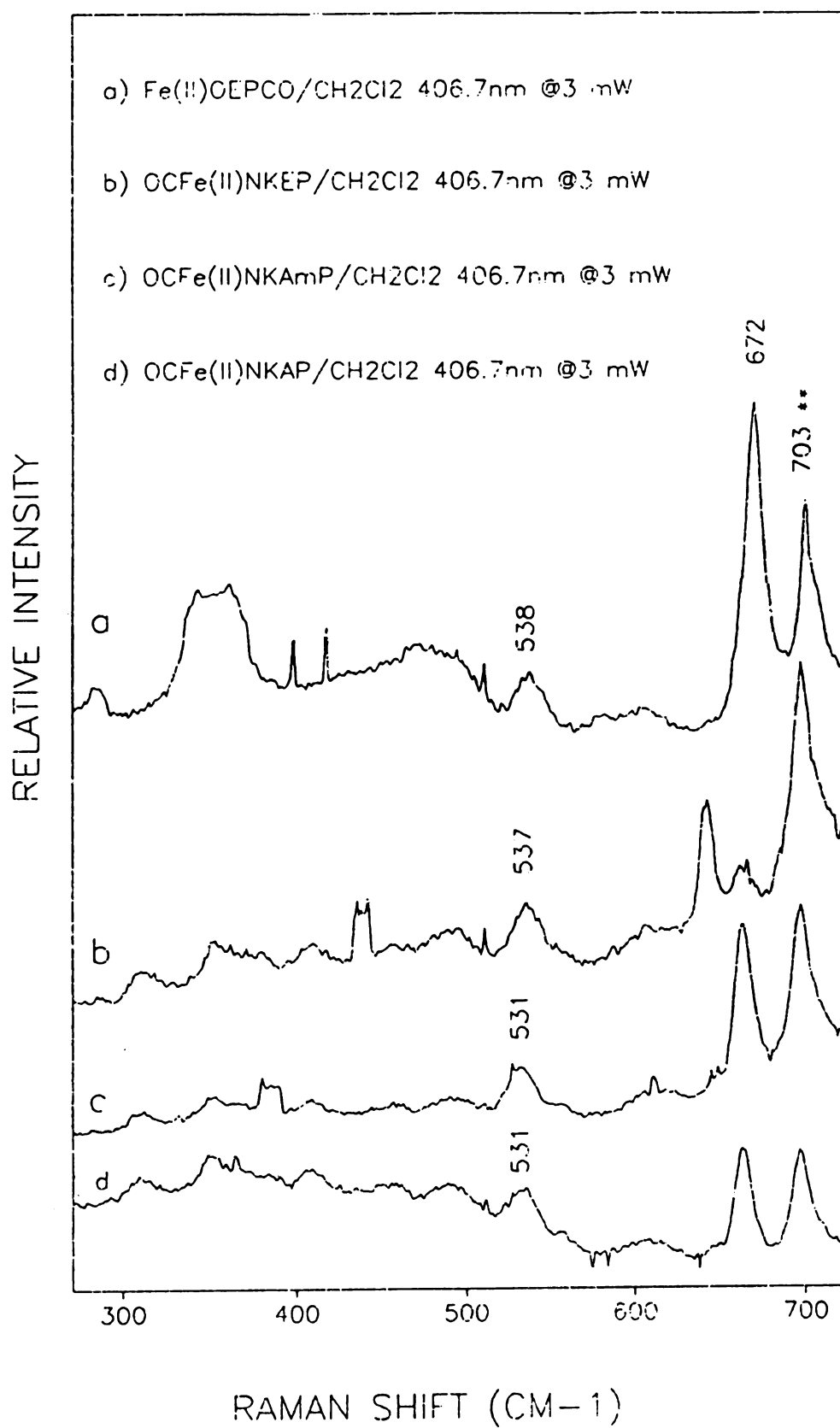
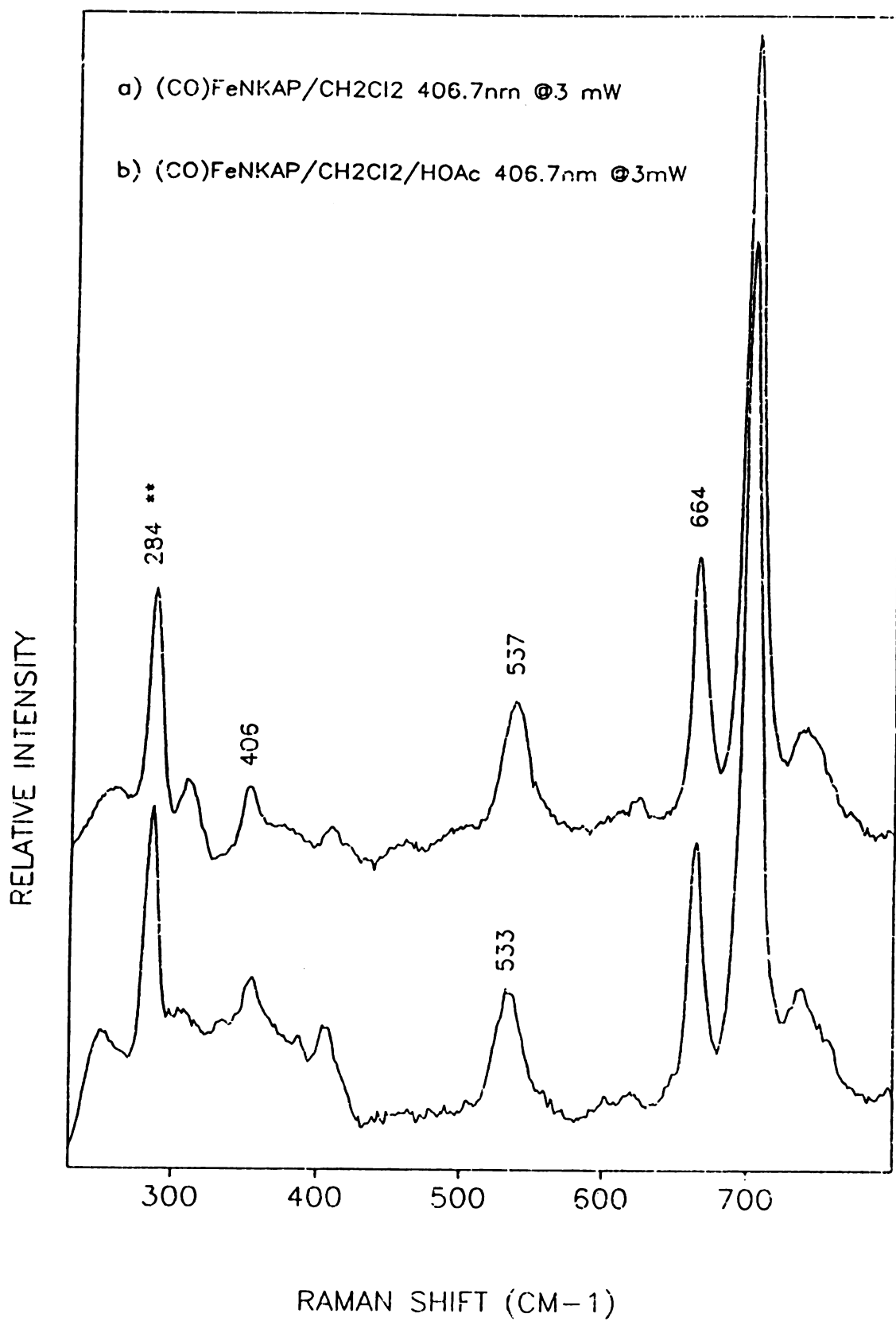


**Figure 5-5** The low frequency resonance Raman spectra obtained with  $\lambda_{\text{ex}} = 406.7$  nm of (a) carbon monoxide bound iron(II)NKAP in  $\text{CH}_2\text{Cl}_2$ . Iron was inserted into free base NKAP in the form of iron(II)carbonyl carbonate. The carbonate anion left the  $\text{COFe(II)NKAP}$  complex in the deprotonated five-coordinate form. (b) carbon monoxide bound iron(II)NKAP in  $\text{CH}_2\text{Cl}_2$  and 2mL of HOAc that would leave the  $\text{COFe(II)NKAP}$  complex in the protonated five-coordinate form.



metalloporphyrins [74]. The domed or out-of-plane metal structure for the five-coordinated complex is consistent with the crystal structure of the oxovanadyl naphthyl Kemp's amideporphyrin [75].

Figure 5-4 represents the low frequency region RR spectra of CO bound iron(II)porphyrins. It was previously established that  $\nu(\text{Fe-CO})$  for CO bound Fe(II)porphyrins is the range of 525 to 540  $\text{cm}^{-1}$  [76]. In Fig. 5-4a we can assign the mode at 538  $\text{cm}^{-1}$  to  $\nu(\text{Fe-CO})$  for the unperturbed CO ligated iron porphyrin. In Fig. 5-4b we detect little, if any, effect on the the frequency of  $\nu(\text{Fe-CO})$  for the Kemp's ester complex. If steric hindrance were a major influence on the frequency of  $\nu(\text{Fe-CO})$  then we would expect a much greater influence from the ester complex. In Figures 5-4 c and d we see that the  $\nu(\text{Fe-CO})$  frequency is shifted by 7  $\text{cm}^{-1}$  compared to the unrestricted COFe(II)OEP complex. Even if we allow one wavenumber for detection limits of the instrumentation we we have an obvious effect on the frequency of  $\nu(\text{Fe-CO})$  for both the amide and acid complexes. Both of which are strong hydrogen bond donors [76].

Figure 5-5 a and b represents the RR spectra of COFe(II)NKAP in the deprotonated and protonated forms respectively. In the deprotonated form of COFe(II)NKAP we detect the frequency of  $\nu(\text{Fe-CO})$  at 537  $\text{cm}^{-1}$  which is within experimental agreement with the frequency of  $\nu(\text{Fe-CO})$  for COFe(II)OEP. In Figure 5-5b we have added 2  $\mu\text{L}$  of acetic acid (HOAc) to the sample that was used to obtain Figure 5-5a. The shift to lower energy for the hydrogen bonding donor of the protonated COFe(II)NKAP complex is in agreement with the frequencies  $\nu(\text{Fe-CO})$  reported in Figure 5-4d.

## 5.6 Discussion

Table II is a summary of the observed frequencies of  $\nu(\text{M-CO})$   $\text{M} = \text{Fe(II)}$  or  $\text{Ru(II)}$  for "unhindered"  $(\text{CO})\text{M(II)OEP}$  or the naphthyl Kemp's porphyrins. The

Kemp's acid and amide compounds are likely to hydrogen bond with CO whereas the Kemp's ester complex would likely act as a hindered structure. If steric hindrance is indeed the factor that most influences the frequency of  $\nu(\text{M-CO})$  then we would expect the frequency for the ester to be the furthest away from the unhindered frequency of  $(\text{CO})\text{MOEP}$ . However, this is not the case in the observed frequencies. In fact the greatest effect on the frequency of  $\nu(\text{M-CO})$  is detected in the 7  $\text{cm}^{-1}$  shift in both NKAP and NKAmP.

This is most likely explained by the hydrogen bonding effect. It may be true that the CO is tilted off axis from the linear M-C-O case but this can also be explained by an attraction of the CO by the adjacent hydrogen bond donors. This situation would then produce a two-fold effect on the vibrational frequencies. One effect would, indeed, be the tilting of CO and the other effect would be polarity induced by the hydrogen bond.

Table II. The observed  $\nu(\text{M-CO})$  {M = Fe(II) or Ru(II)} frequencies for OEP, NKAP, NKEP or NKAmP in methylene chloride. Raman excitations were obtained from  $\lambda_{\text{ex}} = 406.7 \text{ nm}$ .

Compound	Solvent		$\nu(\text{M-CO})$
(CO)RuNKEP	$\text{CH}_2\text{Cl}_2$		564
(CO)RuNKAP	$\text{CH}_2\text{Cl}_2$		560
(CO)RuNKAmP	$\text{CH}_2\text{Cl}_2$		561
(CO)FeOEP	$\text{CH}_2\text{Cl}_2$		538
(CO)FeNKEP	$\text{CH}_2\text{Cl}_2$		537
(CO)FeNKAmP	$\text{CH}_2\text{Cl}_2$		531
(CO)FeNKAP	$\text{CH}_2\text{Cl}_2$		531
(CO)FeNKAP	$\text{CH}_2\text{Cl}_2$	deprotonated	537
(CO)FeNKAP	$\text{CH}_2\text{Cl}_2$	w/HOAc	533

The fact that NKEP has virtually no effect on the frequency of  $\nu(\text{M-CO})$  suggests that steric hinderence is a minor factor affecting bound CO in these compounds. These results would also suggest that steric hinderence from the distatal histidine of hemeoproteins is not an essential element in the proteins ability for ligand discrimination. The observed  $\nu(\text{M-CO})$  frequency for the deprotonated form of NKAP would further suggest that polar interactions in themselves are also not a major factor affecting the ligand binding abilities of hemeoproteins. Indeed, polar effects may be placed on the ligated form of the heme, however, they are most likely the direct result of hydrogen bonding from the distal histidine.

## REFERENCES

- [1] Branden, C. and Tooze, J. *Introduction to Protein Structure*, Garland Publishing, Inc., New York and London, 1991
- [2] Perutz, M. F. *Annu. Rev. Biochem.*, 1979, 48, 327-386
- [3] Perutz, M. F. *Trends. Biochem. Sci.*, 1989, 14, 42-44
- [4] Perutz, M. F.; Fermi, G.; Luisi, B. and Liddington, R. C. *Acc. Chem. Res.* 1987, 20, 309-321
- [5] Perutz, M. F. *Annu. Rev. Physiol.* 1990, 52, 1-25
- [6] Gibson, Q. H. *Biochem. J.*, 1959, 71, 193
- [7] Antonini, E. and Brunori, M. *Hemoglobin and Myoglobin and their Reactions with Ligands*, Elsevier Science Publishers B.V.; Amsterdam, 1971
- [8] Collman, J. P.; Brauman, J. I.; Iveson, B. L.; Sessler, J. L.; Morris, R. M. and Gibson, Q. H. *J. Am. Chem. Soc.*, 1983, 105, 3052-3064
- [9] Lavalett, D.; Tetreau, C.; Mispelter, J.; Momenteau, M. and Lhoste, J.-M. *Eur. J. Biochem.*, 1984, 145, 555-565
- [10] Traylor, T. G.; Tsuchiya, S.; Campbell, D.; Mitchell, M.; Stynes, D. and Koga, N. *J. Am. Chem. Soc.*, 1985, 107, 604-614
- [11] Traylor, T. G.; Koga, N. and Deardurff, L. A. *J. Am. Chem. Soc.*, 1985, 107, 6504-6510
- [12] Traylor, T. G.; Koga, N.; Deardurff, L. A.; Swepston, P. N. and Ibers, J. A. *J. Am. Chem. Soc.*, 1984, 106, 5132-5143
- [13] Springer, B. A.; Egeberg, K. D. Sligar, S. G.; Rohlfs, R. J.; Mathews, A. J. and Olson, J. S. *J. Biol. Chem.*, 1989, 264, 3057-3060

- [14] Collman, J. P.; Brauman, J. J.; Halbert, T. R. and Suslick, K. S. *Proc. Natl. Acad. Sci.*, **1976**, 73, 3333-3337
- [15] Marks, G. S.; Brien, J. F.; Nakatsu, K. and McLaughlin, B. E. *Trends Pharmacol. Sci.*, **1991**, 12, 185-188
- [16] Vandegriff, K. D. and Olson, J. S. *J. Biol. Chem.*, **1984**, 259, 12619-12627
- [17] Lemon, D. D.; Nair, P. K.; Boland, E. J.; Olson, J. S. and Hellmuns, J. D. *J. Appl. Physio.* **1987**, 62, 798-806
- [18] Perutz, M. F. *Nature*, **1970**, 228, 726-734
- [19] Norvell, J. C.; Nunes, A. C. and shoenborn, B. P. *Science*, **1975**, 190, 568-570
- [20] Collman, J. P.; Brauman, J. J.; Halbert, T. R. and Suslick, K. S. *Proc. Natl. Acad. Sci.*, **1976**, 73, 3333-3337
- [21] Hayashi, Y.; Yamada, H. and Yamazaki, I. *Biochem. Biophys. Acta.*, **1976**, 427, 608-616
- [22] Satterlee, J. D.; Teintze, M. and richards, J. H. *Biochemistry*, **1978**, 17, 1456-1462
- [23] Choc. M. G. and Caughey, W. S. *J. Biol. Chem.*, **1981**, 256, 1841-1838
- [24] Phillips, S. E. V. and Schoenborn, B. P. *Nature*, **1981**, 292, 81-81
- [25] Barlow, C. H.; Ohlsson, P.-I. and Paul, K.-G. *Biochemistry*, **1976**, 15, 2225-2229
- [26] Shimada, H. and Caughey, W. S. *J. Biol. Chem.*, **1982**, 257, 11893-11900
- [27] Momenteau, M. and Lavalette, D. *J. Chem. Soc., Chem. Commun.*, **1982**, 341-343
- [28] Satterlee, J. D. *Inorg. Chim. Acta.*, **1983**, 79, 170-172
- [29] Smith, M. L. Ohlsson, P.-I. and Paul, K.-G. *FEBS lett.*, **1983**, 163, 303-305
- [30] Sharma, V. S.; Malayakel, J. E. and Waterman, M. R. *J. Biol. Chem.*, **1982**, 257, 11887-11892
- [31] Stryer, L. *Biochemistry*, Freeman: New York, **1988**, pp 148-150
- [32] Peng, S.-M. and Ibers, J. A. *J. Am. Chem. Soc.*, **1976**, 98, 8032-8036

- [33] Gerothanassis, I. P.; Momenteau, M.; Hawkes, G. E. and Barrie, P. J. *J. Am. Chem. Soc.*, **1993**, 115, 9796-9797
- [34] Kuriyan, J.; Wilz, S.; Karplu, M. and Petsko, G. A. *J. Mol. Biol.*, **1986**, 192, 133-154
- [35] Huber, R.; Epp, and Formanek, H. *J. Mol. Biol.*, **1970**, 52, 349-354
- [36] Padlan, E. and Love, W. *J. Biol. Chem.*, **1974**, 249, 4067-4078
- [37] Norvell, J. C.; Nunes, A. C. and schoenborn, B, P. *Science*, **1975**, 190, 568-569
- [38] Heidner, E. J.; Ladner, R. C. and Perutz, M. F. *J. Mol. Biol.*, **1976**, 104, 707-722
- [39] Quillin, M. L.; Arduini, R. M.; Olson, J. S. and Phillips, G. N., Jr. *J. Mol. Biol.*, **1993**, 234, 140-155
- [40] Kim, K. and Ibers, J. A. *J. Am. Chem. Soc.*, **1991**, 113, 6077-6081
- [41] Kim, K.; Fettingner, J.; Sessler, J. L.; Cyr, M.; Hugdahl, J.; Collman, J. P. and Ibers, J. A. *J. Am. Chem. Soc.*, **1989**, 111, 403-405
- [42] Quillin, M. L.; Brantley, J. R. E.; Johnson, K. A.; Olson, J. S. and Phillips, G. N., Jr. *FASEB*, **1992**, 6, 2687
- [43] Quillin, M. L.; Brantley, J. R. E.; Johnson, K. A.; Olson, J. S. and Phillips, G. N., Jr. *J. Mol. Biol.*, **1993**, 234, 140-155
- [44] Brantley, J. R. E., Jr.; Smerdon, S. J.; Wilkinson, A. J.; Singleton, E. W. and Olson, J. S. *J. Mol. Biol.*, **1993**, 268, 6995-7010
- [45] Hargrove, M. S.; Singleton, E. W.; Quillin, M. L.; Ortiz, L. A.; Phillips, G. N., Jr.; Olson, J. S. and Mathews, A. J. *J. Mol. Biol.*, **1994**, 269, 4207-4214
- [46] Egeberg, K. D.; Springer, B. A.; Sligar, S. G.; Carver, T. E.; Rohlf, R. J. and Olson, J. S. *J. Mol. Biol.*, **1990**, 265, 11788-11795
- [47] Rohlf, R. J.; Mathews, A. J.; Carver, T. E.; Olson, J. S.; Springer, B. A.; Egeberg, K. D. and Sligar, S. G. *Proc. Natl. Acad. Sci.*, **1990**, 265, 3168-3176
- [48] Uno, T.; Nishimura, Y.; Tsuboi, M.; Makino, R.; Iizuka, T. and Ishimura, T. *J. Biol. Chem.*, **1987**, 262, 4549-4556
- [49] Yu, N.-T and Kerr, E. A. in *Biological applications of Raman Spectroscopy*, Spiro, T. G. Ed., John Wiley & Sons, **1988** Chapter 2
- [50] Li, X.-Y. and Spiro, T. G. *J. Am. Chem. Soc.*, **1988**, 110, 6024-6033

- [51] Nagai, M.; Yoneyama, Y. and Kitagawa, T. *Biochemistry*, **1991**, 30, 6495-6503
- [52] Li, T.; Quillin, M. L.; Phillips, G. N., Jr. and Olson, J. S.; *Biochemistry*, **1994**, 33, 1433-1446
- [53] Balasubramanian, S.; Lambright, D. and Boxer, S. *Proc. Natl. Acad. Sci. U.S.A.*, **1993**, 90, 4718-4722
- [54] Smerdon, S. J.; Dodson, G. G.; Wilkinson, A. J.; Gibson, Q. H.; Blackmore, R. S.; Carver, T. E. and Olson, J. S. *Biochemistry*, **1991**, 30, 6252-6260
- [55] Yonetani, T.; Yamamoto, H. and Iizuka, T. *J. Biol. Chem.*, **1974**, 249, 2168-2174
- [56] Phillips, S. E. and Schoenborn, B. P. *Nature*, **1981**, 292, 81-81
- [57] Hanson, J. C. and Schoenborn, B. P. *J. Biol. Chem.*, **1981**, 153, 17-146
- [58] Kitagawa, T.; Ondrias, M. R.; Rousseau, D. L.; Ikeda-Saito, M. and Yonetani, T. *Nature*, **1982**, 298, 869-871
- [59] Lavalette, D.; Tetreau, C.; Mispelter, J.; Momenteau, M and Lhoste, J.-M. *Eur. J. Biochem.*, **1984**, 106, 5132-5143
- [60] Mispelter, J.; Momenteau, M.; Lavalette, D. and Lhoste, J.-M. *J. Am. Chem. Soc.*, **1983**, 105, 5165-5166
- [61] Gerothanassis, I. P.; Momenteau, M and Loock, B. *J. Am. Chem. Soc.*, **1989**, 111, 7006-7012
- [62] Chang, C. K.; Ward, B.; Young, R. and Kondylis, M. P. *J. Macromo. Sci. Chem.*, **1988**, A25, 1307-1326
- [63] Wuenschell, G. E. Tetreau, C.; Lavalette, D. and Reed, C. A. *J. Am. Chem. Soc.*, **1992** 114, 3346-3355
- [64] Bajdor, K. and Nakamoto, K. *J. Am. Chem. Soc.*, **1984**, 106, 3045-3046
- [65] Proniewicz, Z.L.; Bajdor, K. and Nakamoto, K. *J. Phys. Chem.*, **1986**, 90, 1760-1766
- [66] Reczek, C.M.; Sitter, A.J. and Turner, J. *J. Mol. Spec.*, **1985**?6?,
- [67] Schappacher, M.; Chottard, G. and Weiss, R. *J. Chem. Soc., Chem. Commun.*, **1986**, 93-94

- [68] Gold, A.; Jayaraj, K.; Doppelt, P.; Weiss, K.; Chottard, G.; Bill, E.; Ding, X and Trautwein, A.X. *J. Am. Chem. Soc.* **1988**, 110, 5756-5761
- [69] Czernuszewicz, R.S. and Macor, K.A. *Raman spectrosc.*, **1988**, 19, 553-557
- [70] Oertling, W.A.; Kean, R.T.; Wever, R. and Babcock, G.T. *Inorg. Chem.* **1989**, 29, 2633-2645
- [71] Kean, R *Ph.D. Dissertation* Michigan State University, **1987**
- [72] Personal communication with Tony Oertling where he described the "back scatter" set up that was altered to accommodate low temperature spectroscopy.
- [73] Spiro, T.G. (Ed.); *Biological Applications of Raman spectroscopy*, Vol. 3, **1988**
- [74] Prendergast, K. and Spiro, T. G. *J. Am. Chem. Soc.* **1992**, 114, 3793-3801
- [75] The crystal structure for oxovanadyl and (CO)Ruthenium naphthyl Kemp's amideporphyrins have been determined. The manuscript is in preparation.
- [76] (a) Pauling, L. *The Nature of the Chemical Bond*, Cornell University Press, Ithaca, **1960** (b) Pimentel, G.C. and McClellan, A.L. *The Hydrogen Bond*, W.H. Freeman and Co., New York, **1960**